Instituto Politécnico Nacional

CENTRO DE INVESTIGACIÓN EN CIENCIA APLICADA Y TECNOLOGÍA AVANZADA

UNIDAD QUERÉTARO

POSGRADO EN TECNOLOGÍA AVANZADA

MODELACIÓN DE LA CINEMÁTICA DEL VENTRÍCULO IZQUIERDO USANDO IMÁGENES DE RESONANCIA MAGNÉTICA MARCADA

T E S I S

QUE PARA OBTENER EL GRADO DE

MAESTRO EN TECNOLOGÍA AVANZADA

P R E S E N T A

J O E L B A R A J A S Z A M O R A

DIRECTOR DE TESIS: DRA. PETIA RADEVA

CO-DIRECTOR: DR. JOAQUÍN SALAS RODRÍGUEZ

Querétaro, Qro., Diciembre de 2006

SIP-14

INSTITUTO POLITECNICO NACIONAL

SECRETARIA DE INVESTIGACION Y POSGRADO

ACTA DE REVISION DE TESIS

En la Ciudad de Querétaro siendo las 12 horas del día 28 del mes de noviembre del 2006 se reunieron los miembros de la Comisión Revisora de Tesis designada por el Colegio de Profesores de Estudios de Posgrado e Investigación de CICATA Querétaro para examinar la tesis de grado titulada:

Modelación de la Cinemática del Ventrículo Izquierdo usando Imágenes de Resonancia Magnética Marcada

Presentada por el alumno:

Barajas	Zamora	Joel
Apellido paterno	materno	nombre(s)

Con registro: | A | 0 | 5 | 0 | 0 | 6 | 8 |

aspirante al grado de:

Maestro en Tecnología Avanzada

Después de intercambiar opiniones los miembros de la Comisión manifestaron ***SU APROBACION DE LA TESIS***, en virtud de que satisface los requisitos señalados por las disposiciones reglamentarias vigentes.

LA COMISION REVISORA

DR. JOAQUIN SALAS RODRIGUEZ

DR. BOGDAN MIHAI RADUCANU

DRA. SANDRA PUJADAS OLANO

DR. JOEL GONZALEZ BARBOSA

DR. JUAN BAUTISTA HURTADO RAMOS

EL PRESIDENTE DEL COLEGIO

DR. JOAQUIN SALAS RODRIGUEZ

INSTITUTO POLITÉCNICO NACIONAL
CENTRO DE INVESTIGACIÓN EN
CIENCIA APLICADA
Y TECNOLOGÍA AVANZADA
UNIDAD QUERÉTARO

DIRECCION

INSTITUTO POLITÉCNICO NACIONAL

SECRETARÍA DE INVESTIGACIÓN Y POSGRADO

CARTA CESION DE DERECHOS

En la Ciudad de Querétaro el día 7 del mes diciembre del año 2006, el (la) que suscribe Joel Barajas Zamora alumno (a) del Programa de Maestría en Tecnología Avanzada con número de registro A050068, adscrito a CICATA Unidad Querétaro IPN, manifiesta que es autor (a) intelectual del presente trabajo de Tesis bajo la dirección de Petia Ivanova Radeva y cede los derechos del trabajo intitulado Modelación de la Cinemática del Ventrículo Izquierdo usando Imágenes de Resonancia Magnética Marcada, al Instituto Politécnico Nacional para su difusión, con fines académicos y de investigación.

Los usuarios de la información no deben reproducir el contenido textual, gráficas o datos del trabajo sin el permiso expreso del autor y/o director del trabajo. Este puede ser obtenido escribiendo a la siguiente dirección CICATA Unidad Querétaro IPN Cerro Blanco # 141 Colinas del Cimatario c.p. 76090 Querétaro, Qro., México. Si el permiso se otorga, el usuario deberá dar el agradecimiento correspondiente y citar la fuente del mismo.

Joel Barajas Zamora

Modelación de la Cinemática del Ventrículo Izquierdo usando Imágenes de Resonancia Magnética Marcada

Joel Barajas Zamora
Centro de Investigación en Ciencia Aplicada y Tecnología
Instuto Politécnico Nacional
Unidad Querétaro, México

Agradecimientos

Quiero dar las gracias a Joaquín Salas por su apoyo y soporte en la resolución de dudas técnicas y los conocimientos que me ha transmitido desde que he trabajado con él. Además, quiero expresar mi agradecimiento por su ayuda y motivación en mi formación como investigador, así como el desarrollo de habilidades que me ha fomentado tales como la escritura de documentos científicos y la preparación de presentaciones. Sin duda que sus críticas y consejos ha contribuido sustancialmente en la estimulación de estas habilidades básicas en la formación de un investigador. Por otro lado, el apoyo personal de él y de su familia en momentos difíciles para seguir en este camino ha sido invaluable.

A Petia Radeva me gustaría agradecer su paciencia para tratar conmigo y resolver mis dudas, por haber creído en mí cuando comencé a trabajar con ella. La oportunidad de trabajar con ella que junto con Joaquín hicieron realidad. Su apoyo para lograr establecernos a Karla y a mí en otro país y aceptarnos en su grupo de trabajo como si tuviéramos mucho tiempo de conocernos.

Deseo expresar mi reconocimiento a la labor hecha por Jaume García del Centre de Visió per Computador de Barcelona por compartir conmigo su experiencia en el problema, sin la cual el alcance de esta tesis hubiera sido menor. Su aportación al establecer una versión del proyecto sin duda que ha sido de gran ayuda para explorar con mayor profundidad el problema.

A Reydezel Torres, Lucina de la Paz López, Alicia Anaya, Pablo Vera, y a todos los que me han ayudado de alguna manera con los trámites necesarios para culminar este trabajo. Se aprecia sinceramente su ayuda y disposición mostrada. Igualmente, deseo dar las gracias a José Guadalupe Vega por su incansable ayuda en la resolución de diversos trámites relacionados con esta tesis.

Quiero mostrar mi aprecio a mi hermano Víctor Manuel por sus consejos y por haberme dado ánimos para tratar de ir siempre más allá y fomentarme el sentido de superación. Junto con él, mi hermana Ana por su apoyo personal, mi papá por creer en mí, y mi mamá por respetar siempre mis decisiones y respaldarme en tiempos difíciles.

Finalmente, quiero expresar mis agradecimientos y respeto profesional a Karla. Por las innumerables desveladas, la disposición incondicional para ayudarme, sus críticas profesionales, entre otras muchas cosas. Por tranquilizarme en momentos de

excesiva excitación o estimularme cuando era necesario. Sus ideas y observaciones han sido incontables y me han ayudado profundamente a culminar el trabajo que aquí se presenta.

A todos los que aquí menciono y a los que no haya nombrado pero hayan contribuido de alguna manera al completar este paso en mi vida profesional solo les puedo decir una cosa, Gracias.

Índice general

Agradecimientos **3**

Resumen **7**

1. Introducción **9**

2. Materiales y Métodos **13**

3. Resultados **19**

4. Conclusión y Discusión **21**

Apéndices **21**

A. Clinical Background **23**
A.1. Cardiac Diseases: An Important Cause of Death 23
A.2. Heart Structure and Function 23
A.3. Cardiac Measurement Tools 26

B. Previous Work **29**
B.1. Image Preparation 31
B.2. Boundary Surface Extraction 32
B.3. Tag Tracking 33
B.4. 3D Motion Reconstruction 36
B.5. Intersubject Comparison and Statistical Model Formation 38

C. Clinical Framework **41**
C.1. Surface Extraction 41
C.2. Tag Tracking 43
C.3. 3D Motion Reconstruction 43
C.4. Intersubject Comparison 44

D. Improved Deformation in Cardiac Tagged MR Images **45**
D.1. Introduction 45
D.2. Principle of Angle Images 47
D.3. Definitions 47
D.4. Gabor Filters in Tagged MR Images 48
D.5. Motion Tracking using Angle Images 51

E. Correction of Misalignment Artifacts in 3-D Space **53**
E.1. Planes Intersection 54
E.2. Correspondence Measure 56
E.3. Misalignment Correction 56

F. Estimating 3-D Motion from 2-D Components **61**
F.1. From 2-D Images to 3-D Space 62
F.2. Generation of 3D Motion 63
F.3. Interpolation 65

G. Results **67**
G.1. Gabor Filters in Cardiac Tagged MRI 67
G.1.1. Validation Protocol 67
G.1.2. Result Analysis 68
G.2. Misalignment Correction Results 71
G.3. 3-D Motion and Behavior 74
G.4. Myocardial Rotation: a Clinical Measure 75

H. Further Research **79**
H.1. Conclusion and Discussion 79
H.2. Further Research 80

Bibliografía **81**

Publicaciones Relacionadas **91**

Resumen

Las enfermedades cardiovasculares se han convertido en una de las principales causas de muerte en los últimos años. Para poder elaborar un diagnóstico apropiado y así disminuir su influencia dentro de las principales causas de muerte, es necesario contar con herramientas tecnológicas capaces de proporcionar estimaciones cuantitativas en forma confiable. Actualmente hay una gran variedad de equipos disponibles clínicamente los cuales proporcionan descripciones cualitativas a través de imágenes del estado de algunos órganos del cuerpo humano, incluido el corazón. Sin embargo, la interpretación de estas imágenes depende en gran medida del médico que elabora el estudio, lo cual ha afectado considerablemente la incorporación completa de estas técnicas de imagen. Dentro de las modalidades de imagen cardiaca disponibles esta la resonancia magnética. Este tipo de imagen tiene la ventaja de ser una técnica no invasiva, además de brindar la oportunidad de estudiar al corazón *en vivo*, por lo que el uso de ella esta adquiriendo cada vez mayor popularidad. Debido a la uniformidad con que el miocardio se observa en la imágenes de resonancia magnética, solo es posible obtener medidas globales de la deformación de éste. Es por esto que se ha creado una variante de esta forma de imagen en la cual han logrado tener marcajes que pueden ser seguidos en el tiempo. Como dichos marcajes se deforman en la misma medida en que lo hace el miocardio, su seguimiento describe la cinemática de forma confiable. A estas imágenes se les nombra de resonancia magnética marcada.

En esta tesis, se presenta un método para la modelación de la cinemática del ventrículo izquierdo basada en el análisis de imágenes de resonancia magnética marcada. Se presentan un estudio del problema y éste se divide en: segmentación del miocardio, seguimiento de los marcajes, modelación en 3-D, y comparación entre sujetos. Se establece el método usado para la segmentación del miocardio. En el seguimiento de los marcajes se propone una nueva técnica basada en filtros de Gabor, aprovechando la frecuencia característica del patrón de marcaje. Para realizar la modelación se requiere combinar la deformación obtenida de los planos de imagen, por lo que es necesario que éstos estén alineados entre sí. En esta tesis se presenta un método para corregir problemas de desplazamiento entre planos basado en la información mutua normalizada a lo largo de las líneas de intersección. Se sugiere un procedimiento para obtener los vectores de deformación en 3-D a partir de la combinación de vectores en 2-D. Además, se muestra una forma de interpolación para distribuir las deformaciones sobre el miocardio en imágenes de eje corto. Posteriormente, además de los resultados de cada técnica, se exponen un estudio estadísticos de la rotación y torsión del miocardio en una población de sujetos sanos. Por último, una conclusión y discusión son abordadas junto con

algunas líneas futuras de investigación.

Abstract

In recent years, cardiovascular illness have become one of the most frequent causes of death. To elaborate a sound diagnosis, and hence reduce its effects, it has become essential to have images to describe qualitatively the state of the human organs, including the heart. However, the interpretations of these images depends greatly on the physician skills which make it error prone and hence reduce the reliability of these interpretations. One of the techniques available in the area of cardiac imaging is the magnetic resonance. These images have the advantage of being non-invasive, giving the opportunity of studying living hearts, and hence are becoming very popular. Due to the stability of the magnetic resonance myocardium images, it is only possible to obtain global measures about it. On the contrary, tagged can be tracked down in time. Since these tags deform along the myocardium, its cinematic is equivalent to the heart one. These images are called tagged magnetic resonance images. In this thesis, we develop a method to model the left ventriculus cinematics based on tagged magnetic resonance image analysis. Our study includes: segmentation of the myocardium, tracking of the tags, 3-D modeling, and patients comparison. We describe in detail the method used to segment the myocardium. Also, we propose a novel technique to track the tags using Gabor filters using the tag pattern characteristic frequency. Our method to model the myocardium requires to estimate the deformation in the image planes, thus it is necessary to align them. Our study includes a method to solve the plane shift problem based on normalized mutual information along the intersection lines. We suggest a procedure to obtain the deformation vectors in 3-D from their combination in 2-D. Indeed, we develop and interpolation procedure to distribute the deformation on the short axis images. Later on, we show the results and the statistical studies for the myocardium rotation and torsion in a healthy population. Finally, we conclude discussing future lines of research

Capítulo 1

Introducción

Durante los últimos años las enfermedades cardiacas se han convertido en una de las principales causas de muerte en todo el mundo. De acuerdo con la Organización Mundial de Salud (OMS), las enfermedades del corazón representaron el 30 % de las muertes en 2005 en todo el planeta[1]. Este dato las ubica como la principal causa de muerte dentro de las enfermedades no contagiosas, lo cual es de especial trascendencia tomando en cuenta que varias de estas últimas se encuentran erradicadas en muchos países. En México, de acuerdo con el Instituto Nacional de Estadística Geografía e Informática (INEGI), las enfermedades cardiovasculares fueron la primera causa de muerte en personas mayores de 65 años y la tercera en personas de 30 a 64 años de 1994 a 2004[2].

El corazón humano puede ser considerado como un órgano muscular el cual bombea sangre oxigenada hacia el sistema circulatorio encargado de distribuirla por todo el cuerpo humano. Este proceso se realiza en coordinación con los pulmones quienes se encargan de oxigenar la sangre. De tal forma que mediante contracciones del músculo cardiaco el corazón realiza su función. Dos de sus principales partes son el ventrículo izquierdo y el ventrículo derecho. Ambos realizan la tarea principal complementándose entre ellos. Por un lado el ventrículo derecho bombea sangre proveniente del sistema circulatorio hacia los pulmones para ser oxigenada. Por otro lado el ventrículo izquierdo es el responsable de bombear la sangre proveniente de los pulmones hacia el sistema circulatorio. El lapso de tiempo cuando ambos ventrículos pasan de máxima contracción a relajación completa es llamado diástole. Por el contrario, el tiempo entre relajación y máxima contracción se le nombra sístole.

Debido a que numerosas enfermedades cardiacas están relacionadas con disfunciones del ventrículo izquierdo, el análisis de su funcionamiento es de vital importancia para elaborar un diagnóstico apropiado. Como ejemplo se puede citar la isquemia del tejido miocárdico. En este caso, el funcionamiento del ventrículo izquierdo pierde sincronía debido a la atrofia de un segmento de la pared del miocardio ocasionando una disminución en la presión necesaria para la correcta irrigación de la sangre a través del sistema circulatorio.

Actualmente existen varias técnicas de imagen médica capaces de proporcionar una descripción visual de la anatomía y funcionamiento del corazón y sus partes. Estas técnicas van desde ecocardiogramas hasta diferentes tipos de tomografías. To-

das tienen sus ventajas y desventajas y muchas de ellas se complementan o son más usadas para diagnosticar enfermedades específicas. Dentro de las técnicas de tomografía, las imágenes de Resonancia Magnética (MRI) sugieren una alternativa para estudiar el comportamiento global del ventrículo izquierdo. Esta modalidad está basada en la producción de imágenes internas con características físicas y químicas de un objeto con señales de resonancia magnética. Empleando campos magnéticos altos y ondas de radio, el equipo de resonancia colecta y relaciona reflexiones causadas por los átomos del cuerpo para formar las imágenes. Es por esto que esta técnica ofrece imágenes relativamente definidas permitiendo a los médicos observar estructuras internas del cuerpo con gran detalle.

Para poder estudiar la deformación global del ventrículo izquierdo las imágenes de resonancia magnética representan una opción confiable y viable. En una sesión típica de captura de imágenes, una serie de vistas de eje corto y eje largo son adquiridas. Si se considera al ventrículo como un cilindro, las vistas de eje corto son cortes radiales donde el músculo cardiaco se observa como un anillo. Por el contrario, las vistas de eje largo son cortes adquiridos sobre el eje central del ventrículo donde éste puede observarse de base a ápex. De esta forma es posible combinar la información geométrica y de deformación de ambas vistas dado que son complementarias.

A pesar de que las imágenes de resonancia magnética permiten la obtención de parámetros globales de deformación, la uniformidad con que el tejido del miocardio se observa limita su capacidad para saber que pasa dentro de éste. Esta propiedad de la técnica limita su capacidad para obtener un desplazamiento denso a través de la estimación del flujo óptico. Para ofrecer una solución a este problema se ha creado una variante a esta modalidad de imagen, la resonancia magnética marcada. En esta técnica se generan perturbaciones magnéticas en el tejido tal que éstas puedan ser visibles produciendo varios puntos de referencia. Este patrón de puntos marcan el tejido mediante la suma de una señal de radio frecuencia en la magnetización de éste para producir un número de planos de saturación. Este proceso es realizado en dos fases de adquisición. Una para producir un patrón espacialmente modulado en la fase de la magnetización, y la otra para adquirirlo durante un ciclo cardiaco. A este proceso se le llama Modulación Espacial de Magnetización (SPAMM). Para generar un punto de referencia en el tiempo, el arreglo de marcajes es sincronizado con el electrocardiograma para inicializarlo al principio de la sístole cuando la relajación del ventrículo es máxima. Conforme éste se va contrayendo, los marcajes van deformándose de acuerdo a como lo hace el miocardio. Finalmente cuando la diástole ocurre, los marcajes van siendo restaurados a su forma original. Ejemplos de imágenes de resonancia marcada se muestran en la figura 1.1.

Una de las limitaciones de esta variación a la resonancia magnética es la gradual desaparición de los marcajes. Esto ocurre debido a la relajación del tejido a través del tiempo, por lo que al final de ciclo cardiaco los marcajes prácticamente han desaparecido. Para tratar de contrarrestar este fenómeno, se ha creado la Modulación Espacial de Magnetización Complementaria (C-SPAMM). En esta variante, dos imágenes marcadas mediante SPAMM son creadas con un desfase de 180° y restadas entre sí. Sin embargo, la principal desventaja de esta modificación es el tiempo de adquisición que típicamente es de 18 segundos, lo cual requiere que el paciente aguante la respiración mientras se realiza el estudio. Este inconveniente limita el uso de C-SPAAM dado que el esfuerzo para soportar la respiración durante este tiempo es considerable. Para una mayor descripción de los principios clínicos,

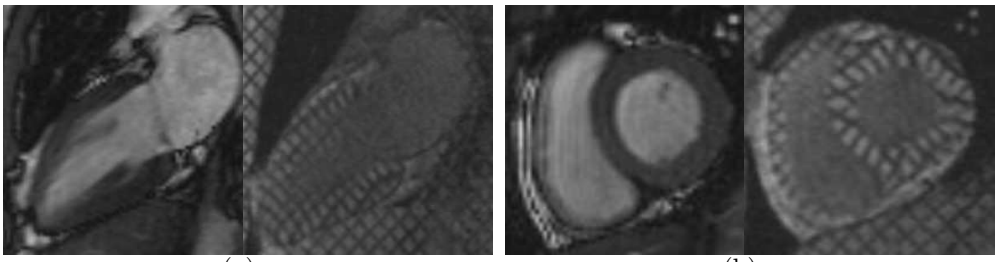

(a) (b)

Figura 1.1: Imágenes de resonancia magnética y su representación en resonancia marcada. (a) Imágenes de eje largo en el final de la sístole. (b) Imágenes basales de eje corto en el final de la sístole.

vease el apéndice A.

Para fines de esta tesis, se han empleado imágenes SPAMM para el análisis de la cinemática del ventrículo izquierdo. El equipo de adquisición de resonancia magnética usado es un Siemens Avanto de 1.5 Teslas el cual se encuentra en el Hospital de la Creu Blanca en Barcelona España. Las imágenes son proporcionadas por los cardiólogos Francesc Carreras Costa y Sandra Pujadas Olano del Hospital de la Santa Creu i Sant Pau y del Hospital de la Creu Blanca respectivamente.

En esta tesis, la cinemática del ventrículo izquierdo es analizada basandonos en imágenes de resonancia magnética marcada. A partir de un conjunto de imágenes de eje corto y de eje largo, las deformaciones en 3-D son inferidas. El flujo óptico para cada píxel en los planos de imagen es calculado. Posteriormente, estos planos son alineados para que concuerden entre ellos en el espacio 3-D. Después, los vectores de desplazamiento calculados para los puntos de intersección entre planos son combinados para obtener las deformaciones en 3-D en ellos. Finalmente, esta información es distribuida en las vistas de eje corto para completar las deformaciones obtenidas sobre ellas. Adicionalmente, la rotación y torsión del ventrículo izquierdo son examinadas para proporcionar una potencial herramienta médica. Un estudio de las técnicas existentes para el análisis de imágenes de resonancia magnética marcada es desarrollado en el apéndice B.

Capítulo 2

Materiales y Métodos

El análisis de las imágenes de resonancia magnética marcada puede ser dividido en los siguientes pasos[3]:

- Preparación de imágenes
- Segmentación del miocardio
- Seguimiento de los marcajes
- Reconstrucción de la deformación en 3-D
- Comparación entre sujetos y generación de un modelo estadístico

La preparación de imágenes consiste en realizar un preprocesamiento con el fin de excluir ciertos errores inducidos por la técnica de adquisición. Este paso es de especial importancia cuando se usan los niveles de gris en el análisis. La falta de una escala de grises estandarizada y la variación del fondo de las imágenes son algunos de los problemas que deben corregirse. Sin embargo, la solución que se presenta aquí está basada en una caracterización espectral de las imágenes lo cual disminuye considerablemente estos errores. Además de esta ventaja, debido a las características técnicas del equipo de resonancia las imágenes presentan un fondo uniforme alrededor del corazón. Es por esto que se ha suprimido este preprocesamiento en el método presentado en esta tesis.

Para la segmentación del miocardio se ha designado usar las imágenes de resonancia convencional o CINE. A causa de la ausencia de los marcajes en estas imágenes el ventrículo izquierdo es más fácil de segmentar. Debido a que las secuencias que se obtienen del equipo comercial contienen información espacial en formato DICOM (Digital Imaging and Communication in Medicine), es posible establecer correspondencias geométricas entre una imagen CINE y una marcada. Por lo tanto, al diseñarse un protocolo de adquisición en el cual para las vistas marcadas se obtenga sus correspondientes en CINE, una segmentación hecha en esta modalidad puede llevarse a las imágenes marcadas. De esta forma se toma ventaja de ambas modalidades para obtener resultados más acertados.

En la segmentación de las imágenes de eje corto se ha usado el método desarrollado por García *et al.*[4]. En esta solución el miocardio es inicializado mediante

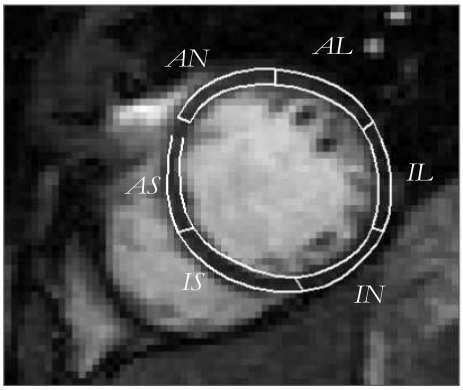

Figura 2.1: Segmentación del ventrículo izquierdo para vistas de eje corto de acuerdo a la *American Heart Association (AHA)* *AN* - Anterior. *AL* - Anterolateral. *IL* - Inferolateral. *IN* - Inferior. *IS* - Inferoseptal. *AS* - Anteroseptal.

una serie de puntos localizados manualmente los cuales describen al miocardio en seis regiones: anterior, anteroseptal, inferoseptal, inferior e inferolateral, de acuerdo a la *American Heart Association*[5]. Dichas regiones se muestran en la figura 2.1. Mediante estos puntos la forma del miocardio es alterada de acuerdo a un mapa de deformaciones calculado a través del seguimiento de los marcajes. Sin embargo, deformar esta forma con base únicamente en esta información puede conducir a segmentaciones no validas debido a errores en el seguimiento. Para resolver este problema se emplean los modelos de forma activa (ASM).

En ASM una forma puede ser representada mediante un conjunto de puntos los cuales la describen. Para nuestro caso tenemos 6 regiones dándonos 6 puntos en el epicardio y 6 en el endocardio. Para completar la forma, los puntos intermedios entre regiones pueden ser obtenidos mediante *splines* o *snakes*, donde estos segmentos son interpolados a un polinomio de un orden determinado[6].

Una vez las curvas han sido definidas, se crea un modelo estadístico capaz de corregir errores en ellas y adaptarlas a unas plausibles. Aunque la creación de una base de formas plausibles parece ser una tarea viable para ser hecha automáticamente, en general esta base se crea manualmente para garantizar la mayor certeza posible. Teniendo este conjunto de entrenamiento, se hace un análisis de componentes principales para reducir la dimensionalidad de las formas y tener un rango de ellas creíble. Por tanto, una corrección en la deformacin puede hacerse con base en el rango obtenido. Una explicación más detallada de esta segmentación es presentada en el apéndice C.

Habiendo estimado la segmentación, se realiza el seguimiento de los marcajes. Dentro de las métodos propuestos para resolver el problema están los que se basan en la extracción de los marcajes y su seguimiento. Una vez deformados, la información de desplazamiento obtenida se distribuye en el área del miocardio. Uno de los principales problemas de esta manera de atacar el problema es el desvanecimiento de los marcajes ocasionado por la relajación del tejido a través del tiempo. Para disminuir este problema, uno de los procedimientos mayormente aceptados es mediante la obtención de imágenes de ángulo. A través del uso de la técnica de fase

armónica (HARP) es posible obtener esta caracterización[7]. Debido a la frecuencia de los marcajes, el espectro común de una imagen de resonancia magnética marcada muestra una serie de picos armónicos centrados en múltiplos enteros de la frecuencia de estos. Por lo que una imagen marcada puede verse como una señal modulada en esta frecuencia. De tal forma que en HARP se propone extraer el primer pico armónico y filtrarlo únicamente en un lado del espectro de la imagen generando un repuesta compleja. Al obtener la fase de la salida, se puede establecer ésta como una propiedad material de cada punto en la respuesta. Por lo que, mientras los marcajes sean capaces de generar picos armónico, el seguimiento de la fase es robusto. La principal ventaja de esta caracterización es la posibilidad de calcular el flujo óptico para cada píxel de la imagen.

A pesar de las mejoras incorporadas por HARP, la naturaleza de esta técnica es global. Cuando los marcajes no han sido deformados la detección de ellos es trivial dado que el contenido de frecuencias en toda la imagen es en general el mismo. Sin embargo, conforme los marcajes se van deformando el contenido va variando en forma local por lo que éste tiene diferente distribución en distintas regiones. Debido a que la extracción del primer armónico asume una frecuencia predominante en toda la imagen, en muchas ocasiones pierde deformaciones locales. Para mejorar este problema, en esta tesis hemos aplicado un banco de filtros de Gabor para realizar esta caracterización.

Un filtro de Gabor puede considerarse como una envolvente Gausiana modulada por una senoidal compleja. El espectro de Fourier de éste resulta ser igualmente una Gausiana pero con desviaciones estándar invertidas y centrada en la frecuencia de la senoidal. Debido a que el filtro es una función compleja su espectro no es simétrico respecto a la frecuencia cero, lo cual produce un resultado similar que con HARP. Sin embargo, al aplicar varios filtros se puede saber cual se adapta mejor por zonas en la imagen mediante la magnitud de la respuesta. Por lo que para mejorar su adaptación, se localiza el primer pico armónico, se genera un rango de filtros alrededor de esta frecuencia y se aplica cada uno a la imagen. La imagen final se forma extrayendo la máxima magnitud por píxel de las distintas respuestas. Mediante este análisis se logra una mejor descripción del contenido de frecuencias de los marcajes por región. Como el resultado de la combinación de filtros es también una imagen compleja, se puede extraer su fase y formar una imagen de ángulo más acertada que con HARP.

Una vez que se tienen imágenes de ángulo capaces de permanecer constantes a través de la secuencia, se aplica un algoritmo de seguimiento para obtener el flujo óptico para cada punto del miocardio. Para este caso, se aplica una adaptación del método de Newton-Raphson para la obtención ceros de una función. En este problema se asume que el valor de fase se mantiene constante por lo que se busca el punto en el cual esto se cumple alrededor de su posición original en la siguiente imagen de la secuencia permitiendo resolución subpíxel en la búsqueda[7]. En la figura 2.2 se muestra un ejemplo del flujo óptico obtenido. Para una explicación más detallada del seguimiento de los marcajes véase el apéndice D.

Para el análisis de las imágenes de eje largo se realiza el mismo proceso que en eje corto. Sin embargo, la segmentación del ventrículo no se lleva a cabo. Esto es debido a que, para fines de esta tesis, estas imágenes se usan únicamente para completar la deformación en 3-D del ventrículo y no se extraen parámetros específicos de ellas. Como es posible encontrar las intersecciones entre un conjunto de imágenes

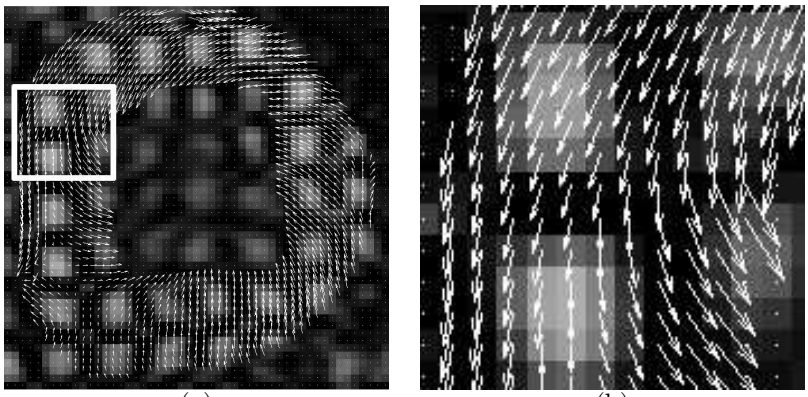

(a) (b)

Figura 2.2: Ejemplo de deformaciones obtenidas mediante el flujo óptico en las imágenes de ángulo. (a) Vectores de deformación calculados. (b) Región seleccionada.

de eje corto y otro de eje largo, la segmentación realizada en uno de ellos puede ser reflejada en el otro para los puntos de intersección. Por otro lado, en eje largo la región del ápex resulta difícil de segmentar además de que teóricamente en este punto del ventrículo su grosor es muy pequeño.

Una vez que los mapas de deformación han sido obtenidos, para reconstruir la deformación en 3-D es necesario correlacionar la información de los planos de eje corto con los de eje largo. Para poder realizar esta reconstrucción es necesario asumir que las secuencias de imágenes han sido tomadas en el mismo lapso de tiempo. No obstante, lo que ocurre a la práctica es que las secuencias son adquiridas una a una y en diferentes tiempos. Para realizar la captura, se le pide al paciente que aguante la respiración mientras la secuencia es gravada. Un problema típico es que la posición del ventrículo no es la misma en todas la secuencias a causa de movimientos del paciente o desplazamientos inducidos por su respiración[8]. Para solucionar este problema de registración, en esta tesis se presenta un método basado en el uso de la Información Mutua Normalizada (NMI)[9]. En la figura 2.3 se muestran algunos ejemplos de las intersecciones entre planos de eje corto y largo.

En el método presentado en esta tesis, se calculan las líneas de intersección entre los planos de todas la capturas usando la información DICOM. A estos planos se les asocia la primera imagen de las secuencias CINE y se establece un rango de valores a partir de una región de interés seleccionada manualmente. Posteriormente se extraen los niveles de grises a lo largo de estas líneas formando parejas de valores entre planos. Si hay una buena correspondencia entre ellos, estos valores tenderán a ser iguales. La comparación de estos niveles se ha hecho usando la Información Mutua Normalizada la cual permite variaciones en contraste o falta de uniformidad en el fondo.

Una vez establecida una medida de adaptación entre planos, se ha empleado un método de optimización para maximizarla. Para esto, el espacio de búsqueda se ha establecido igual al número de planos menos uno multiplicado por tres. Esto sale de que cada plano es trasladado libremente en 3-D. El método de optimización usado es una versión particular del gradiente descendente desarrollada en [10]. De esta

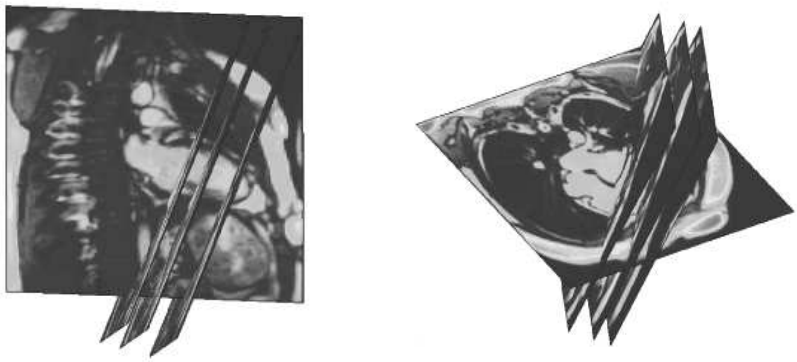

(a) (b)

Figura 2.3: Ejemplos de intersecciones entre planos en una sesión de imagen típica. (a) Intersecciones entre una vista de eje largo y tres de eje corto. (b) Otra vista de eje largo donde los dos ventrículos pueden observarse con tres vistas de eje corto.

forma los planos son ajustados para obtener una buena correspondencia entre ellos y poder lograr una acertada descripción de la anatomía del ventrículo izquierdo. Este método es detallado más profundamente en el apéndice E.

Habiendo ajustado las vistas disponibles, la obtención de las deformaciones completas puede realizarse con mayor certeza. A lo largo de las líneas de intersección entre los planos hay desplazamientos obtenidos del seguimiento de las fases. En esta tesis, las deformaciones en 3-D son calculadas a partir de la combinación de los vectores sobre cada plano. Teniendo la información completa de deformación en estas intersecciones, el resto de los desplazamientos sobre los planos de eje corto es interpolado para la componente ortogonal a los marcajes. Este método permite tener mapas de deformación para las segmentaciones del miocardio en vistas de eje corto. Debido a la naturaleza de las deformaciones cerca del ápex y a la probabilidad de error en la interpolación en esta región, los desplazamientos en las vistas de eje largo no han sido completados. Los detalles técnicos de este técnica son desarrollados en el apéndice F.

Capítulo 3

Resultados

Para validar las mejoras del método de seguimiento de los marcajes expuesto en esta tesis, se ha elaborado una comparación basada en la correlación entre las imágenes deformadas de acuerdo al mapa de desplazamiento obtenido. La técnica de alineación desarrollada ha sido validada mediante movimientos inducidos en forma aleatoria a los planos. En general, este método mejora considerablemente las deformaciones obtenidas en 3-D. Esto es porque las correspondencias entre planos resultan ser más acertadas. En la figura 3.1 se muestra un ejemplo de los vectores en 3-D calculados para las vistas de eje corto.

Para crear una herramienta robusta y que pueda usarse en los ambientes clínicos, es necesario realizar un modelo estadístico que refleje un comportamiento estable entre sujetos sanos como primer paso. En esta tesis, se analiza la rotación del ventrículo izquierdo en distintas latitudes desde la base hasta el ápex. Este parámetro ha sido definido como el cambio de ángulo de una imagen a otra en la misma secuencia obtenido de representar las deformaciones en forma polar respecto al centro del miocardio[4]. De esta manera, ha sido estudiada la relación de este parámetro con la latitud de la vista de eje corto en el ventrículo. Adicionalmente, la torsión, definida como la diferencia de rotaciones entre la base y el ápex, ha sido estudiada. Para analizar los esquemas de validación y los resultados numéricos,

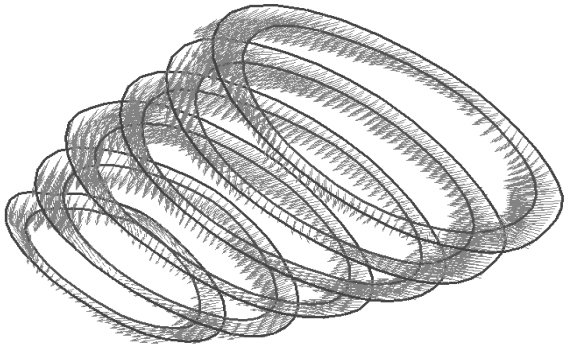

Figura 3.1: Vectores de deformación calculados para el ventrículo izquierdo en 3-D.

véase el apéndice G.

Capítulo 4

Conclusión y Discusión

Una nueva técnica para caracterizar las imágenes de resonancia magnética marcada ha sido descrita en esta tesis, la cual es capaz de manejar el problema del desvanecimiento de los marcajes. Un método certero para alinear las vistas de eje corto y eje largo entre sí ha sido presentado, el cual ha sido capaz de eliminar desplazamientos provocados por el movimiento del paciento o su respiración. Mediante el estudio del comportamiento de la medida de alineamiento y los vectores de intersección, se ha detectado que hay más de una solución al problema, lo cual pone a prueba el método de optimización usado.

Un método para reconstruir las deformaciones en 3-D libre de asunciones ha sido diseñado, el cual está basado en los puntos de intersección entre los planos de eje corto y los de eje largo. Además un algoritmo para combinar los vectores de deformación en 2-D de cada uno de los planos ha sido detallado. Se ha presentado una manera de interpolación para distribuir las deformaciones obtenidas en las líneas de intersección sobre todo el área del miocardio en vistas de eje corto.

Por último, la rotación del miocardio y la torsión del ventrículo izquierdo han sido estudiadas. Se ha presentado un análisis estadístico sobre un conjunto de sujetos sanos. Esto se ha hecho con le fin de introducir estos parámetros en el diagnóstico clínico. Para esto el primer paso es crear una línea base fundamentada estadísticamente. Posteriormente, la comparación entre esta base de sanos y alguna patología debe ser estudiada para poder presentar una herramienta médica ampliamente aceptada. Para una descripción más detallada de estos puntos y las posibles líneas de investigación futura véase el apéndice G.

Apéndice A

Clinical Background

A.1. Cardiac Diseases: An Important Cause of Death

In recent years, the treatment of cardiac diseases have become an extremely relevant issue. According to the World Health Organization (WHO), among the non communicable diseases, cardiovascular deficiencies were the leading cause of death responsible for 30 % of all defunctions around the world in 2005 (about 17,5 millions). These were followed by cancer and chronic respiratory diseases[1]. In figure A.1 this distribution is shown.

In Mexico, ischemic heart diseases represented the 5 % of the total number of deaths in 2002, just after diabetes mellitus which was the first cause[1]. It denoted 52 thousands of people for a single year. In table A.1 the main causes are listed. Moreover, according to the National Institute of Informatics Geographic and Statistics (INEGI) cardiovascular diseases were the first cause of death in people over 65 and the third cause in people from 30 to 64 years old from 1994 to 2004[2]. Therefore, the importance of creating reliable tools to asses cardiac diagnosis has become a priority.

There are several cardiac diseases which are related with myocardial dysfunctions such as ischemia, coronary artery diseases (CAD) and acute infraction among others[11]. These are consequences of an asynchronous ventricular motion along the cardiac muscle. Then, the reliable estimation of the heart motion is a powerful tool to detect abnormal patterns in order to emit an accurate diagnosis and design an efficient treatment.

A.2. Heart Structure and Function

The human heart can be considered as a muscular pump. While most of the hollow organs of the body have muscular layers, the heart is almost entirely muscle. It functions by contractions causing the muscle cells to shorten during the cardiac cycle. The muscle is composed of intercalated disks which are connections between two adjacent cardiac cells. These disks help the cells to contract rapidly as a unit. It is important for the heart to function properly since this muscle can also contract more powerfully when it is stretched slightly. Additionally, when the ventricles are

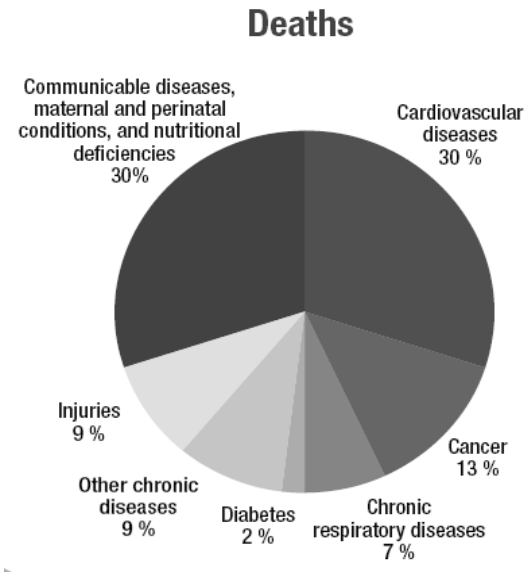

Figura A.1: Main causes of death for 2005 around the world. The total number of deaths was 58 million, where non communicable diseases were estimated to account for 35 million. 16 million of these occurred in people aged under 70[1].

Cuadro A.1: Major causes of death for all ages in Mexico during 2002. From the WorldOrganization of Health [1].

	Deaths in thousands	
Causes	Number	%
All Causes	469	100
Diabetes Mellitus	55	12
Ischaemic Heart Disease	26	6
Cerebrovascular Disease	26	6
Perinatal Conditions	26	6
Cirrhosis of the Liver	24	5
Chronic Obstructive Pulmonary Diseases	16	4
Lower Respiratory Infections	15	3
Congenital Anomalies	12	3
Road Traffic Accidents	12	3
Hypertensive Heart Disease	10	2

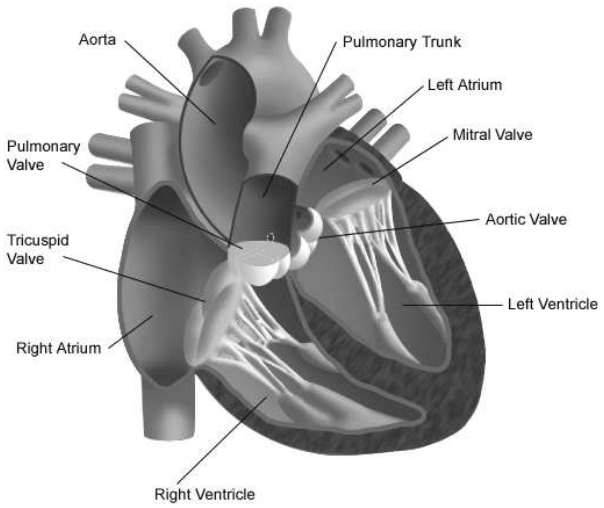

Figura A.2: Schematic heart anatomy[15].

filled, they are stretched beyond their normal resting capacity. Consequently, a more powerful contraction is achieved ensuring that the maximum amount of blood can be forced from the ventricles to the arteries during each beat[12, 13].

Anatomically, the heart is composed of four chambers, two atria and two ventricles. The atria are responsible for receiving blood from the veins leading to the heart. When they contract, the blood is pumped into the ventricles. Then, the heart receives deoxygenated blood from the upper body via the superior vena cava, and from the lower body via the inferior vena cava. These two veins join together to return the deoxygenated blood to the right atrium. The right atrium is separated from the right ventricle by an atrioventricular valve, also known as the tricuspid valve, which ensures that the blood only flows in one direction. Next, the blood from the right ventricle is sent into the lungs where it is oxygenated. Once the blood is purified, it returns to the left atrium through the left atrioventricular valve, also called as mitral valve or bicuspid valve, and then into the left ventricle. Finally, the blood from this is returned to the systemic circulation via the aorta, the largest artery of the body[14]. This process is called a cardiac cycle since it is repeated periodically. Respect to the left ventricle, the region after the mitral valve and the aortic valve is named as base or basal section. The opposite side of the base along the long axis of the ventricle is named as apex or apical section. Figure A.2 depicts the heart anatomy.

The pressures associated with the filling and emptying of the cardiac ventricles are referred to as diastole and systole. Diastole is the pressure measured in the arterial system when the ventricles are relaxed and filled with blood. Systole is the pressure associated with ventricular contraction, when the blood is being pushed into the systemic and pulmonary circulations. The heart can vary the speed of its

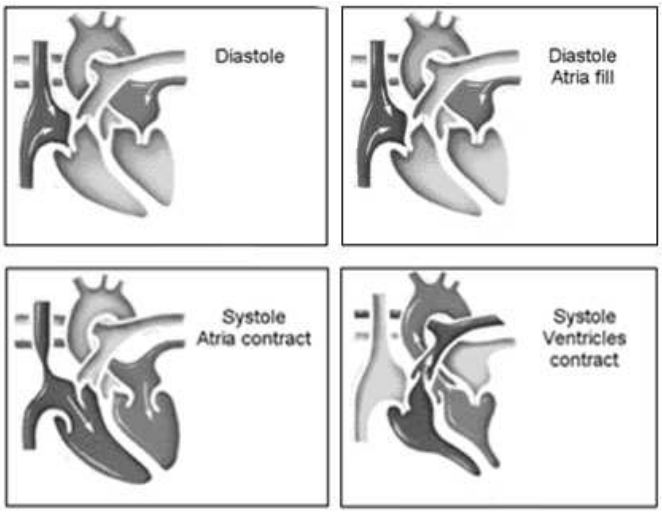

Figura A.3: From left to right and from top to bottom the cardiac cycle. In the top the diastole period is shown while in the bottom the systole is illustrated.

contractions based on feedback received from the body and the brain. When the body requires more oxygen, such as during exercise or when frightened, the heart increases its rate of contraction. When the heart is noticed that more oxygen is needed, it begins beating faster and increases the heart rate[14]. In figure A.3 the heart function is drawn.

A.3. Cardiac Measurement Tools

The left ventricular function has been demonstrated to be highly associated with ischemic diseases[11]. The myocardium is of especial interest for physicians since it constitutes the wall muscle of the left ventricle. Then, a detailed description of the complex myocardial function useful for diagnosis can not be observed easily. Common imaging tools, such as cardiac ultrasound and angiography are unable to extract more specific motion information than just the heart boundary deformation.

Within tomographic imaging techniques, Magnetic Resonance Imaging (MRI) suggests an alternative imaging modality to estimate cardiac motion since it can measure the global parameters of the cardiac motion. This technique is based on producing images of internal physical and chemical characteristics from an object with nuclear magnetic resonance signals. Using strong magnetic fields and radio waves, MRI collects and correlates deflections caused by atoms into images[16]. Thus, MRI offers relatively sharp pictures that allow physicians to see internal bodily structures with great detail. In order to appreciate the heart anatomy and motion, two general angle views have been established. A long axis view is said to be an image perspective where the left ventricle is observed along its longest axis. In contrast, a short axis view is said to be an image perspective where the left ventricle is appreciated radially. Here, its orientation is orthogonal to the longest axis of the ventricle. In addition, the short axis views are identified depending on

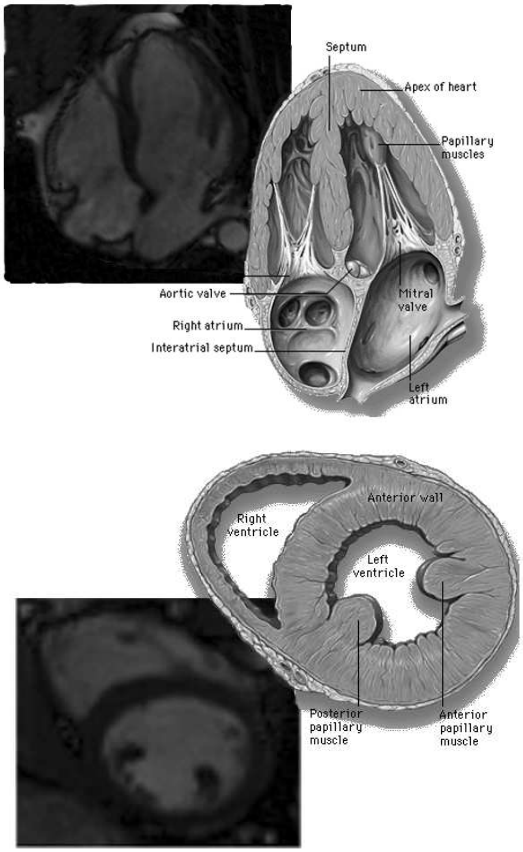

Figura A.4: Examples of MR images compared with the a schematic anatomical explanation. On the top a long axis of the left ventricle is shown. On the bottom a middle short axis of the left ventricle is illustrated. Schematic images obtained from [17].

the long axis region (i.e. basal, middle, or apical). Examples of two MR images and their schematic relations are illustrated in figure A.4.

However, MRI does not posses reliable landmarks to follow a specific type of tissue, therefore local measures within the tissue can not be achieved. This lack of landmarks undermines the estimation of local motion such as rotation and mechanical strain in the cardiac tissue. To create a reliable type of marking in these images, Tagged Magnetic Resonance was created. Here, some magnetic perturbations in the magnetized material (the heart wall) are created such that these can be visible. These patterns are generated by adding Radio Frequency (RF) signals to the magnetization of the material in order to produce a few saturated planes in the heart wall. Then the Tagged MR images are generated from 2 acquisition phases, one to produce a spatiality modulated phase pattern of magnetization in the heart wall, and other to acquire this pattern in one cardiac cycle. This process is called Spatial Modulation of Magnetization (SPAMM)[18, 3, 19]. The pattern

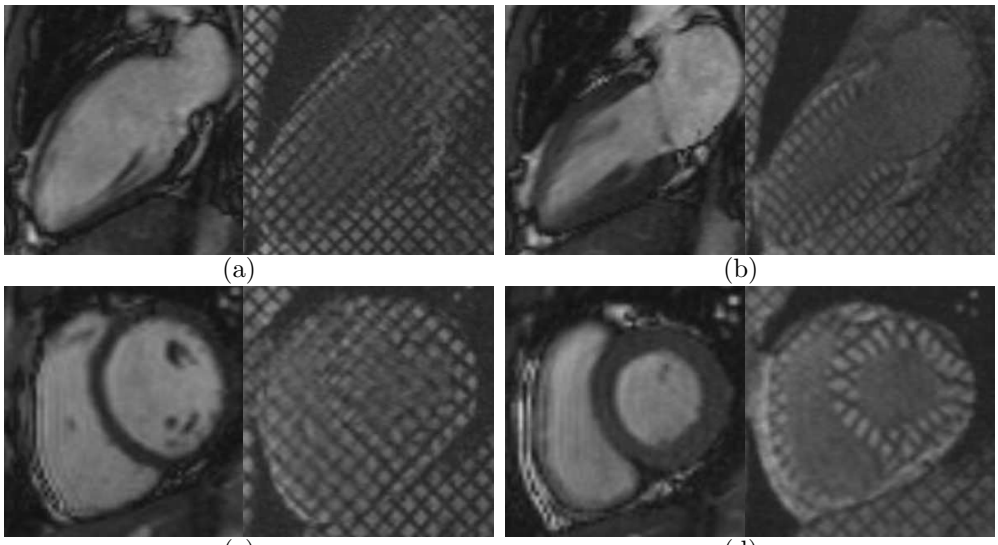

Figura A.5: MR images and their corresponding tagged version. (a) Long axis view at the beginning of the systole. (b) Same perspective at the end of the systole. (c) Basal short axis view at the starting of the systole. (d) Same view at the end of the systole.

created is synchronized with the electrocardiogram to initialize the tagging marks at the beginning of the systole when the contraction of the ventricle is the least. As the systole occurs, the myocardium contracts, and the tagging marks are deformed based on this contraction. Finally, when the diastole happens, these marks are restored to their original form. In figure A.5 a short axis and a long axis images are shown. Here, the MR images are compared with the tagged ones. It can be observed how it is not possible to estimate the motion within the myocardial tissue in the MR images. On the other hand, this motion is described with more detail by the tag deformations.

One weakness of these tagging marks is the tag fading due to the muscle relaxation. Here, the tags tend to blur along the time such that, at the end of the cardiac cycle these practically have disappeared. To minimize this fading effect the complementary SPAMM, or C-SPAMM, is applied. In this technique two tagged images with SPAMM patterns that are 180° out of phase with each other are subtracted. However, the main disadvantage of this improvement is the acquisition time. It typically takes around 18 seconds to performed the tagging and capture all the sequence for one cardiac cycle. As a result, the acquisition of one cycle several times is done. It suggests that some of the images could be misaligned because of the patient respiration and movement[3].

Apéndice B

Previous Work

Since the development of tagged Magnetic Resonance (MR) images [19, 18], many imaging techniques has been proposed to estimate cardiac dynamics and motion. Before this advance in radiology, it was not possible to compute cardiac motion reliably as the myocardium is a highly uniform tissue in conventional MR images (CINE images). Unfortunately, due to the time needed by most of the available approaches, tagged MRI has not become clinically viable. However, in recent years, many improvements have been done in the speed of the imaging sessions, analysis process, and the accuracy of the systems has been ameliorated significantly. Some examples of conventional CINE images and tagged MR images are shown in figure B.1.

The analysis of tagged MR images allows the measurement of global and regional cardiac functions due to the tagging improvement over the CINE images. According to Axel *et al.*[3], this analysis can be divided in five steps:

- Image Preparation
- Boundary Surface Extraction
- Tag Tracking
- 3D Motion Reconstruction
- Intersubject Comparison and Statistical Model Formation

Image preparation step consists basically in removing image artifacts and standardizing the gray level of the images. It is necessary when gray levels are used directly to performed tracking or to ease the boundary surface extraction step. In this step, the myocardium mass is segmented by delineating the epicardium and endocardium, and performing the extraction of the ventricular boundary. Some global function measures, such as ventricular mass, stroke volume, cardiac output, among others, can be extracted from tagged cardiac MR images through the obtention of boundary surfaces of the left ventricle. These measures are comparable to those from CINE images[20]. In addition, both type of images can be correlated making possible to perform a good segmentation in CINE MR images and apply it to tagged MR images. By doing it, we can take advantages of both sequences.

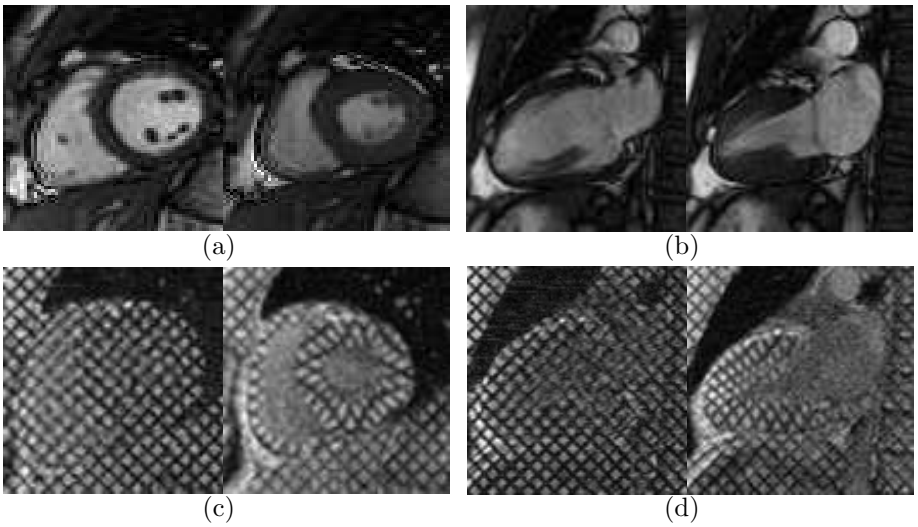

Figura B.1: Example CINE and tagged MR images. (a) CINE images of the left ventricle in a short axis (SA) view at the starting of the systole and at the end systole. (b) CINE images of the left ventricle in a long axis (LA) view at the starting of the systole and at the end systole. (c)-(d) The corresponding tagged MR images of (a) and (d) respectively.

The performed segmentation can be useful in the determination of some of the local functional measures, such as wall surface curvature and thickening[21]. It has been used to ease the tag line tracking and 3D motion reconstruction[22, 23]. By tracking the motion of the tag lines within images of the heart wall, deformation maps can be built [24, 25, 26, 7]. Some of the proposed approaches are based on the tags extraction and the propagation of the their deformation to obtain dense displacement fields[27]. Some others are based on a physic model of the tagging process to estimate a dense displacement map using optical flow techniques[7, 28, 29, 30].

Given a 2D dense deformation field obtained from a number of single short axis (SA) and long axis (LA) planes, and their orientation, a full 3D deformation field can be reconstructed, which more fully characterize the motion of the myocardium[22, 31, 32, 33, 34]. However, only a number of planes can be obtained yielding some gaps between planes. Thus an interpolation should be performed in a certain way and, due to the complex motion of the heart, it represents a challenging task. On the other hand, some researchers have suggested to fit a model to the available data and deform it based on the 2D motion measurements and a smoothness constraint[32, 35, 36, 37].

Intersubject comparisons, which consist in obtaining motion parameters invariant through subjects, should be computed to create a baseline to assist the cardiologists in diagnosis. Some comparisons have already been performed with statistical models of regional contractility[3] enabling the generation of clinical results. In fact, due to the lack of a reliable validation technique, this practice is usual in many approaches. The correlation among deformation parameters, between healthy people

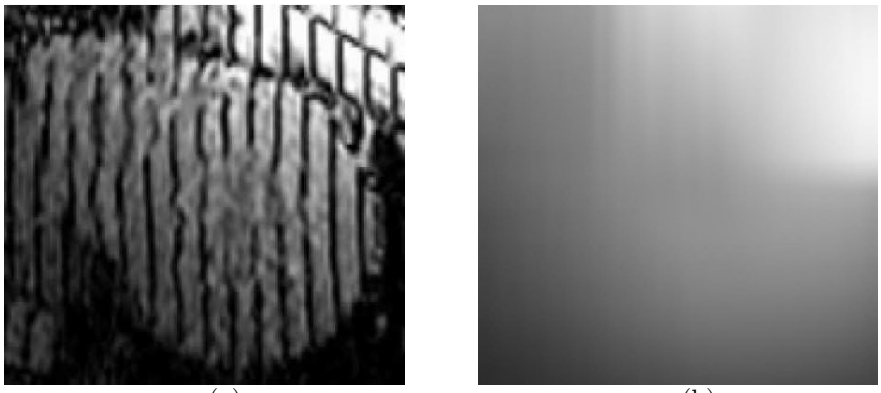

(a) (b)

Figura B.2: Example of background intensity variation problem in a cardiac tagged MR image. (a) MR image with a problem in the variation of the background intensity pixels. (b) Background intensity distribution. Images taken from [24].

and with some kind of pathology is explored in some medical articles[38]. However, because of a variety of discrepancies in the way of getting these parameters, and the processing time of many approaches which could be hours, the integration of the tagged MR imaging as a clinical practice has been delayed.

In this chapter, the steps in which the problem is divided are explored. Certain advantages and disadvantages of the tendencies to solve the problem are discussed. Additionally, representative results from these approaches are shown.

B.1. Image Preparation

Image preparation process typically includes three steps: suppression of background intensity variation due to non-uniform RF fields, suppression of thermal noise, and normalization of image intensities which vary from subject to subject[3]. In general, these problems are caused because the nature of MR imaging process itself provokes undesired artifacts[1]. Although some scientists have treated the problem of suppressing background intensity variation in MR images and thermal noise[39, 40, 41], this problem has received less attention. It is mainly because, due to the high variation of grey levels in MR images, the proposed approaches to find myocardial deformation are usually based on more reliable image features, such as frequency distribution. In any case, there are image artifacts that should be corrected. Figure B.2 shows an example of a tagged MR image with this problem.

The lack of an absolute scale for MR image intensities causes the variation of nominal intensity for a given tissue among different subjects. Although this problem has been treated in brain MR images[42], this variations are less critical in cardiac tagged MR images. Essentially, it is because the intersubject comparison are done based on motion estimates, and the boundary extraction techniques usually performed some kind of normalization. Nonetheless, Montillo *et al.*[41] have applied a

[1]For a detailed description of the physics and process of MR imaging and its artifacts including thermal noise, and non-uniformed RF fields, consult [16].

method of normalization previously applied on brain MR images.

Because of improvements in MR imaging techniques and MR scanners, this problem is becoming less important. Even though some variations in background intensities are present and thermal noise is susceptible to appear, most of the proposed approaches to estimate cardiac motion do not address this problem. The work showed in this thesis has been done using a Siemens Avanto magnetic resonance equipment of 1.5 Tesla. In particular, the supplied images do not show this problem. Therefore, it has been preferred to avoid this preprocessing.

B.2. Boundary Surface Extraction

Boundary surface extraction consists in the delineation of the epicardium and endocardium in MR images in order to segment the myocardial muscle. If a 3D analysis is desired, this extraction should be done in the space to generate a surface capable of isolate the left ventricle.

The extraction of the endocardial and epicardial surfaces of the heart from tagged MR images is challenging for several reasons. The tag lines and the distribution of the pixels values around the myocardium are some of the difficulties. Image artifacts and noise should be suppressed. It is recommended to remove the tag lines, but there is evidence that given a boundary surface extraction obtained from CINE MR images, it can be reflected in tagged MR images.

In any case, the features outlining the boundaries must be identified in order to extract them. Additionally, the image data generally sample the volume of the heart with some gaps and non-uniformed spacing between images planes, and due to the complex geometry of the heart this task is particularly difficult.

Many times, it is more relevant for the physicians to estimate the motion of the heart instead of achieving an efficient boundary extraction. Thus, many researchers have resorted to do this task manually and focussed on the development of methods in other aspects of the analysis[22, 23, 35]. Nevertheless, some approaches have been proposed to solve the problem by semi-automatic methods in which a user-guide active geometry was employed to locate the boundaries of the myocardium[43, 44].

In the same line, García *et al.*[4] have proposed a method to delineate the epicardium and endocardium of the left ventricle in short-axis tagged MR images. Here, after placing a set of points at the beginning of the sequence, the myocardium contours are completed and deformed according to the estimated motion. It is achieved using Active Shape Models (ASM) technique, which allows us to deform a given model based on a set of shapes previously learned, letting a smooth active shape capable of correct errors during the deformation[45]. Thus, a set of possible shapes of the myocardium, segmented by cardiologist, are chosen. Then a group of landmarks are specified establishing a point distribution model, and the covariance matrix of this distribution is built. Having this matrix, the eigenvalues and eigenvectors are computed, and a range of different myocardial shapes are obtained. Thereafter, a Principal Component Analysis (PCA) is implemented. Figure B.3 shows an application of the method.

The idea of ASM has already been applied to 3D models in CINE MR images[46]. As it was mentioned before, it is possible to establish a point-to-point correspondence between a given tagged MR image and CINE MR image acquired at the same

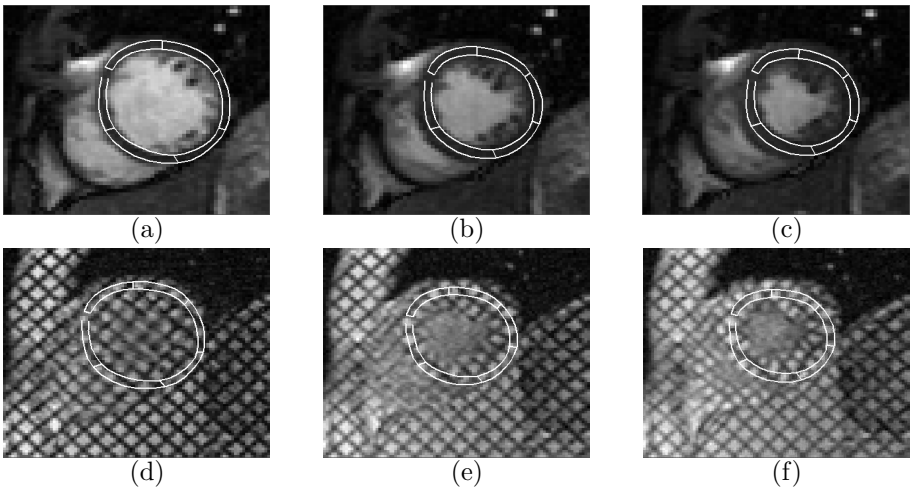

Figura B.3: Segmentation proposed by García *et al.*[4]. A segmentation is initialized by placing twelve points and automatically generating the initial shape in the CINE image. Later the proposed shape is deformed according to the calculated motion from the tagged MR sequence and adapted to a valid deformed shape using ASM. (a) First initialization in the CINE sequence. (b) A mid-systole CINE image after deforming the shape. (c) An end-systole CINE image with the performed shape. (d)-(f) Corresponding tagged MR images of (a)-(c).

orientation. So, even though some methods based on tagged MR images have been developed[37, 47, 48], the segmenting problem has been more studied in CINE MR images[46, 49, 50], due to the interest of estimating global measures such as wall thickening and volume variation. Basically, it is proposed to start from a set of manually segmented images, and then create a volume from them. So, an automatic generation of landmarks is achieved from a triangulation process using the marching cubes method[51].

Even when relevant approaches have been done to solve this problem in CINE MR images, it is still an active research area. A reliable method to pick consistent landmarks among subjects is still a challenging problem, and a fully automated method has not arrived yet. Additionally, more research needs to be done to succesfully mix CINE and tagged MR images.

B.3. Tag Tracking

Probably the most studied issue of the entire problem, tag tracking is actually the essence to estimate the cardiac motion. During acquisition of MR images, tagging planes are created in the heart in an orthogonal direction to the image plane. These tag planes are manifested as dark bands through the myocardium. To reconstruct the myocardial motion, the intensity heterogeneity representing the tagged planes must be tracked through the cardiac cycle. Because the tracking is constrained to the image plane, only limited components of the 3D myocardial motion can be recovered from a given set of 2D image data.

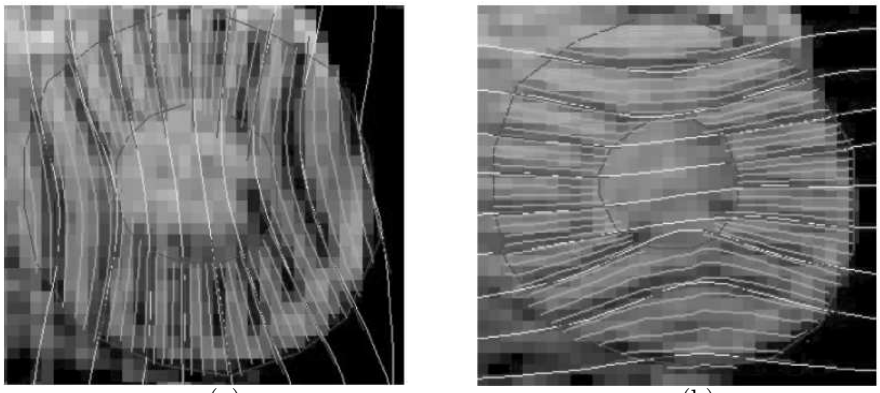

(a) (b)

Figura B.4: Cardiac deformation estimated using a mesh of B-Splines. Here deformation between tags is calculated by interpolating the motion from a mesh of B-Splines. (a) Interpolated deformation from the vertical tags. (b) Interpolated deformation from the horizontal tags. Results taken from [27].

The proposed methods to extract motion from tagged images are based on using different aspects of the myocardial intensity heterogeneity, including: tracking the dark tag bands as intensity minima, employing optical flow, or using harmonic phase (HARP) methods. The last two methods do not explicitly track the tags, instead a complete tracking of each pixel is performed.

The first method involves the development of a model of the time-varying intensity profile of a tag line. Although some methods typically begin by having a manual location of the tags, these can be segmented using approaches such as morphological operations to identify dark bands in the image[25], matched filters[35, 37], or a Gabor filter bank[24, 52]. While the latter two techniques tend to be relatively robust with respect to tag fading, a limitation of all tag line tracking methods is that temporal correspondences are available only for pixels along the tag lines and not for the pixels between them. Some methods have been developed to improve this limitation by creating a mesh based on B-Splines and estimating the deformation of them[32, 53]. Based on this deformation, an interpolation step has been proposed to estimate a dense displacement field[27]. It is shown in figure B.4. However, this is susceptible to propagate errors and to introduce artifacts due to the interpolation. A somewhat related tag tracking approach is the use of nonrigid registration to match corresponding tagged regions[34]. Here a interpolation is achieved based on registration.

Optical flow-based techniques try to overcome the limitation of relatively sparse tag data and provide a spatially dense estimate of the 2D apparent motion field. The basis for this technique is a brightness constraint equation[54]. Thus, this method involves estimating the spatial gradient of the intensity image, using finite differences of the intensities at neighboring pixels, and the temporal intensity derivative. It is estimated by subtracting the intensity at a pixel from one time-frame to the next in CINE acquisition.

Even though some methods assume the time derivative of the brightness to be

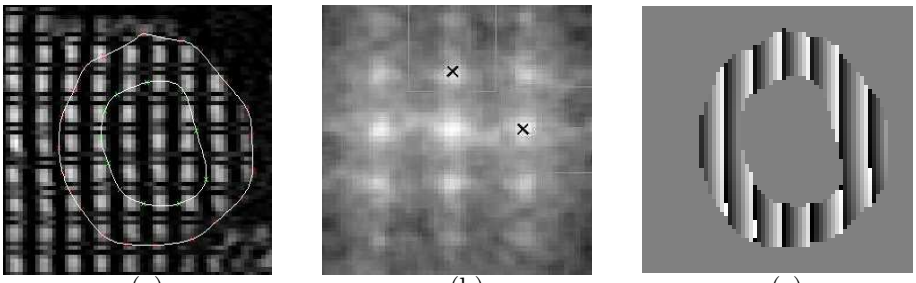

(a) (b) (c)

Figura B.5: Example of the application of HARP to obtain the Angle Images. (a) A tagged MR image at end diastole. (b) Fourier transformed in decibels of the image. (c) Obtained Angle Image by isolating the first horizontal harmonic peak, extracting the inverse fourier transformed, and computing the phase value of the complex response (black pixels represent phase values of $-\pi$ and white pixels represent $+\pi$). For clarity, the myocardium has been delineated.

zero[55], *i.e.* a given pixel preserves its brightness value through the entire sequence, the intensity of the myocardial pixels may actually experience significant changes due to tag fading, through plane motion, and noise artifacts. Several strategies have been proposed to either preprocess the images to suppress the effects of the tag fading[56] or to model the tag fading portion of the variation based on the MR imaging physics[54].

In Spatial Modulation of Magnetization (SPAMM) tagging pulse sequences, tags are generated with a sinusoidal cross-sectional intensity profile. Hence, at any point on or between tags, the tissue has both a magnetization intensity and a spatial phase of the periodic tag magnetization pattern that are dependent on position[3]. In addition, it has been shown that a given tagged MR image can be written as a sum of multiple complex images obtained from the isolation of a number of harmonic peaks and filtered them[29].

Harmonic Phase (HARP) takes advantage of these features of the tagged MR images. So, it is possible to track the phase of the tissue tagging pattern in *Angle Images*, which are a representation of this phase for each pixel[7, 28]. Thus, angle images are derived from the phase of the complex image that is computed from the inverse Fourier transform of one of the harmonic peaks, usually the first one which corresponds to the frequency of the sinusoidal tags. Figure B.5 illustrates how the harmonics are present in the spectrum of the image.

In HARP processing, one spectral peak is extracted from the raw Fourier data of the tagged MR image, and the assigned phase value is assumed to be an intrinsic property of the tissue. For instance, this method can be viewed as an effective optical flow in the spectral domain. However, it may not be reliable near the edges of the heart wall due to partial volume effects, such as the through-plane effect as it is shown in figure B.6. In addition, there are some limitations due to the essence of the method. Although the discontinuities from $-\pi$ to π can be handled by an interpolation step in the complex image instead of in the phase image, the numerical stability is not guaranteed completely due to this wrapping. Notice that the aliasing of the phase for shifts greater than 2π can lead to ambiguity equivalent during the

tracking. Additionally, the global nature of this approach has demonstrated to be insufficient in high local deformations of the myocardium[24, 52].

Despite of the weakness of HARP, this is actually one of the most popular methods to estimate myocardial motion from tagged MR images. Its capability to estimate dense displacement maps in 2D short axis and long axis views of the left ventricle has contributed significantly to find parameters of medical importance such as ventricular torsion and rotation indices[57], which can be correlated among healthy people and with some kind of hear disease.

B.4. 3D Motion Reconstruction

Once a method to estimate 2D deformation has been implemented and there are 2D displacement fields, a reconstruction of the 3D information can be compiled. While the extension from plane motion to space motion seems natural due to the availability of orthogonal views, this issue is still an open research area.

When the motion is obtained based on one tagging direction, only one component of the real deformation can be derived. One example is shown in figure B.2(a). When 2D tagging are performed by the MR equipment during the scanning session, two components of the motion can be obtained. Figure B.5(a) shows an example of 2D tagging. Note that the estimated motion here is apparent since it represents a projection of the real one. In addition, the effect of through-plane emerges through the time. This effect occurs when the myocardium becomes thicker due to the contraction of the left ventricle through the orthogonal axis of the image. Figure B.6 depicts this effect.

It is possible to stack tag lines from adjacent images to form a tag sheet by inferring the correspondences[22, 58]. So, at tag sheet intersections, all three components of the motion can be measured. When optical flow methods are used (spatial or spectral), two components of the motion can be estimated at every pixel. However, it is not possible to measure three components of motion for any given point from 2D tagging methods. There have been proposed methods such as slice following[59] or SENC method[60], which may help to eliminate this limitation.

A variety of approaches have been suggested to compile 2D information into a dense, smoothly varying, 3D motion field[32, 35, 36, 37]. In general, these methods involve fitting a model, using an optimization function which balances fidelity of the final 3D motion field to the 2D motion measurements and a smoothness constraint. This constraint either interpolates missing information, such as motion between the sparse tag sheet intersections, or suppresses errors in harmonic phase motions fields. An example of a typical model is shown in figure B.7 done by Radeva *et al.*[32].

Several researches have modelled the motion of the left ventricle with a reduced number of parameters in the hopes of obtaining a more revealing description of normal and pathological motion, which is a typical validation technique. Declerk *et al.*[61] have employed a 3D B-spline tensor product to reconstruct the deformation field. The motion is modelled as a 4D continuous displacement function in time and space. More general splines have also been proposed including both 3D splines[32, 35, 37], and 4D spline models[62] that treat time as the fourth dimension. These models often have difficulties capturing the motion of the apex. To compensate this limitation, both prolate spheroidal coordinates[3, 35] and 4D planispheric

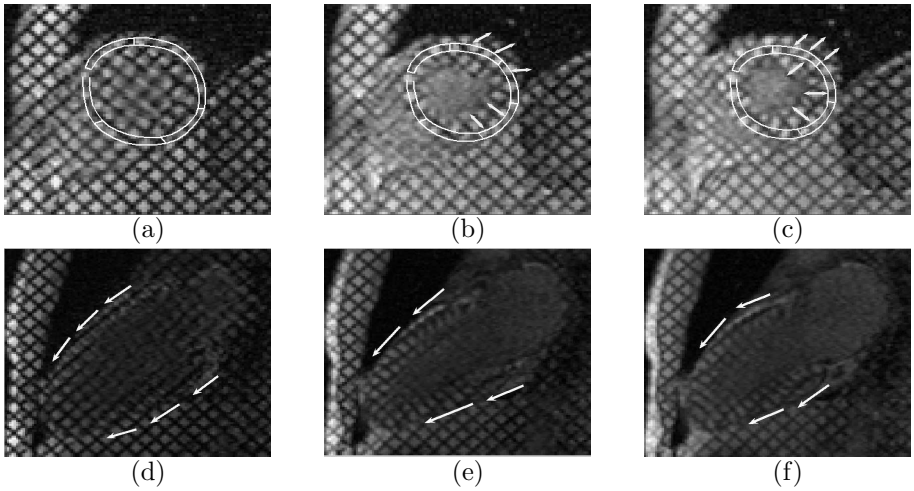

Figura B.6: Through-plane motion effect. This effect is produced when the myocardium becomes thicker than it is at the beginning in short axis views. It is because the contraction observed in long axis views, from base to apex, provokes an apparent increment in the myocardium mass. (a) Initial segmentation in short axis. (b) Mid-systole short axis view. (c) End systole short axis view. (d) Long axis view at the starting systole. (e) Mid-systole long axis view. (f) End systole long axis view.

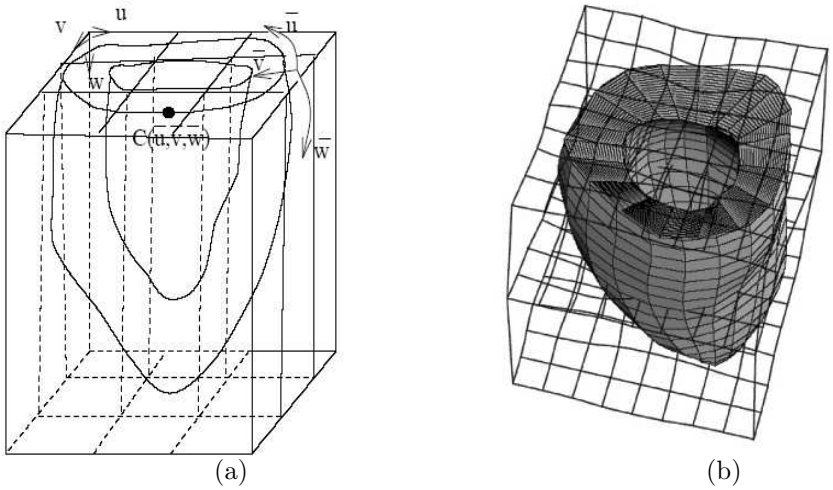

Figura B.7: Model used by Radeva *et al.* in [32] to estimate the deformation of the left ventricle. (a) Coordinate system of the B-Solid (u, v, w) and the left ventricle model $(\bar{u}, \bar{v}, \bar{v})$. (b) Left ventricle model located in the B-Solid.

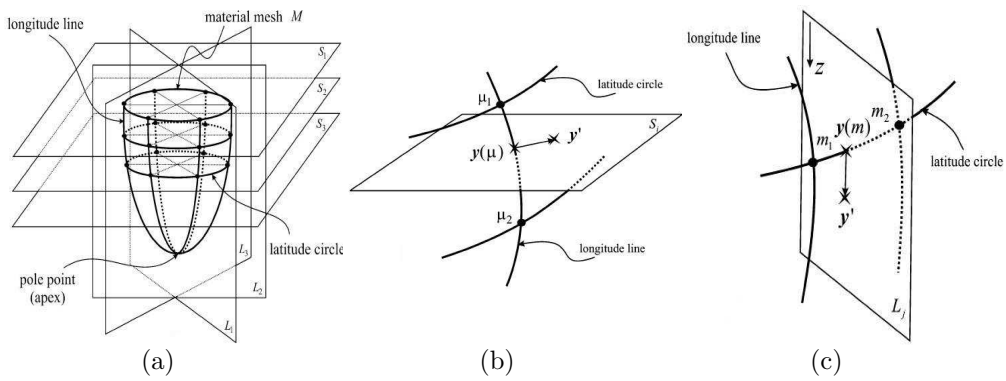

Figura B.8: (a) Material mesh used to estimate the motion of the left ventricle. S_i is a short axis image plane and L_j is a long axis image plane. M is the material mesh. (b) Diagram of the intersection of the material mesh and image planes, as well as a description of the in-plane motion of intersection points in SA. (c) The same for LA views. A detailed description is presented in [33].

coordinates[61] have been used to increase the numerical stability over spherical coordinates when reconstructing the motion at the apex of the left ventricle.

In any case, the introduction of a model adds, in a certain way, a bias to a specific model of deformation which depends on the flexibility of it. As it is mentioned above, HARP takes advantage of phase invariance produced by taking the tagged MR images as modulated images in 2D. This idea has already been carried to 3D analysis by Pan *et al.*[33]. Here a simple mesh is imposed to the set of image views of the left ventricle, short axis and long axis. From these views, under the idea of phase constancy, a 3D vector of phases is initialized for each of the mesh points, so a tracking is performed for each of the three dimensions. In order to deal with the sparsity of the available data, a interpolation method is computed to estimate the motion of a mesh mark out of the image views. Figure B.8 shows the general mesh used and how it is deformed to estimate the motion.

A typical imaging session is composed of a number of imaging captures. Here, the required views are acquired during different breath holds. A necessary assumption to reconstruct 3D motion is to consider all the views as *instantaneously acquired*, since currently it is not possible to generate a set of tagged MR image sequences at the same time. So, a potential patient movement and a displacement of the left ventricle due to respiration can lead to misalignment errors. Some methods have been proposed to solve the problem in conventional CINE MR images[63]. Thus, due to the source of this data, it is susceptible to occur in tagging sequences too. Figure B.9 shows some examples of misalignment.

B.5. Intersubject Comparison and Statistical Model Formation

Intersubject comparison is probably the most useful benefit for cardiologists. Regardless of how well motion is computed, a given scheme is practically useless if

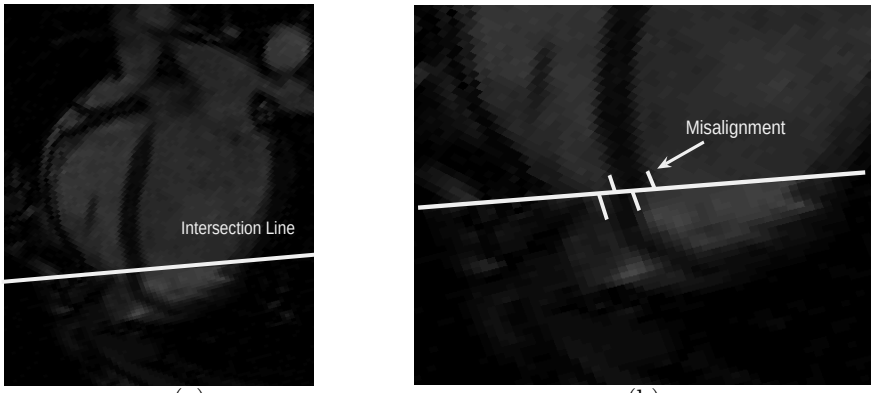

(a) (b)

Figura B.9: Example of misalignment between a given short axis and long axis views. The intersection of both planes is shown. Here some misalignments are present in the correspondences of the wall of the left ventricle.

a comparison among subjects is not possible. Although some methods use synthetic images to validate their results, a typical validation technique used in many approaches is to establish a division between healthy people and those with some kind of pathology. Thus, an intersubject comparison is intrinsically established. However, only the motion parameters can be compared and not the deformation model fittings.

Generally, the imaging protocol is not fulfilled completely and it is difficult to obtain the same views for every patient. Even when these views could be localized for each patient, the left ventricle size is not always the same yielding a scaling issue. Thus, to establish a number of landmarks invariant through patients is not an easy task.

Few methods have been suggested to solve the problem in conventional CINE MR images. The use of 3D ASM have been proposed to generate an automated 3D segmentation invariant through subjects[46, 49]. Firstly, an ideal model is adapted to fit the image data of a given patient. Secondly, the landmarks are created automatically in the deformed model. Finally, these are used as an entrance to the ASM atlas[46]. Thus, the landmarks are created with some certainty of being the same through subjects, and it is possible to reconstruct the left ventricle in 3D from sparse and arbitrarily oriented MR image views[49]. In figure B.10 some of these results are shown.

In spite of the advancements done in automated 3D landmarks generation through subjects, it has not been applied to tagged MR images yet. The correspondence between conventional CINE MR images and tagged MR images is still being studied. Nonetheless, the generation of comparable motion data among subjects is under development. The creation of a standard set of parameters and shapes for healthy people is the first step in the introduction of tagged MR imaging to clinical diagnosis. Later, comparisons of parameter and shape data are generally studied among a variety of pathologies, yielding a strong tool for diagnosis.

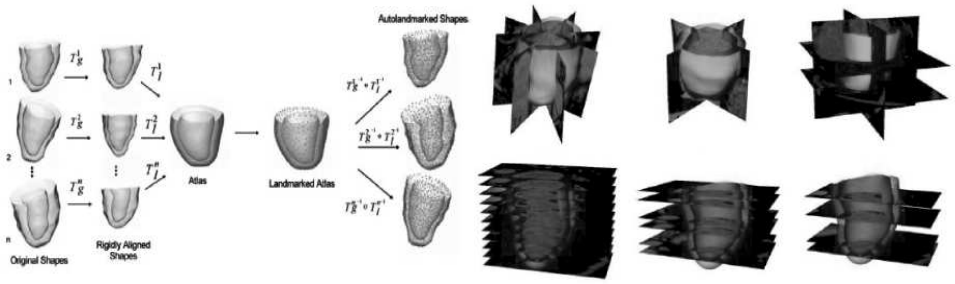

(a) (b)

Figura B.10: Automatic 3D segmentation invariant through subjects. (a) Adaptation of and ideal model and the automatic generation of landmarks. (b) Proposed segmentation after the use of 3D ASM. Results taken from [49].

Apéndice C

Clinical Framework

In this approach, the estimation of the left ventricular motion is treated. Although some researchers have analyzed the motion of the right ventricle[23], it is more useful for cardiologists to study the left ventricle. It plays an extremely important role since it distributes the blood for the entire body while the right ventricle pumps the blood to the lungs. In addition, several studies suggest that some of the heart diseases are related with the left ventricle performance[38], and there are some physicians interested in analyzing the left ventricular rotation and torsion[57]. As a result, the approach proposed in this thesis is focussed on the estimation of the rotation and torsion, and on the modelling of the left ventricular motion as a volume to study their behavior. Here, only the systole of the cardiac cycle is analyzed, because the tagging sequence is synchronized with the electrocardiogram so as to start the tagged MRI sequence at the beginning of the systole, and because of the tag fading through the time, only during this period of the cycle reliable tagging marks can be preserved.

In spite of the improvements done to tagged MR images by the image preparation step, in this approach it has been preferred to skip it since the gray scale images are no used for tag tracking. Even when some variations in background intensities are present and thermal noise is susceptible to appear, in this approach a frequency analysis is used to generate the features to track. In particular, the supplied images do not show the problem of the background intensity variations. These have acquired using a Siemens Avanto magnetic resonance equipment of 1,5 Tesla.

C.1. Surface Extraction

In order to produce reliable measures, a segmentation of the short axis (SA) views has been implemented. Here, the method proposed by García *et al.*[4] is used. In this approach, the left ventricle is initialized by manually placing a set of landmarks and dividing the left ventricle in six regions (anterior, anteroseptal, inferoseptal, inferior, inferolateral, anterolateral), according to the *American Heart Association*[5]. These regions are shown in figure C.1. Having this segmentation, the myocardium shape is deformed according to a dense displacement map calculated from the tag tracking step, generating a new shape. However, adapting the contours based only on this information usually drives the segmentation to implausible

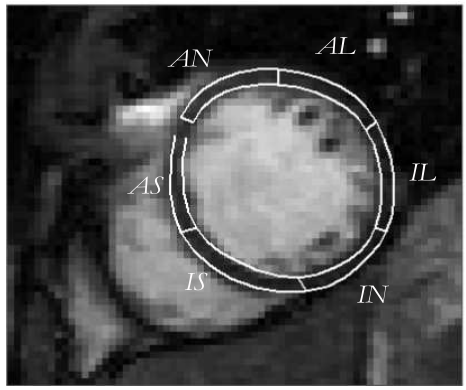

Figura C.1: Left ventricular segmentation for SA views proposed by the American Heart Association (AHA). *AN* - Anterior. *AL* - Anterolateral. *IL* - Inferolateral. *IN* - Inferior. *IS* - Inferoseptal. *AS* - Anteroseptal.

shapes. It is mainly because of image artifacts and errors in the tracking. Thus, to solve this problem the Active Shape Models (ASM)[45] are used.

In ASM a shape can be thought as a set of landmarks. The configuration of these points are invariant under a certain transformation, such as translation, rotation, and scaling. Good points for landmarks should be consistently located from one image to another. These ones could be T junctions, projections, points of high curvature, biological landmarks, among others. This representation allows a compact description of a shape. There are some points between landmarks which are called pseudo-landmarks. These are necessary to complete the shape, but these are not essential in the model definition. Formally, let $\mathbf{x}_i$ be a vector describing the n points corresponding to each landmark of the ith shape, this shape is defined as the following set:

$$\mathbf{x}_i = (x_{i0}, y_{i0}, x_{i1}, y_{i1}, \ldots, x_{ik}, y_{ik}, \ldots, x_{in-1}, y_{in-1})^T.$$

In the case of segmenting the left ventricle, the dividing points between regions are used. Since there are six regions, as it is shown in figure C.1, 12 points are used to represent the ventricular shape in SA views, 6 for the epicardium divisions and 6 for their projections onto the endocardium. The rest of the shape is modelled by deformable models, such as splines and snakes[6].

Once the landmarks have been defined, landmarking process is performed to create a statistical model. Although their placement seems feasible to be done automatically, it usually implies manual localization. Thus, a training set of the left ventricle is created manually to establish a statistical model. Here a Principal Component Analysis is performed to reduce the dimensionality of $\mathbf{x}_i$, and to have a range of plausible shapes. Therefore, a correction to the shape deformed can be done based on a set of valid ones. A detailed description of the method used and the application of ASM in medical image analysis, is presented in [6].

C.2. Tag Tracking

Once a segmentation of the left ventricle is performed in SA views, it is necessary to establish a method to estimate its motion. One of the improvements done in cardiac MR images is the development of tagged MR imaging[19, 64]. It is a variant of the conventional CINE imaging which generates a tag pattern within the tissue. This pattern is represented by a grid of dark bands which deform according to the heart during the cardiac cycle. Hence, in order to estimate an accurate description of the ventricular motion, a technique to calculate the tracking of this tags has to be performed so as to find their deformation.

A wide range of techniques and approaches to estimate the tag tracking have been developed. One of the most popular methods is *Harmonic Phase* (HARP)[7]. It is based on the extraction of the first harmonic peak of the fourier transform of the tagged MR images. Then, the inverse fourier transform of this peak, a complex image, is obtained. There is a direct correlation between the phase discontinuities and the tagging marks. In addition, this value has the important property of being invariant through the sequence despite of the tag fading. Thus, it is used for tracking instead of the direct gray value, because of its stability and the opportunity to track not only the tagging marks, but also each of the pixels between tags. In this thesis, the idea of HARP is used to estimate the myocardial motion on the image planes.

Due to the nature of the fourier transform, in practical cases the use of HARP provokes several mistakes, especially when there are high local deformations in the myocardium. For example, there exist cases where three tagging marks are too close that they are reported to be only two but widely separated. These type of mistakes are extremely important at the time of performing the tracking, because they could affect the overall deformation of an entire region. Consequently, an alternative scheme is suggested in this thesis to improve these mistakes.

A method to generate the phase maps is proposed to improve the tag tracking. Here, the phase maps are created too, but the method to obtain them is different. The Gabor filters, a special case of wavelets, are employed in this approach. These filters have the advantage of achieving optimal resolution in both, the spatial and the frequency domains. Thus, when there are regions of high local deformation in the myocardium, the Gabor filtering is a suitable technique to solve the problem.

Having the phase maps, the tracking of each value is solved by an iterative method[7]. The phase invariant property is assumed through the sequence to computed the displacement maps. It allows the estimation of the optical flow for each pixel, but using the phase value as the feature to track.

C.3. 3D Motion Reconstruction

Once the displacement information has been estimated for each of the SA planes, a 3D motion reconstruction can be estimated by calculating the displacement information in the long axis (LA) views and correlating them with the SA ones.

In order to calculate the displacement information from the LA views, the method applied for the SA planes is applied too. However, there has not been implemented a segmentation step. It is because it is possible to project each of the performed segmentation on the LA views. Thus, to estimate the ventricular deformation on

this view a simple region of interest containing the left ventricle is chosen, then the phase maps are found, and the displacement fields are calculated.

During an imaging session, it is possible to obtain spatial information of each of the planes. A translation of the initial corner of the image, two orientation vectors, and a scale factor to convert pixels into millimeters are stored automatically with each image as part of the Digital Imaging and Communications in Medicine (DICOM) standard information. Having this information, it is possible to place each view in a common space and find correspondences among views.

When the displacement information is calculated for single views, two apparent motion components are found from two orthogonal tagging marks. The real motion of left ventricle corresponds to a more complex three dimensional deformation, which can be calculated by relating the two dimensional displacement maps of each image and building a more realistic deformation field. Hence, the displacement information calculated for the image views is assumed to be a projection of the real one. Thus, the intersection between a SA view and a LA one is calculated, then the displacement information of both views are combined to build the three dimensional deformation for these points. Finally, this information is disseminated through the segmented myocardium to complete the estimated motion.

To correct possible misalignments among the 2D views, a framework based on the intersection lines have been developed. It is based on the use of the Normalized Mutual Information (NMI) in registration problems[9]. Here, the problem turns to be an optimization issue where a particular version of the steepest descendent method developed in [10] has been implemented.

C.4. Intersubject Comparison

In order to create a useful diagnostic tool for cardiologist, it is necessary to establish a baseline to distinguish between healthy patients and those with some kind of pathology. It suggests, as a first step, to generate this baseline supported by a huge set of healthy people parameters. Thus, the constancy of the obtained results and the statistics of them need to be stable.

In this thesis, the rotation and torsion parameters in SA views are studied. The rotation is ordered by their relative position according to the long axis of the left ventricle, *i.e.* base, middle, apex. The torsion represents a global measurement of the left ventricle where the difference between the basal and apical rotation is computed. Here, the image data used were obtained from healthy volunteers. The current database consists of 8 real cases. The rotation results have generated a well defined tendency during the systole. The diastole has not been analyzed because of the fading effect, which could cause a false deviation within the experiment, since it is not guaranteed the generation of reliable deformation information.

Apéndice D

Improved Deformation in Cardiac Tagged MR Images

One of the tasks in the analysis of tagged MR images is the tag tracking. There exist many approaches to solve the problem, which can roughly be divided into three groups according to what they use to extract the motion. One of the most popular methods to achieve this task is the harmonic phase (HARP) method developed by Osman *et al.*[7]. They introduce the concept of Angle Image. It is basically a representation of a tagged MR image which recovers the relative position of the tissue respect to the distorted tags. Thus, cardiac deformation can be estimated. In this chapter, a novel approach to generate Angle Images using a bank of Gabor filters in short axis cardiac Tagged MR images is described. The proposed method improves the Angle Images globally obtained by HARP, with a local frequency analysis. It is proposed to use the phase response of a combination of a Gabor filter bank, and take advantage of it to find a more precise deformation field of the left ventricle. The accuracy of the method over HARP is demonstrated by several experimental results.

D.1. Introduction

Cardiovascular diseases have arisen as one of the main causes of mortality in recent years. A complete knowledge of the heart function, and how pathologies affect local and global myocardial contractility, would lead to a more accurate diagnosis. As the myocardium is a highly uniform tissue, when it is depicted in conventional CINE MR images, only the displacement of myocardial wall boundaries is appreciated. Tagged MRI (figure D.1) is a variant of this technique which generates a tag pattern within the tissue. It is represented by a grid of dark bands, which deform according to the heart during the cardiac cycle. This pattern is called SPAMM (Spatial Modularization of Magnetization)[18, 64].

Since the appearance of Tagged MRI [19, 64], several computational techniques have been developed in order to extract motion information from these images. Some of them treat tags as sparse features that have to be tracked, while others directly retrieve dense displacement maps. Regardless of the method, all of them

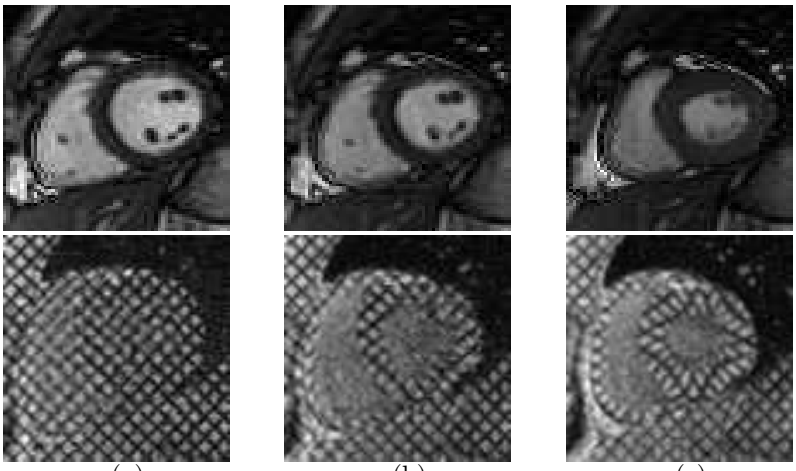

(a) (b) (c)

Figura D.1: Examples of cardiac CINE MR images and tagged MR images. The first row contains the CINE MR images, while the second shows the corresponding tagged MR images. (a) Left ventricle at the starting of the systole. (b) Left ventricle images during the systole. (c) Left ventricle at the end of the systole.

share the same aim, which is to obtain automatically (or semiautomatically) these maps that cover the whole myocardium.

Harmonic Phase (HARP) is one of these methods which is based on the extraction of the first harmonic peak from the Fourier spectrum of the image. Then the phase image is generated from the extraction of this peak, which is called *Angle Image* [7]. Thus, the tracking process consists of tracing image pixels with the same phase parameter. Although this approach gives a good global estimation of heart motion, it treats the image by an approximation of one frequency of the tags to all the image. In practice, the myocardium deforms through the time, and the frequency of the tags changes locally. This processing can overestimate locally the heart deformation. In addition, it is not an easy task to design a bandpass filter that can achieve good resolution in spatial and frequency domains. When the first harmonic peak is not well concentrated, HARP increases the its bandwidth. Therefore, if the tagging lines deform a lot locally, the method is susceptible to increase the error.

On the other hand, Z. Qian *et. al.* [65] have proposed a variant to localize the tags by using Gabor filters based on the limitations of HARP [24]. They proved that Gabor filters are more reliable to recover the tags than HARP when there is a high level of deformation locally. However, they use this approach only to localize the tags which implies a lack of dense displacement maps as it can be done with Angle Images used by HARP.

This chapter is focus on the Angle Images due to the fact that these images are strongly related to the movement of the myocardium in tagged MR images. This concept is explained in section D.2. A new method based on the use of Gabor filters to obtain them from a local analysis is presented, which is strongly inspired in HARP. It can be said that the proposed technique behaves as local HARP. In section

D.3, the Gabor filter fundamentals are described. In section D.4, the application of this filtering tool to tagged MRI to obtain Angle Images is stated while in section D.5 the tracking method is presented. Finally, in section G.1, some experimental results are shown.

D.2. Principle of Angle Images

According to Osman and Prince in [28], a Tagged MR image can be expressed as sum of multiple images:

$$\psi = \sum_{k=-K}^{K} \psi_k,$$

where ψ_k is a complex image whose phase is called Angle Image, and it is linearly related to the true motion of each point in the myocardium [4, 29]. By this fact, the phase of points becomes an intrinsic property of the tissue that remains constant during the cardiac cycle. Therefore, tracking tissue points is equivalent to track their phases.

Angle images are very similar to tagged MR images, except that they seem to have tags that are sinusoidal patterns. There are two of these patterns, a cosine pattern and a sine pattern, which correspond to the real and imaginary parts of the complex response after filtering one of the harmonic peaks ψ_k from the tagged MR image power spectrum. When the heart moves, the described pattern of each angle image changes. For example, contraction of the heart tissue provokes the crests of the sinusoidal pattern to get closer, while elongation causes the crests to separate each other.

Consider the 1D tag pattern shown in figure D.2. The initial pattern changes by a deformation and fading. It can be observed that the phase response changes as well, but in a more limited way. In fact, the phase of a given point does not change due to motion [29]. Because of this property, it is possible to track one point in the image, generate a dense displacement field, and calculate different motion parameters, like rotation, deformation, among others.

D.3. Definitions

The Gabor filter was introduced by Daugman firstly in [66]. It is an special case of wavelets [67], and is essentially a Gaussian g modulated by a complex sinusoid s. In 2D, a Gabor filter has the following form in the spatial domain:

$$h(x, y) = g(x', y') \cdot s(x, y),$$

where $g(x', y')$ and $s(x, y)$ are defined as:

$$g(x', y') = \frac{1}{2\pi\sigma_{x'}\sigma_{y'}} \exp\{-\tfrac{1}{2}[(\tfrac{x'}{\sigma_{x'}})^2 + (\tfrac{y'}{\sigma_{y'}})^2]\},$$

$$s(x, y) = \exp[-i2\pi(Ux + Vy)].$$

The rotation of the Gaussian is established by:

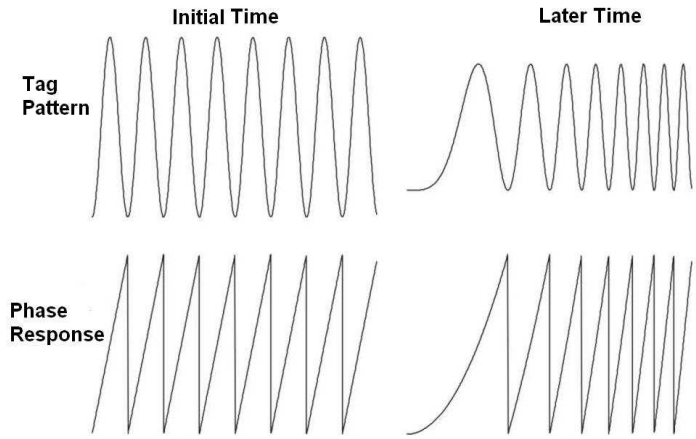

Figura D.2: Principle of Angle Images. A sinusoidal tag pattern and its phase response at the initial time, and a short time later.

$$x' = x\cos\theta + y\sin\theta, \quad y' = -x\sin\theta + y\cos\theta.$$

x' and y' represent the spatial coordinates rotated by an angle θ. $\sigma_{x'}$ and $\sigma_{y'}$ are the standard deviations for the Gaussian envelope and they may not coincide necessarily. This allows us to deal with anisotropic envelopes. An aspect ratio λ and its orientation are defined as:

$$\lambda = \frac{\sigma_{x'}}{\sigma_{y'}}, \quad \phi = \arctan V/U$$

where U and V represent the 2D frequencies of the complex sinusoid.

It is well known that the Fourier transform $H(u,v)$ of $h(x,y)$ is a Gaussian centered on (U,V). Thus, the Gabor filter can be treated as a bandpass filter, and can achieve optimal resolutions in both, the spatial and frequency domains [24].

D.4. Gabor Filters in Tagged MR Images

A tagged MR image can be seen as a CINE MR image modulated by a sinusoidal tag profile. Although this tagging pattern could have crisp geometric profiles, this change only generates a sequence of equally spaced peaks needed to approximate a square signal. Hence, a single peak contains the enough information of the original signal in order to reconstruct it. As a matter of fact, it possible to regenerate the tagging pattern at other orientation by taking advantage of this idea[68]. Thus, the main goal is to perform a reliable filtering technique robust to local tag frequency changes.

As it is mentioned above, a Gabor filter is a bandpass filter with a Gaussian envelope. Then, by extracting the central frequency of the first harmonic peak ψ_1, it is possible to isolate this peak and take advantage of the Gabor resolution achievement. In order to localize it, a region of interest is designed, which depends on the pattern analyzed in 2D orthogonal tagging, then a search of the maximum value

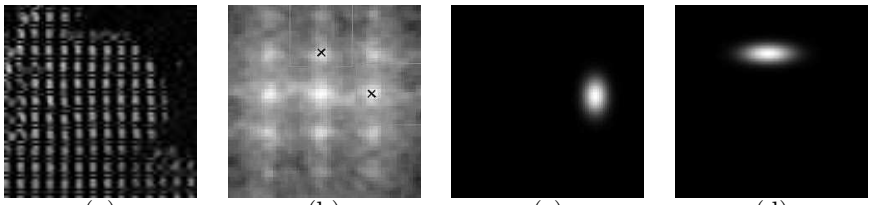

(a) (b) (c) (d)

Figura D.3: Examples of Gabor filters centered at the first harmonic peak in both directions of tagging. (a) Short axis MR image at the starting of the systole. (b) Power spectrum of the MR image. (c) Filter designed to analyze the horizontal peak. (d) Filter designed to analyze the vertical peak.

in this area is performed. Figure D.3(c) shows the localization of these frequencies for a given image.

The bandwidth of the filter has been established through $\sigma_{x'}$ and λ. Thus, the value of $\sigma_{x'}$ is fixed by:

$$\sigma_x = \frac{1}{\sqrt{U^2+V^2}},$$

where (U, V) are the frequencies of ψ_1 of the input image [24]. The orientation of the Gaussian has been designated to be equal to the orientation of the complex sinusoid, $\theta = \phi$ [69].

The intersections between both orthogonal tagging marks in 2-D generate a harmonic peak with an angle orientation of 45^0 between the orthogonal ones. It should be ignored since each component of the 2-D motion is contained in the distribution of the tagging marks in each direction. Thus, it has been designed $\lambda = 2$ to isolate the desired peak. Figure D.3(c) shows the Gabor filter for the horizontal peak, while the figure D.3(d) displays the filter for the vertical one.

Based on this analysis, we can verify that applying a Gabor filter centered on the first harmonic peak is a variant of HARP. The only difference is the shape of the filter. Therefore, we can deal with the phase response of the filtered image as an Angle Image, and estimate a displacement field by tracking points with the same estimated phase. However, applying only one filter does not improve HARP at all. It is because it roughly assumes one frequency for all the image, and it generates a level of error especially when large local deformations are present.

By designing a set of Gabor filters, the most relevant information for a specific frequency can be recovered. In [65], an approach using Gabor filters is described. However, they suggest to vary the central frequency of the first harmonic peak by the equations:

$$\begin{aligned} U' &= \Re\{(U + i \cdot V) \cdot m \cdot \exp(i \cdot \Delta\phi + \omega), \\ V' &= \Im\{(U + i \cdot V) \cdot m \cdot \exp(i \cdot \Delta\phi + \omega) \end{aligned}$$

where m, $\Delta\phi$ and ω, are parameters to vary, and deal with the ω map as a phase image which is recovered from the maximum response of the filters tested for each pixel. U and V are the central frequency of the first harmonic peak. The ranges of the parameters are established as:

$$m \in [0{,}85, 1{,}3], \quad \Delta\phi \in [-\pi/12, \pi/12], \quad \omega \in [-\pi, \pi]$$

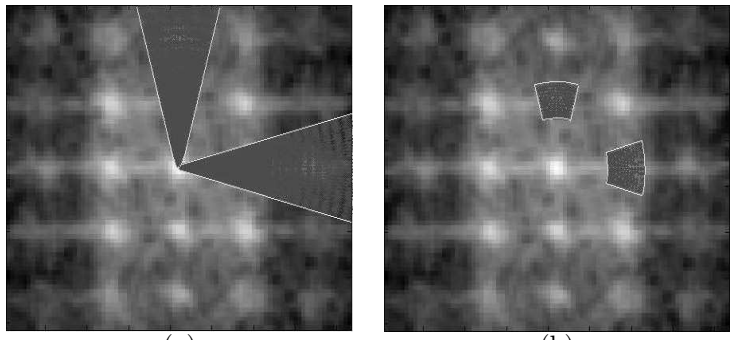

(a) (b)

Figura D.4: Scanned space of frequencies for the horizontal and vertical first harmonic peak. (a) Scanned space suggested in [65]. (b) Mapped space tested to look for local variations of the central frequency.

Although the advantages of the Gabor filters are used, the variations in the frequency space is out of range, because it tests Gabor filters with frequencies that are out of a possible deformation in the tags, as it is shown in the figure D.4(a). In fact, as the Gabor filters reaches low frequencies, it is more influenced by the contours of the heart. Additionally, it has a high computational cost besides HARP and the method proposed, and it suggests the estimation of a displacement map based on the parameters of the filters that maximize the response.

On the other hand, it is proposed to deal with the phase response obtained from the use of a set of Gabor filters, which were generated by varying the central frequencies according to the following equations:

$$U' = \Re\{(U + i \cdot V) \cdot m \cdot \exp(i \cdot \Delta\phi)\},$$
$$V' = \Im\{(U + i \cdot V) \cdot m \cdot \exp(i \cdot \Delta\phi)\},$$

where m represents a linear variation on the frequency, and $\Delta\phi$ represents a angle orientations of the frequency. In other words, m represents whether how the tags open among them, elongation in the heart tissue, or how the tags shorten among them, tissue contraction. Because the Gaussian envelope of the Gabor filters is adaptable to the 2-D frequency orientation, and the bandwidth is a function of the frequency, it is possible to modulate m and $\Delta\phi$ to map the frequencies that could be present in the cardiac motion. Thus, a more precise Angle Image can be built by creating a Gabor filter bank, and taking the highest response for each pixel. The parameters used to modulated are in the following ranges:

$$m \in [0{,}8, 1{,}2], \quad \Delta\phi \in [-\pi/12, \pi/12].$$

These ranges map to frequencies that are around the center of the first harmonic peak. It is expected to match the local patterns mostly in this space. The scanned space is shown in the figure D.4(b).

Based on this analysis, it is proposed to modulate the bank of Gabor filters to recover a more accurate local deformation. The phase of the complex image generated by the extraction of the maximum response of the filtered images at each pixel is taken. It is done in order to create the Angle Images locally. Figure

D.5 displays some examples of Gabor power spectra used. The filters shown were generated to analyze the first horizontal harmonic peak. The effects of modifying the parameters m and $\Delta\phi$ can be observed. The m parameter moves the center of filter horizontally, while $\Delta\phi$ rotates the central frequency and the orientation of the filter. In figure D.6 the complete method is depicted graphically.

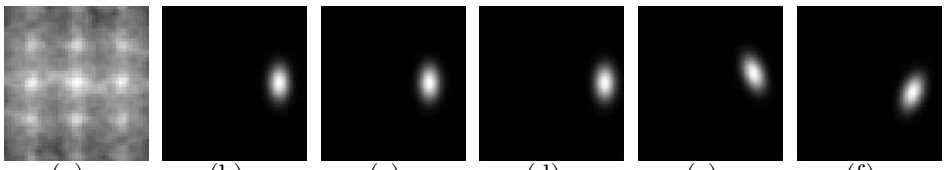

(a) (b) (c) (d) (e) (f)

Figura D.5: Examples of power spectra of Gabor filters (a) Power spectrum of a Tagged MRI at the starting of the systole. (b) First chosen filter (c) Shifted filter, $m = 0{,}8$, $\Delta\phi = 0$. (d) Shifted away filter: $m = 1{,}2$, $\Delta\phi = 0$. (e) Positive rotated filter: $m = 1$, $\Delta\phi = -\pi/12$. (f) Negative rotated filter: $m = 1$, $\Delta\phi = -\pi/12$

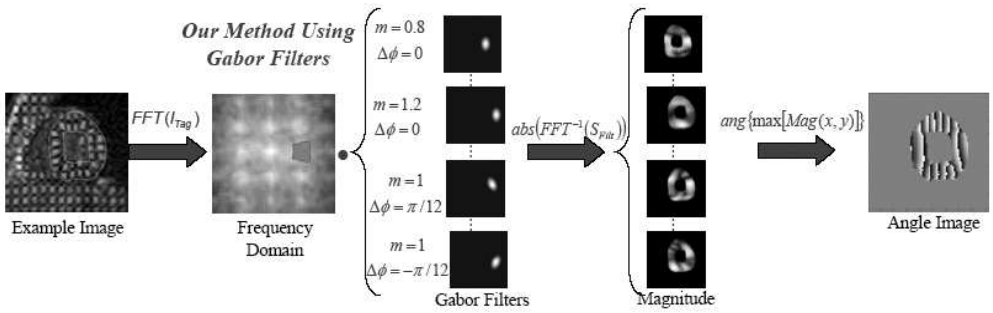

Figura D.6: Schematic representation of the method. First, the fourier transformed of a tagged MR image is obtained. Then, a set of Gabor filters is applied to image around the first harmonic peak. The maximum amplitude of the image filtered is extracted for each pixel to form a single output. Finally, the phase response is used as an Angle Image.

D.5. Motion Tracking using Angle Images

Having the angle images, the tracking of each value is solved by using an iterative method. It is based on the assumption of phase as a material property, *i.e.* invariant through the sequence for a given point. Let $\phi = [\phi_1, \phi_2]$ be a pair of phases of the angle images I_1 and I_2 obtained from the analysis of both orthogonal tagging marks directions. Consider a point located at $\mathbf{y}_m$ at time t_m. If y_{m+1} is the apparent position of this point at time t_{m+1}, then we have:

$$\phi(\mathbf{y}_{m+1}, t_{m+1}) = \phi(\mathbf{y}_m, t_m).$$

It provides the basis for tracking $\mathbf{y}_m$ from t_m to time t_{m+1}. Hence, the problem can be solved by finding a certain $\mathbf{y}$ that satisfies:

$$\phi(\mathbf{y}, t_{m+1}) - \phi(\mathbf{y}_m, t_m) = \mathbf{0}, \tag{D.1}$$

and then set $\mathbf{y}_{m+1} = \mathbf{y}$. Thus, a solution to the equation D.1 has turned to be a multidimensional nonlinear root finding problem. It can be solved iteratively using the Newton-Raphson method. The iteration of the method has been defined as:

$$\mathbf{y}^{(n+1)} = \mathbf{y}^{(n)} - [\nabla\phi(\mathbf{y}^{(n)}, t_{m+1})]^{-1}[\phi(\mathbf{y}^{(n)}, t_{m+1}) - \phi(\mathbf{y}_m, t_m)] \tag{D.2}$$

where ∇ is the gradient with respect to $\mathbf{y}$. There are some details in the practical implementation of equation D.2. The estimation of the gradient involves the use of a wrapping function to deal with the discontinuities from π to $-\pi$, while the calculation of $\phi(\mathbf{y}^{(n)}, t_{m+1})$ requires to perform a certain interpolation. A detailed description of this implementation is explained in [7].

Apéndice E

Correction of Misalignment Artifacts in 3-D Space

Cardiac diseases have become one of the most common causes of death in recent years. Magnetic Resonance (MR) images from the heart provide an opportunity to study the anatomy and functions of the heart *in vivo*. As a result, it is becoming a widely used clinical tool to elaborate an accurate diagnosis. Many approaches have been developed to estimate the motion of the left ventricle, which are based on the initialization of a 3-D model and its deformation[70]. Then, it is required a good correspondence between the image planes in the space to achieve a proper description of the left ventricle volume[46].

A typical imaging session is composed of a number of imaging captures. Here, the required views are acquired during different breath holds. A necessary assumption to reconstruct a 3D model is to consider all the views as *instantaneously acquired*. As a result, a potential patient movement and a displacement of the left ventricle due to respiration can lead to misalignment artifacts[8]. Although some researchers have claimed that the development of more powerful and faster scanners skips the problem[50], this issue has still relevance in many clinical studies.

Some approaches have been proposed to solve the problem. One of them is a method based on registering a 3-D volume with sagittal and axial images as a preprocessing step to build a high resolution dynamic heart model from coronal slices[71]. Here, a line-by-line mean square difference is minimized. In same direction, Lötjönen *et al.*[63] have proposed the registration of a 3-D volume by the use of the Normal Mutual Information (NMI)[9]. They treat the image pixels as volumetric pixels (voxels) by assigning a thickness equal to the slice separation between parallel short axis (SA) planes, and interpolating the voxel size using nearest neighbor in long axis (LA) views. However, it introduces some errors to the analysis due to the approximation. It is because there could be a gap of up to 15mm considering 6 SA views, and taking into account that the thickness of the myocardium is no more than 12mm, this assumption becomes important. An alternative option could be to treat the thickness of the frame as it is reported by the image acquisition, but in order to achieve a good image quality it should be no less than 6mm which is still significant. Additionally, the proposed optimization method suggests the movement of a randomly chosen slice in the direction of its gradient and maximizing its NMI,

which causes a bias depending on the slice. Moreover, this method uses a constant step size of the movement which can provoke a uncertainty of when it has arrived to a maximum besides the slow convergence.

In this chapter, it is proposed an alternative solution to the problem of misaligned MR images in a 3-D reconstruction of the left ventricle, by treating the MR images as planes on the space, and using the NMI as a measure of registration which is maximized using a particular variant of the steepest descendent method. In figure E.1 typical intersections among planes of a given patient are shown. It is suggested to use the intersection line between a given SA plane and an intersecting LA one, sample it, and extract the gray values associated with this points in both images. Then the NMI is estimated for these values generating an alignment measure. Thus, all of NMI values obtained from the intersections between the SA and LA views are combined to generate a global measure of alignment. Later, all of the images are moved simultaneously in order to arrive to a maximum by the steepest descendent method using a non constant step size. As an enhancement to reach a global maximum, the step size is altered to jump out of a possible local maximum along the gradient direction.

E.1. Planes Intersection

Having a SA MR image and a LA MR image, it is possible to obtain their spatial information from the DICOM headers respect to a common coordinate system, allowing the estimation of geometrical correspondences among all the views. A translation of the initial corner of the image, two orientation vectors, and a scale factor to convert pixels into millimeters are stored automatically. Hence, the equation of each of the image plane can be calculated.

Let I_{SA_i} be a short axis plane *i-th* of a total of N short axis planes, and I_{LA_j} be a long axis plane *j-th* of a total of M long axis planes, thus there exist a line intersection, $\mathbf{l_{ij}}$, between them which can be obtained from their plane equations by finding 2 points of this line. It can be expressed as:

$$\mathbf{l}_{ij} = \mathbf{r}_0 + t\mathbf{w},$$

where $\mathbf{r}_0$ is a point on the line, t is a free parameter, and $\mathbf{w}$ is a unitary vector parallel to the line. In order to find the pixel values along $\mathbf{l}_{ij}$ on I_{SA_i} and I_{LA_j}, it has to be placed on each of the image spaces. Thus, a point $\mathbf{p}_{l_{ij}} = \mathbf{l}_{ij}(t_0)$ can be expressed on the image spaces $\mathbf{p}_{SA_i} \in U_{SA_i}$ and $\mathbf{p}_{LA_j} \in U_{LA_j}$, from the image plane I_{SA_i} and I_{LA_j} respectively, as follows:

$$\mathbf{p}_{SA_i} = \left[\mathbf{r}_x^{SA_i}\mathbf{r}_y^{SA_i}\mathbf{r}_z^{SA_i}\right]^{-1}\left(\mathbf{p}_{l_{ij}} - \mathbf{o}_{SA_i}\right), \tag{E.1}$$

$$\mathbf{p}_{LA_j} = \left[\mathbf{r}_x^{LA_j}\mathbf{r}_y^{LA_j}\mathbf{r}_z^{LA_j}\right]^{-1}\left(\mathbf{p}_{l_{ij}} - \mathbf{o}_{LA_j}\right), \tag{E.2}$$

where $\mathbf{r}_x^{SA_i}$,$\mathbf{r}_y^{SA_i}$,$\mathbf{r}_z^{SA_i}$, are the direction of the x-axis, y-axis, and z-axis of U_{SA_i} respectively, while $\mathbf{o}_{SA_i}$ is a translation of the initial corner of I_{SA_i}. In the same manner, $\mathbf{r}_x^{LA_j}$,$\mathbf{r}_y^{LA_j}$,$\mathbf{r}_z^{LA_j}$ and $\mathbf{o}_{LA_j}$, are the descriptors of the space U_{LA_j}. Here the points $\mathbf{p}_{SA_i}$ and $\mathbf{p}_{LA_j}$ are in $\Re^3$. However, since these points lie on $\mathbf{l_{ij}}$, the z-coordinate is equal to zero. Hence, after reducing the dimensionality of the points

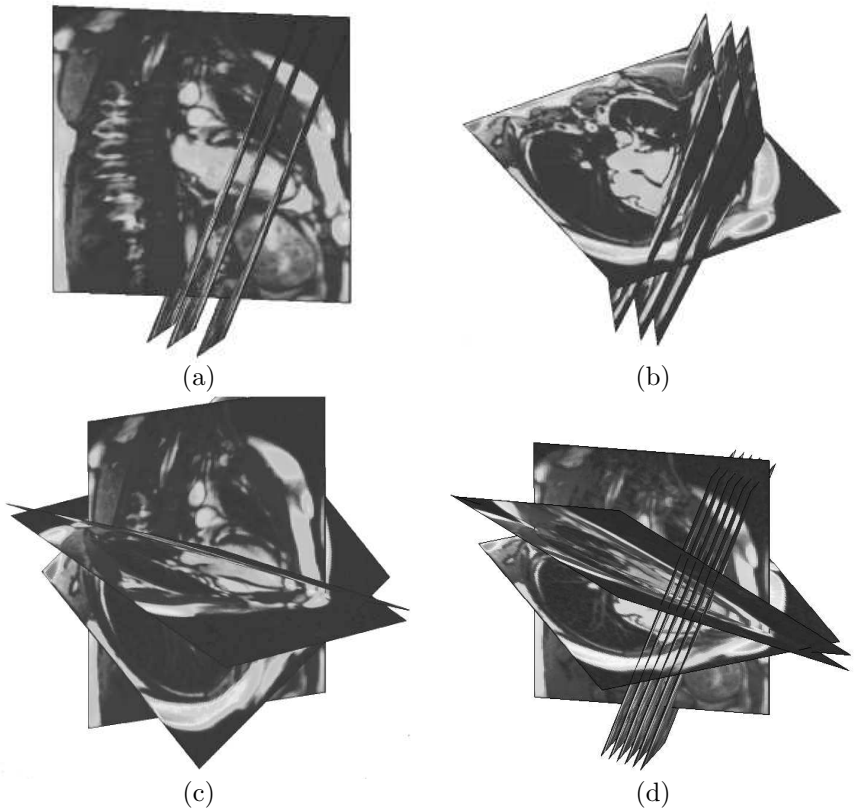

Figura E.1: Example of intersections among planes. (a) One LA plane vs three parallel SA. (b) A different LA view where both ventricles are observed vs three SA. (c) Four intersected LA planes used for one study. (d) All the available planes for a certain study, six parallel SA vs four LA intersected planes.

to $\Re^2$ and applying a scale factor, these points can be expressed in pixels in U_{SA_i} and U_{LA_j} respectively. Therefore, by applying Eq. (E.1) and Eq. (E.2), a pair of gray values can be obtained for a single point $\mathbf{p}_{l_{ij}}$ coming from each of the images planes I_{SA_i} and I_{LA_j}, at the points $\mathbf{p}_{SA_i}$ and $\mathbf{p}_{LA_j}$ respectively.

Once the intersection line has been estimated, the image ranges are intersected to guarantee the availability of gray values along the line. Then, the resulting line segment is sampled to generate a fixed number of points $\mathbf{p}_{L_{ij}}$. By using Eq. (E.1) and Eq. (E.2), the points on I_{SA_i} and I_{LA_j} can be found. However, the corresponding gray values are only available for integer values of $\mathbf{p}_{SA_i}$ and $\mathbf{p}_{LA_j}$. We have observed that typically the myocardium in the SA and LA views have a thickness of 4-6 pixels (7,9-11,9mm), which means that a simple rounding of $\mathbf{p}_{SA_i}$ and $\mathbf{p}_{LA_j}$ is not suitable. Hence, it has been performed a linear interpolation of the gray values along the sampled line so that $\mathbf{v}_{SA_i}$ and $\mathbf{v}_{LA_j}$ approximate continuous lines with reliable image values. To avoid any kind of bias, the sampling process has been designed using the parameter t so as to have the same points regardless of the order.

E.2. Correspondence Measure

Having $\mathbf{v}_{SA_i}$ and $\mathbf{v}_{LA_j}$, the problem turns to be a registration issue with two gray value vectors available. Thus, the Normalized Mutual Information (NMI)[9] has been employed to measure the correspondence between $\mathbf{v}_{SA_i}$ and $\mathbf{v}_{LA_j}$, and, as a result, between I_{SA_i} and I_{LA_j}. The NMI, S, is defined as:

$$S(\mathbf{v}_{SA_i}, \mathbf{v}_{LA_j}) = \frac{H(\mathbf{v}_{SA_i}) + H(\mathbf{v}_{LA_j})}{H(\mathbf{v}_{SA_i}, \mathbf{v}_{LA_j})}, \tag{E.3}$$

where $H(\mathbf{v}_{SA_i})$ and $H(\mathbf{v}_{LA_j})$ are the marginal entropies of $\mathbf{v}_{SA_i}$ and $\mathbf{v}_{LA_j}$ respectively, and $H(\mathbf{v}_{SA_i}, \mathbf{v}_{LA_j})$ is the joint entropy of both vectors. Based on information theory, the gray values reported on the intersection vectors can be treated as discrete random variables[9]. Thereby, these entropies are defined as:

$$H(\mathbf{v}_x) = -\sum_{x \in \mathbf{v}_x} p\{x\} \log p\{x\} \tag{E.4}$$

$$H(\mathbf{v}_x, \mathbf{v}_y) = -\sum_{x \in \mathbf{v}_x} \sum_{y \in \mathbf{v}_y} p\{x, y\} \log p\{x, y\}. \tag{E.5}$$

Here $p\{x\}$ represents the probability distribution of v_x, while $p\{x, y\}$ is the joint distribution of v_x and v_y. Thus, for this case in order to calculate the distribution of $\mathbf{v}_{SA_i}$,$\mathbf{v}_{LA_j}$, and their joint probability, the number of bins has been adjusted according to the number of samples of the intersection vectors. It is mainly because the gray values in a given $\mathbf{v_x}$ can vary until thousands, and by selecting a region of interest, the variety of gray values can be little, which allows some bins to be 1 or 2 undermining the measure. Thus, the number of bins has been established to be the ratio between the number of elements of $\mathbf{v_x}$ and a density factor experimentally determined. For this case this number varies from 20 to 40 based on the number of samples. In addition, a preprocessing step has been performed to the images available. Here, the logarithmic of the image is computed, which improves the gray distribution and compresses its range[72]. Because the sampling process assures the selection of the same points regardless the order, it is guaranteed that:

$$S(\mathbf{v}_{SA_i}, \mathbf{v}_{LA_j}) = S(\mathbf{v}_{LA_j}, \mathbf{v}_{SA_i}).$$

E.3. Misalignment Correction

One of the main causes of misalignment among MR image planes is respiration[8]. During an imaging session, the patient is asked to hold the breath while the images are acquired. Long periods of time, up to 20 seconds, provoke the patient to inhale small quantities of air which cause a certain movement of the heart. We have performed an experiment where a patient is scanned while this effect is introduce during a cardiac cycle. It is shown in figure E.2. It can be observed that there is a certain level of rotation. Nonetheless, the left ventricular motion can be assumed to be a translation. Thus, we have selected a region of interest which contains the myocardium, and tried to fit the image planes by translations, since we are interested in the left ventricle.

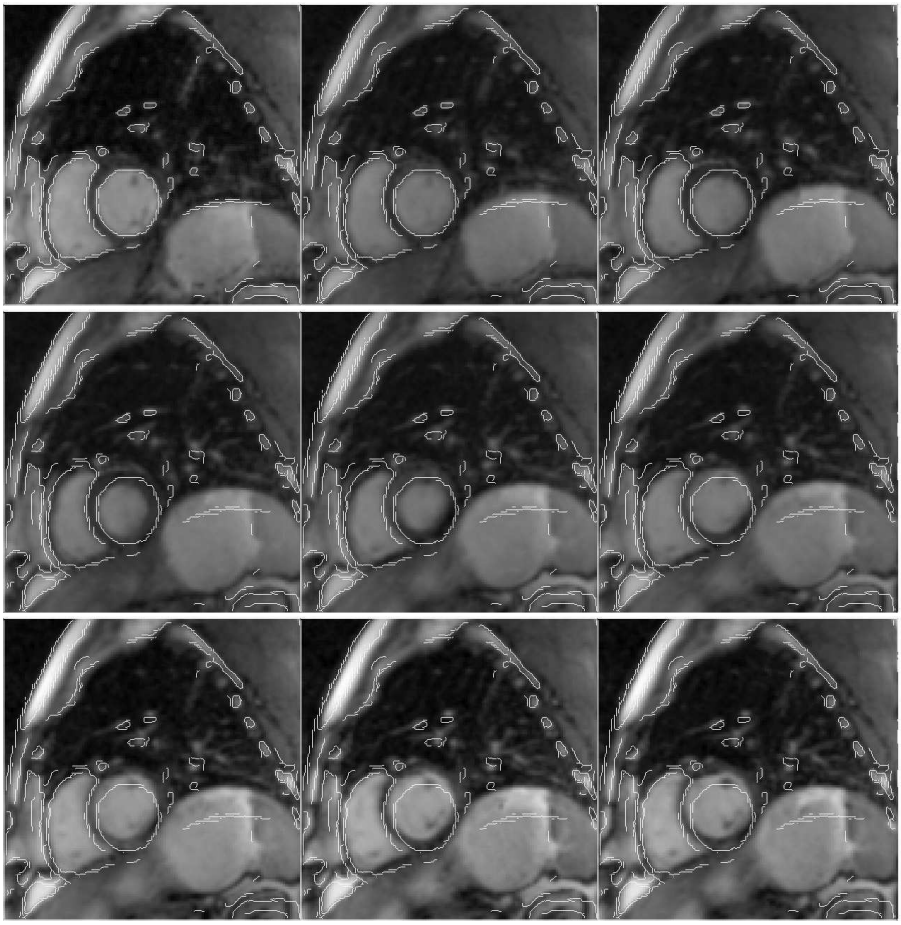

Figura E.2: From left to right and from top to bottom, a cardiac cycle sequence from a patient with the motion artifact due to respiration. The contours of the first frame have been added for better visualization

The movement artifacts can also be observed from the intersection vectors $\mathbf{v}_{LA_j}$ and $\mathbf{v}_{SA_i}$. As an example, in the figure E.3 a typical misalignment artifact is shown. Since we are interested in the analysis of the left ventricle, it has been selected a region of interest where the left ventricle is appreciated. Although the problem can be treated as moving one plane until $S(\mathbf{v}_{SA_i}, \mathbf{v}_{LA_j})$ is maximum and repeating the process until it converges for all the N short axis and M long axis planes, the main drawback of this is that a movement in one SA plane, affects the alignment with the other LA planes which intersect it. Consequently, we have designed a method to correct misalignments among the image planes by moving all the planes simultaneously.

It has been calculated a global measure of alignment C to be maximized in this registration problem. A simple approach is to use the mean of $S(\mathbf{v}_{SA_i}, \mathbf{v}_{LA_j})$ for all the intersections between the N SA views and the M LA ones. However, because of the NMI probabilistic properties, it has been designed C as follows:

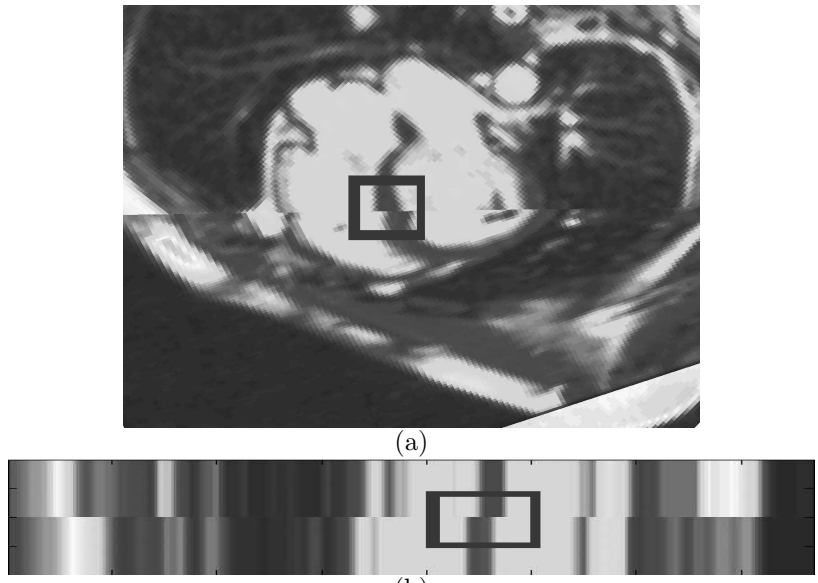

(a)

(b)

Figura E.3: Example of misalignment between a SA plane and a LA one. The square area represent the interventricular septum. (a) The SA and LA images in a common 3-D space. (b) The intersection vectors displayed one against the other.

$$C = \frac{\sum_{i=1}^{N} S(\mathbf{u}_{SA_i}, \mathbf{u}_{LA}) + \sum_{j=1}^{M} S(\mathbf{u}_{LA_j}, \mathbf{u}_{SA})}{N+M},$$

where

$$\mathbf{u}_{SA_i} = \left[\mathbf{v}_{SA_{i1}}^T, \mathbf{v}_{SA_{i2}}^T, \ldots, \mathbf{v}_{SA_{iM}}^T\right], \quad \mathbf{u}_{LA} = \left[\mathbf{v}_{LA_{i1}}^T, \mathbf{v}_{LA_{i2}}^T, \ldots, \mathbf{v}_{LA_{iM}}^T\right],$$

$$\mathbf{u}_{LA_j} = \left[\mathbf{v}_{LA_{j1}}^T, \mathbf{v}_{LA_{j2}}^T, \ldots, \mathbf{v}_{LA_{jN}}^T\right], \quad \mathbf{u}_{SA} = \left[\mathbf{v}_{SA_{j1}}^T, \mathbf{v}_{SA_{j2}}^T, \ldots, \mathbf{v}_{SA_{jN}}^T\right].$$

Here $\mathbf{v}_{SA_{ij}}$ and $\mathbf{v}_{LA_{ij}}$ represent the intersection vectors $\mathbf{v}_{SA_i}$ of the SA view *i-th* with the LA *j-th*. Thus, we have estimated the NMI for all the intersections for a given plane, and computed the mean for all the planes.

There is a translation $\mathbf{o}_x$ of each of the image planes in a common space of dimension 3. If:

$$\mathbf{d} = \left[\mathbf{o}_{SA_2}^T, \mathbf{o}_{SA_3}^T, \ldots, \mathbf{o}_{SA_N}^T, \mathbf{o}_{LA_1}^T, \mathbf{o}_{LA_2}^T, \ldots, \mathbf{o}_{LA_M}^T\right],$$

it can be said that $C = f(\mathbf{d})$, where $\mathbf{d} \in \Re^{3(N+M-1)}$. Therefore an optimization method can be applied to maximize C so as to find the best fitting of the image planes.

In order to maximize C, it has been used the steepest descent method explained in [10]. The gradient, ∇C, respect to $\mathbf{d}$ is estimated using finite differences by the central-difference equation of order $\mathbf{O}(h^2)$ for each dimension. Because of the definition of C, the implementation of ∇C can be simplified by finding $\mathbf{u}_{SA_{ij}}$ and $\mathbf{u}_{LA_{ij}}$ just for the intersection planes where d_k belongs to. Thus, the iteration of $\mathbf{d}$ is constrained along the line:

$$\mathbf{d}_{k+1} = \mathbf{d}_k + \gamma \mathbf{g}_k$$

where $\mathbf{g}_k$ is the direction of ∇C_k. Here, the step size γ is found from a single parameter maximization of

$$\phi(\gamma) = C(\mathbf{d}_k + \gamma \mathbf{g}_k).$$

It has been designed γ to be increased each time when C tends to be a local maximum and, by solving the single parameter maximization of $\phi(\gamma)$, C could be attracted to a higher maximum. If γ returns to the same value range in spite of the perturbation, the algorithm is left to converge to this maximum.

Apéndice F

Estimating 3-D Motion from 2-D Components

A typical TMRI session is composed of several imaging captures, where some are short axis (SA), while others are long axis (LA) views of the left ventricle. These orientation captures are used in order to have enough information of the ventricular motion. Once a set of SA and LA image planes for a given patient are acquired, it is possible to place each point from these planes into a 3-D space based on the DICOM headers provided by the imaging equipment. As it is discussed in section E.1, the DICOM information allows us to place an image plane into a common 3-D space, and to estimate the intersection lines among all the planes. As a result, it is possible to have motion information of two images from their intersection points. This estimated deformation can be treated as the *real* motion because it can be observed at two different angles *simultaneously*, which can complete the on-plane displacement.

Because of the 2-D tagging marks in the images, the points along the intersection line are associated with two deformation vectors. However, the real dimension of the displacement vector for these points is 3 which means that there is redundancy. Consequently, a method to combine the on-plane vectors into a 3-D displacement vector for a given intersection point needs to be developed. Here, these vectors can be assumed to be projections of the 3-D one.

Once the 3-D deformation vectors have been reconstructed for the intersection points, there are some remaining points along each of the image planes whose 2-D deformation maps are obtained from the tracking process. These maps can be considered as *reliable* since they were obtained from the image information. Thus, the missing deformation component could be interpolated based on the intersection points motion. Later, this information is used to complete the 2-D on-plane motion. Here, the missing component on the image coordinate system is interpolated independently of the others.

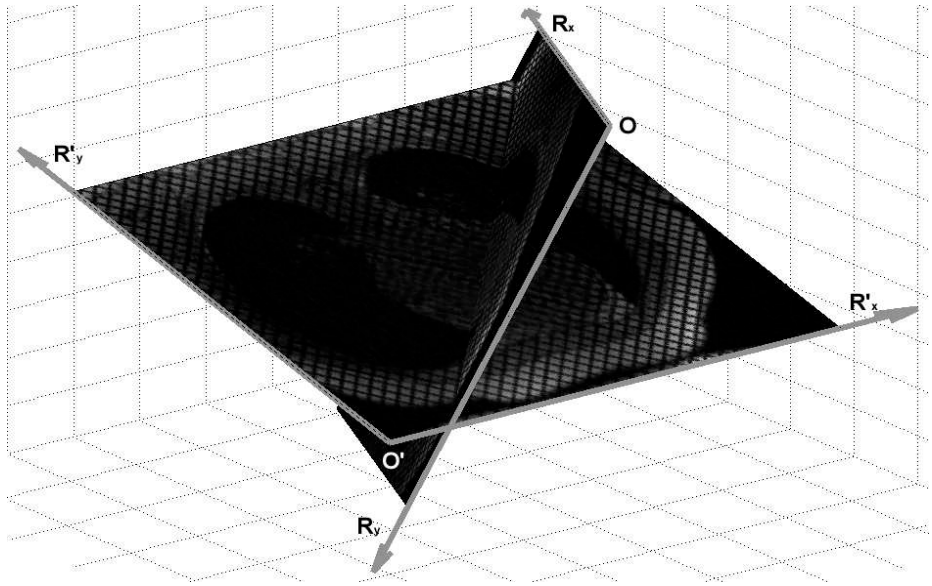

Figura F.1: A short axis and a long axis Tagged MR images in the 3-D common space. The orientation vectors ($\mathbf{R}_x$, $\mathbf{R}_y$), and the translation vector ($\mathbf{O}$) are illustrated for each frame. The dashed symbols represent the available information for the long axis frame.

F.1. From 2-D Images to 3-D Space

Spatial information from DICOM headers respect to a common coordinate system can be extracted in order to estimate geometrical correspondences among all the views. In addition, it is possible to obtain a point $\mathbf{p}^w$ in the 3-D common space corresponding to one $\mathbf{p}^u$ in an image space. Figure F.1 shows the available information for each of the frames.

Let $\mathbf{o}^w = [o_x, o_y, o_z]^T$ be a displacement vector, and $\mathbf{r}_x = [r_{1x}, r_{1y}, r_{1z}]^T$, $\mathbf{r}_y = [r_{2x}, r_{2y}, r_{2z}]^T$, and $\mathbf{r}_z = [r_{3x}, r_{3y}, r_{3z}]^T$ be three unitary orthogonal vectors which correspond to the direction of each axis of a coordinate system U in a 3D space W. Therefore, a point $\mathbf{p}^u$ can be represented by $\mathbf{p}^w$ as follows:

$$\mathbf{p}^w = [\mathbf{r}_x \mathbf{r}_y \mathbf{r}_z]\, \mathbf{p}^u + \mathbf{o}^w. \tag{F.1}$$

For our case, the vectors $\mathbf{r}_x$, $\mathbf{r}_y$, and $\mathbf{o}^w$ are obtained from the DICOM headers. $\mathbf{r}_z$ is calculated by the cross product of $\mathbf{r}_x$ and $\mathbf{r}_y$. Hence, it is feasible to find the 3D points in W, corresponding to the on-plane 2D points after applying a scale factor from the DICOM information to transform pixels into millimeters, and expanding the 2D vectors to 3D by fixing the z-coordinate to be 0 in the coordinate system U.

By applying the Eq. (F.1), the deformation maps, obtained by the tracking process presented in section D.5, can be transformed from the image space to the common space. It allows us to combine the motion obtained from each image to a global motion of a volumetric myocardium.

F.2. Generation of 3D Motion

Once the intersection between a SA view and a LA view is calculated, as developed in the section E.1, the 3D motion can be estimated for the intersection line based on the on-plane motion obtained from the tracking process for each view. Let $\mathbf{p}^0 \in W$ be a point inside of the ventricle volume at time t_0 which lies along the intersection line, $\mathbf{l}_{ij}$, between a SA plane *i-th* and a LA plane *j-th*, thus by applying Eq. (E.1) and Eq. (E.2), there exists a point $\mathbf{p}^0_{SA_i} \in U_{SA_i}$ on the *i-th* SA view at time t_0 that is associated with a final point $\mathbf{p}^1_{SA_i} \in U_{SA_i}$ at time t_1 obtained from the on-plane tracking, and a point $\mathbf{p}^0_{LA_j} \in U_{LA_j}$ on the *j-th* LA view at time t_0 paired with a final point $\mathbf{p}^1_{LA_j} \in U_{LA_j}$ at time t_1 obtained from the same process. By Eq. (F.1), the points $\mathbf{p}^1_{SA_i}$ and $\mathbf{p}^1_{LA_j}$ can be transformed into $\mathbf{p'}^1_{SA_i} \in W$ and $\mathbf{p'}^1_{LA_j} \in W$ respectively.

The real motion which moves the point $\mathbf{p}^0$ to a point $\mathbf{p}^1$ at time t_1 is composed of the on-plane motion estimated in each of the views. It can be assumed that the displacement vectors, $\mathbf{p'}^1_{SA_i} - \mathbf{p}^0$ and $\mathbf{p'}^1_{LA_j} - \mathbf{p}^0$, are projections of the real displacement $\mathbf{p}^1 - \mathbf{p}^0$. Let $\mathbf{l}_{SA_i}$ and $\mathbf{l}_{LA_j}$ be two lines defined as:

$$\mathbf{l}_{SA_i} = t_{SA_i}\mathbf{r}_z^{SA_i} + \mathbf{p'}^1_{SA_i} \tag{F.2}$$

$$\mathbf{l}_{LA_j} = t_{LA_j}\mathbf{r}_z^{LA_j} + \mathbf{p'}^1_{LA_j} \tag{F.3}$$

where t_{SA_i} and t_{LA_j} are the unknown variable of the lines along the direction of $\mathbf{r}_z^{SA_i}$ and $\mathbf{r}_z^{LA_j}$, which correspond to the unitary vectors of the z-direction of each of the image planes respectively. In order to find the real motion, it should be found t_{SA_i} and t_{LA_j} such as the lines $\mathbf{l}_{SA_i}$ and $\mathbf{l}_{LA_j}$ intersect each other, which corresponds to $\mathbf{p}^1$, because $\mathbf{p'}^1_{SA_i} - \mathbf{p}^0$ and $\mathbf{p'}^1_{LA_j} - \mathbf{p}^0$ are its projections on each of the planes. Then, by fixing $\mathbf{l}_{SA_i} = \mathbf{l}_{LA_j}$, the system can be expressed as:

$$\begin{bmatrix} r_{z1}^{SA_i} & -r_{z1}^{LA_j} \\ r_{z2}^{SA_i} & -r_{z2}^{LA_j} \\ r_{z3}^{SA_i} & -r_{z3}^{LA_j} \end{bmatrix} \begin{bmatrix} t_{SA_i} \\ t_{LA_j} \end{bmatrix} = \begin{bmatrix} p'^1_{LA_j1} - p'^1_{SA_i1} \\ p'^1_{LA_j2} - p'^1_{SA_i2} \\ p'^1_{LA_j3} - p'^1_{SA_i3} \end{bmatrix} \tag{F.4}$$

where according to the number of solutions to $\begin{bmatrix} t_{SA_i} \\ t_{LA_j} \end{bmatrix}$ there are the following cases:

1. ∞ or 0 solutions if there are 3 rows linearly dependent
2. 1 solution if 1 row is linearly independent

The first case is possible when $\mathbf{l}_{SA_i}$ can be expressed by a lineal combination of $\mathbf{l}_{LA_j}$. This situation needs the SA plane and the LA plane to be parallel allowing whether no intersection lines, or infinity intersection lines between them, which is not the case since by definition these planes are intersected. Therefore, one solution can be assured to Eq. (F.4). Figure F.2 shows a graphical explanation of the method.

Theoretically there should be one solution for Eq. (F.4), but it is not always the case due to inexact measurements an errors during the tracking . Thus, the solution is found by the approximation of a residual factor using the least-squares

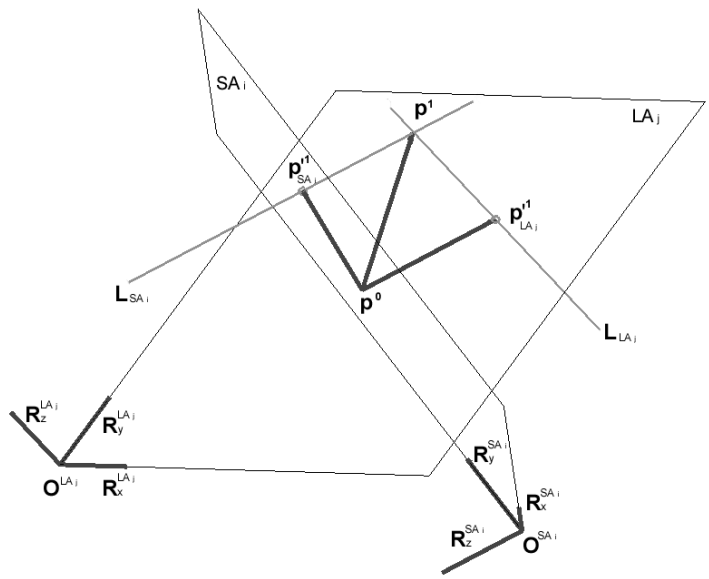

Figura F.2: One of the intersection points has been picked to illustrate our reconstruction method. The vectors $\mathbf{p}'^1_{SA_i} - \mathbf{p}^0$ and $\mathbf{p}'^1_{LA_j} - \mathbf{p}^0$ represent the SA and LA on-plane deformation, and the vector $\mathbf{p}^1 - \mathbf{p}^0$ shows the real 3D motion. Here $\mathbf{l}_{SA_i} \| \mathbf{r}_z^{SA_i}$ and $\mathbf{l}_{LA_j} \| \mathbf{r}_z^{LA_j}$.

method[73] to satisfy the expression as close as possible. Eq. (F.4) is expressed in the standard form $A\mathbf{x} = \mathbf{b}$ where A is the matrix composed of the vectors $\mathbf{r}_z^{SA_i}$ and $-\mathbf{r}_z^{LA_j}$ in the columns, $\mathbf{x}$ is the unknown vector $\begin{bmatrix} t_{SA_i} \\ t_{LA_j} \end{bmatrix}$, and $\mathbf{b}$ represents the constant vector $\left[\mathbf{p}'^1_{SA_i} - \mathbf{p}'^1_{LA_j}\right]$. Then, the norm of the residual $\mathbf{r}$ is minimized, where $\mathbf{r} = A\mathbf{x} - \mathbf{b}$.

It can be demonstrated that the minimum-norm least squares solution to a linear system $A\mathbf{x} = \mathbf{b}$, that is, the shortest vector $\mathbf{x}$ that achieves

$$\min_{\mathbf{x}} \|A\mathbf{x} - \mathbf{b}\|$$

is unique, and is given by

$$\mathbf{x} = A^{\dagger}\mathbf{b}$$

where $A^{\dagger}$ is the pseudoinverse of A. If $U\Sigma V^T$ represents the singular value decomposition of A, then $A^{\dagger}$ is defined as

$$A^{\dagger} = V\Sigma^{\dagger}U.$$

Here the matrixes V and U contain the right and left singular vectors of A respectively, while $\Sigma^{\dagger}$ is a matrix of the same size than A whose diagonal contains the inverse of the singular values of A[73].

Hence, by solving the system for $\begin{bmatrix} t_{SA_i} \\ t_{LA_j} \end{bmatrix}$, it can be guaranteed uniqueness and the intersection point of $\mathbf{l}_{SA_i}$ and $\mathbf{l}_{LA_j}$ which corresponds to the desired point $\mathbf{p}^1$

can be calculated by evaluating either Eq. (F.2) or (F.3) for the solution found. Therefore, the real 3-D displacement for each of the intersection points has been estimated.

F.3. Interpolation

At this point the full 3-D motion has been calculated for the intersection points between the SA and the LA views. However, there are points from the SA plane which have on-plane motion information only. Although this motion information can be represented in the common coordinate system W, it depicts only a projection of the real motion. Nonetheless, the full motion of the intersected points can be represented in U_{SA_i} by Eq. (E.1) yielding the intersection points contribute to the z-coordinate motion information.

With the motion information of the z-coordinate for certain points, it is possible to performed an interpolation to sparse it through the segmented myocardium in SA views. Thus, to complete the 3-D information for the rest of points the z displacement map is interpolated using the method proposed in [74]. For the points where a triangulation is possible, a linear interpolation is performed. The points where this is no possible, the estimation of the z-coordinate is computed by the nearest neighbor technique. As a result, the 3-D motion information is completed for the rest of the points inside the segmented region, for all the SA views of a patient. It offers the advantage of calculating the z motion component regardless of the tracking process components avoiding any kind of bias. Therefore, the missing deformation information is evaluated based on the observed motion from the intersection points.

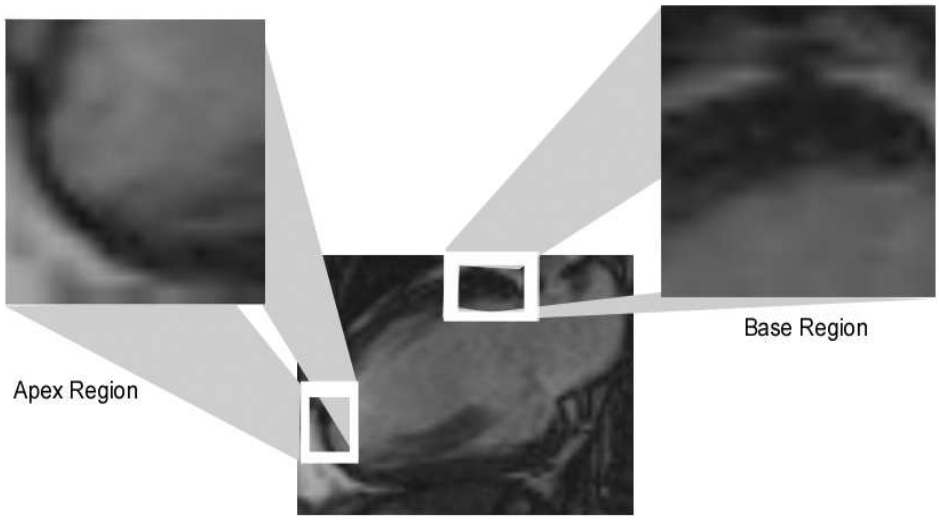

Figura F.3: A LA image where the difference in thickness is appreciated. One region of the apex and one of the base has been expanded at the same scale.

Although the same idea of interpolation can be used to complete the LA on-

plane motion, this has not been used because of the nature of the LA movement. The observed movement on the SA planes can be considered as a rotation combined with a lower level of radial translation respect to the center of the myocardium. However, the motion information distinguished from the LA is more complex. It roughly consists of a translation from base to apex during systole, but near the apex the deformation is more complex and the myocardium is thinner. Consequently, by applying the interpolation method, the z values near the apex on the LA views can be influenced by the nearest intersection line, provoking an erroneous interpolation. The difference in thickness of the left ventricle in LA can be observed in figure F.3. Here, the magnitude of this variation is susceptible to cause the spread of little information through large regions, increasing the error rate.

Apéndice G

Results

G.1. Gabor Filters in Cardiac Tagged MRI

The use of the Gabor Filters in the characterization of the Tagged MR images to be tracked has been explained in chapter D. There, the concept of angle images has been discussed and a novel method to improve their obtention has been proposed. In this section, several results are presented to demonstrate the effectiveness of the method. Firstly, a qualitative analysis is discussed. Here, the method has been tested with 1-1 SPAMM images, low-quality images, and with C-SPAMM images, high-quality sequences. C-SPAMM images have the feature that the fading effect is less than in 1-1 SPAMM. It has been done in order to corroborate the theory that the flaws of HARP are caused by high local deformation of the tagging marks regardless of the fading effect. Additionally, a quantitative test has been performed in order to estimate some statistical data. Here a validation protocol has been developed based on the use of the 2-D correlation coefficient between two matrices. All of these experiments have been elaborated using real data from healthy patients.

G.1.1. Validation Protocol

In the field of medical image analysis one of the main issues is to elaborate a validation scheme. The natural scarcity of healthy patients in hospitals and the lack of a ground truth in the estimation of some parameters are factors which undermine the evaluation of a given technique. In spite of the option of creating synthetic data to analyze, there is frequently a gap between what is simulated and what is a real data. As an example, it is worthy to mention that there has not been developed a reliable evaluation method in the problem of estimation the motion of the heart based on Tagged MR images.

To validate the improvement of the Gabor filters method over HARP in terms of a more precise tracking of pixels over the systole, it has been deformed a given Tagged MR image based on the displacement fields estimated by the proposed framework and HARP. Later on,the resulting images are compared to the next image in the sequence. It can be expected that both images are equal theoretically. Hence, the image with less difference represents the more accurate deformation.

Let I_0 and I_1 be two Tagged MR images at time t_0 and t_1 respectively, and

Ψ_x^0 and Ψ_y^0 be the x and y-displacement information for each of the myocardial pixels $\mathbf{p}_i$ on the image I_0. Thus, an image I_1' has been generated by translating and interpolating each of the gray value from the image I_0 based on the motion information Ψ_x^0 and Ψ_y^0. To measure the likelihood between I_1 and I_1', the 2-D correlation coefficient has been employed. Hence, the similarity measure has been defined as follows:

$$r(A,B) = 1 - \frac{\sum_m \sum_n (A_{mn} - \bar{A})(B_{mn} - \bar{B})}{\sqrt{(\sum_m \sum_n (A_{mn} - \bar{A})^2)(\sum_m \sum_n (B_{mn} - \bar{B})^2)}} \tag{G.1}$$

where $\bar{A}$ and $\bar{B}$ represent the mean of the gray values of A and B, while A_{mn} and B_{mn} represent the image value at the m row and the n column for the images A and B respectively. Thus, by evaluating the equation G.1 for I_1 and I_1', the similarity of the images can be measure, and consequently the efficiency of the methods can be evaluated. Here $r(A,B) = 1$ means that both images are completely different, while $r(A,B) = 0$ means that A and B are exactly the same.

G.1.2. Result Analysis

Once a validation protocol has been stated, some results will be analyzed. Firstly a number of extreme cases are tested to show the effectiveness of the method. It is done to display some quality results. Later on, some numerical results are displayed by using the validation scheme to support the proposed framework statistically.

Typically during systole the Tagged MR images suffer large deformations near the end systole, but at the beginning these are slight. Thus, the method has been tested with three images of the same patient for one sequence at different time points. Figure G.1 shows an example of the method proposed to obtain the Angle Image versus HARP based method. As it is illustrated, in the first image the both techniques report practically the same results (low deformation). In the second image, some differences are shown. These are essentially that Gabor filters follow better the tags deformation. However, the deformation in the myocardium is not highly significant, and the result generated by HARP is still efficient. In the third image a greater difference between HARP and the method proposed is observed. For this image, HARP has lost one tag completely in the upper center of the myocardium (squared area). Here the frequency has increased because of the vertical tags approximation, while the frequency in other sections of the myocardium has decreased, and HARP is not prepared to deal with this issue. Hence, it tends to blur the frequencies of the myocardium, and it generates an Angle Image with smoothed deformations. In fact, it is possible to lose tags, as in this example, when the frequency of the tags changes a lot locally due to motion, as in several regions increases while in others decreases. On the other hand, the method proposed creates a more precise Angle Image. In this example, despite of the fading of the tags, all the tags are recovered, and deformations are accurately generated.

The images discussed above have low quality, especially because of the tag fading. Even when the suggested approach generates better results than HARP, there are some errors due to the quality of the images. In figure G.2 another example is shown

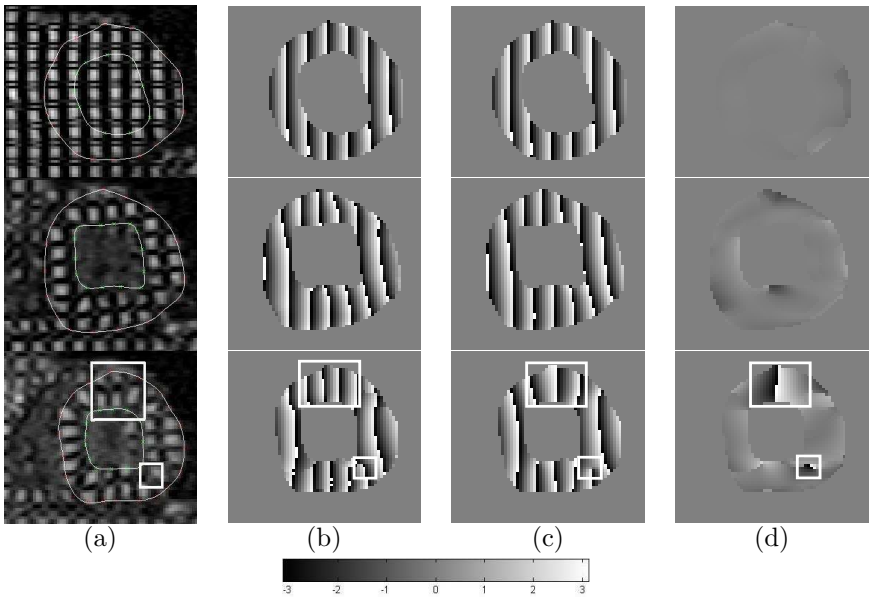

Figura G.1: Examples of Angle Images obtained for the first horizontal harmonic peak using Gabor filters and HARP. (a) Original Tagged MR images in short axis during systole. (b) Angle Images generated by our method. (c) Angle Images produced by HARP. (d) Difference between the methods. The left ventricle has been delineated for a better understanding. Tags can be identified in the Angle Images through the discontinuities from $-\pi$ to $+\pi$.

with a higher quality images. From this example, it can be seen that the proposed method describes better the behavior of the tags deformation than HARP. This image, from the end systole, shows a contraction to the center of the left ventricle. The results shown by HARP have several problems in the tag recovery. There are regions where certain tags are lost. In addition, the deformations reported by HARP are not as accurate as the results obtained since these are smoothed. The differences between methods are shown in figure G.2(d) and (h). The squared areas highlight the regions where the variations are more significant.

There are several diseases which are correlated with the motion of the heart, such as coronary artery disease or ischemia heart disease[38]. These pathologies require the calculated myocardial deformation to achieve a good diagnostic. Thus, in order to generate relevant information for clinical usage, the measurement of the myocardial deformation using Gabor filters is shown in figure G.3. Displacement maps are obtained using phase tracking as described in section D.5, which allows subpixel resolution. It can be observed that the field estimated describes the rotation of the myocardium despite of the quality of the images. From the magnitude of the displacement, it can be noted the distribution of the deformation over the myocardium. These parameters are useful to determine when the heart is rotating under the baseline, and elaborate the appropriable diagnostic.

In addition, the method has been compared with HARP based on the accuracy of the deformation fields. It has been done using the validation protocol presen-

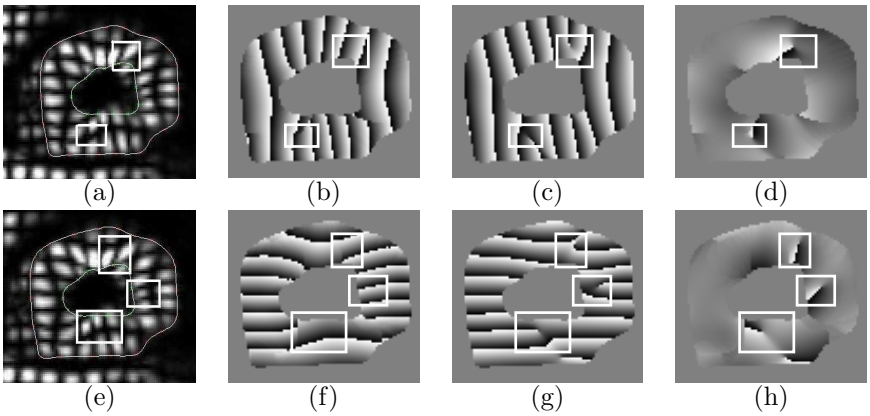

Figura G.2: Example of Angle Images obtained using Gabor filters and HARP. (a) Original Tagged MR images at the end systole. (b) Angle Image of the horizontal harmonic peak using Gabor filters. (c) Angle Image of the same peak using HARP. (d) Difference of (b) and (c). (e) Original image. (f) Angle Image of the vertical harmonic peak. (g) Angle Image of the same peak using HARP. (h) Difference of (f) and (g).

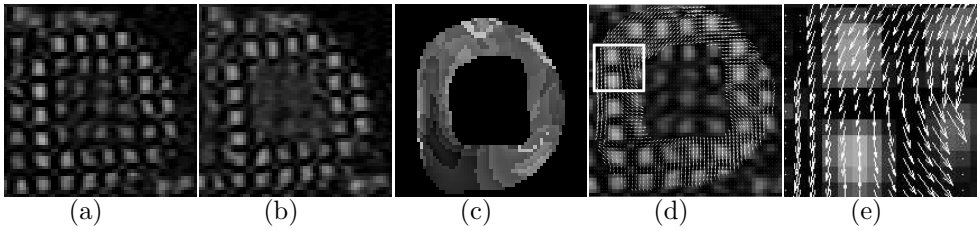

Figura G.3: Measured deformation. (a) A systole image. (b) Next image in the sequence. (c) Calculated magnitude of the displacement. (d) Measured displacement. (e) Highlighted region.

ted in section G.1.1. Since the likelihood measure, equation G.1, is based on the means of the images and square differences, the corresponding index calculated for an image from an specific sequence is not comparable with other sequences at different location of the left ventricle. It is because the morphology of the heart is not the same from base to apex, and consequently the myocardial area is different. Moreover, there are several variations in the shape of the left ventricle from subject to subject such as the thickness of the walls and the size of the radius of the ventricle, among others. Therefore, the results are shown for each of the sequence tested independently.

The similarity measure has been calculated for 3 SA Tagged MR image sequences, from base to apex, for 2 healthy patients. The corresponding plots for each sequence are shown in figure G.4. Here, the plots exhibit the behavior of the likelihood indexes through the systole. For this experiment, the systole period is composed of 7 frames. Then, the (x_i, y_i) value represents the evaluation of equation G.1 between the interpolated image I'_{x+1} and the I_{x+1}. Thus, the graphs illustrate the accuracy

for the method through the systole sequence for a given SA sequence. The test has been performed for the HARP based method, and for the one developed here, while the difference is shown.

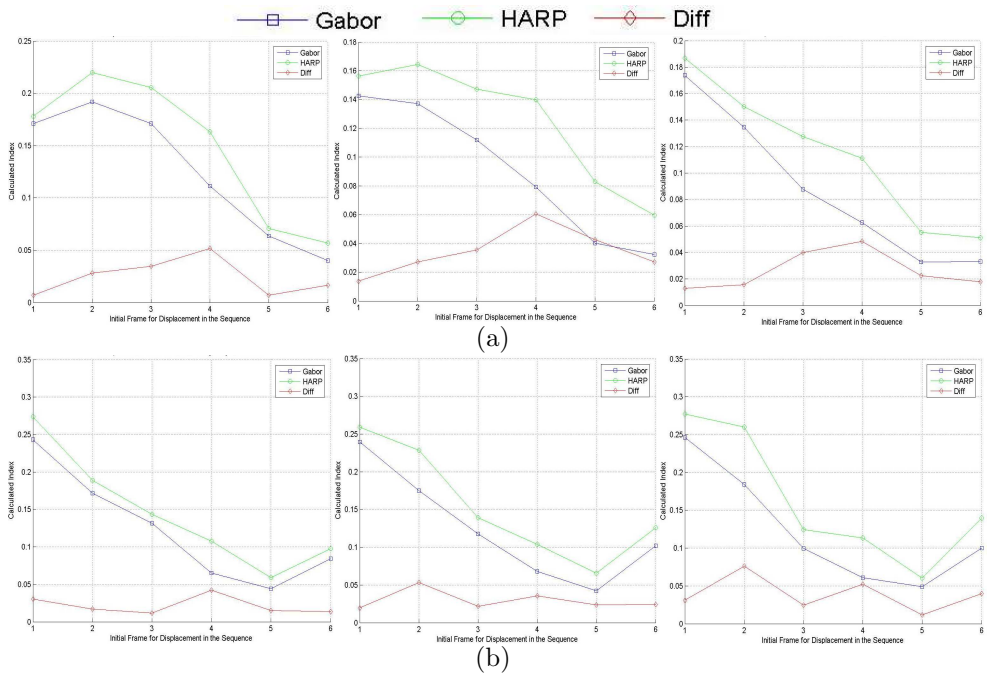

Figura G.4: Similarity measure behavior through the systole. From left to right, parallel SA accuracy from base to apex. The y-axis represents the likelihood index and the x-axis is the frame number of the systole sequence. The measure is described for two patients (a) and (b).

As it is depicted, the Gabor based method seems to be more accurate than the HARP based. For this test the tracking method used is the same. The difference between the both indexes is positive for the entire sequence. It means that the interpolated image is more similar to the next image in the sequence with the Gabor based technique than with HARP. The reason for the observed descending tendency is the disappearance of the tagging marks corresponding to the blood.

G.2. Misalignment Correction Results

As discussed in chapter E, one problem before boarding the 3-D motion reconstruction is to align the imaging planes to concord among them. Here, an approach to correct this artifact has been detailed. In this section, the alignment method is tested with a set of healthy patients. Due to the lack of the ground-truth, the results for a particular case is shown to illustrate the effectiveness of the method qualitatively. The intersection vectors are displayed, in addition to an initialization of a left ventricular model before an after the method application. To evaluate the

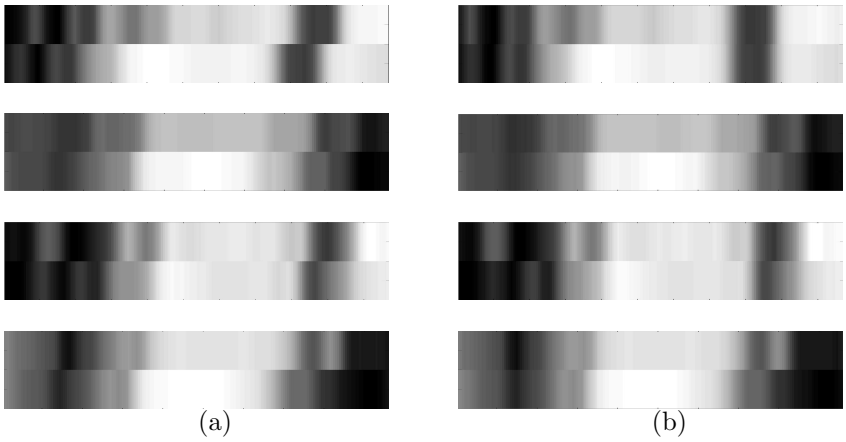

Figura G.5: Some of the most significant misalignment artifacts in a real patient and the alignment performed by the proposed framework are shown. (a) Intersection vectors as acquired from the imaging session. (b) Misalignment artifacts corrected by our method.

framework statistically, a synthetic test has been performed where the planes are moved intentionally at random. Then, the method is expected to realign the planes.

The scheme proposed has been tested with a set of 12 healthy patients. Each case is composed of 7 parallel SA views from base to apex, and 4 LA views. In 3 of these views both ventricles are shown, and in the remaining 1 just the left ventricle is observed. The pixel spacing is 1,98 by 1,98mm for SA and 1,77 by 1,77mm for LA. The slice thickness is 8mm for SA and 6mm for LA. It is selected a region of interest in a SA view, and applied our framework to this region, which is propagated to the other SA planes.

The method has been applied in patients where movement artifacts have been observed by inspecting the intersection vectors. Then, some qualitative results are shown in figure G.5 for one real case. Here some of the intersection vectors are shown before and after the alignment, showing a good registration between them. It should be noticed that all the planes have been moved simultaneously until a global fitting is achieved. In addition, the method has been applied to a different patient to initialize a 3-D model to recover the ventricular anatomy. In figure G.6 the model is shown with and without alignment. It can be observed that the model aligned is smoother and more plausible, especially in the middle of the long axis where the planes are less congruous among themselves in the initial model. It should be noted that it is a continuous model where certain interpolations are performed and a smoothing process is applied.

However, the performance of our framework can not be evaluated with the data from real patients due to the lack of the ground-truth, *i.e.* the movements during the imaging session. In order to overcome this problem, we have chosen one real patient, aligned it, and moved each of the planes by a random number from a given range. Even though there is a propagated error, it provides a good evaluation of our method. Thus, we have selected the patient case presented in figure G.5 to be misaligned by 10 iterations at different displacement ranges. Then, each slice is

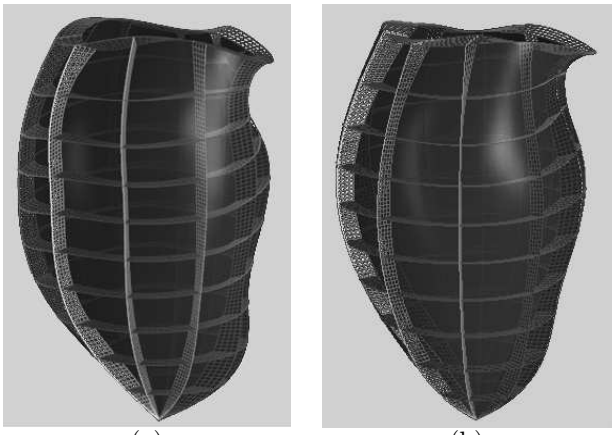

(a) (b)

Figura G.6: Initialization of a 3-D model to recover the anatomy of the left ventricle from MR images. (a) Initial model without plane alignment. (b) Model after alignment.

moved along the three axis by a random number. The results of this experiment are shown in tables G.1 and G.2. Here, it can be observed that when the induced displacement increases, the error increases as well. It is mainly because the plane could be out of the myocardial region. However, it should be noted that these errors are smaller than a pixel (1,98mm), which in terms of the myocardial thickness (12mm) represents an accuracy of 87 %.

Cuadro G.1: Mean Displacement Error in milimeters for each XYZ coordinate in different movement ranges in the LA Slices

Range	X	Y	Z
$\pm 3mm$	$0{,}5018 \pm 0{,}2597$	$0{,}4653 \pm 0{,}2028$	$0{,}4650 \pm 0{,}1985$
$\pm 4mm$	$0{,}8790 \pm 0{,}4373$	$1{,}0790 \pm 0{,}3603$	$0{,}8199 \pm 0{,}3725$
$\pm 5mm$	$1{,}0590 \pm 0{,}4339$	$0{,}8545 \pm 0{,}4540$	$0{,}6827 \pm 0{,}2169$
$\pm 6mm$	$1{,}5728 \pm 0{,}5630$	$1{,}3308 \pm 0{,}4575$	$0{,}9359 \pm 0{,}3711$
$\pm 7mm$	$1{,}5337 \pm 0{,}5840$	$1{,}5227 \pm 0{,}7223$	$1{,}8049 \pm 0{,}8195$

Cuadro G.2: Mean Displacement Error in milimeters for each XYZ coordinate in different movement ranges in the SA Slices

Range	X	Y	Z
$\pm 3mm$	$0{,}5359 \pm 0{,}2402$	$0{,}2776 \pm 0{,}1412$	$0{,}4599 \pm 0{,}1731$
$\pm 4mm$	$0{,}6415 \pm 0{,}3420$	$0{,}7213 \pm 0{,}3287$	$0{,}6814 \pm 0{,}3035$
$\pm 5mm$	$0{,}7910 \pm 0{,}3428$	$1{,}1546 \pm 0{,}3356$	$0{,}6610 \pm 0{,}3229$
$\pm 6mm$	$0{,}7004 \pm 0{,}2197$	$1{,}0097 \pm 0{,}4079$	$0{,}9686 \pm 0{,}3285$
$\pm 7mm$	$1{,}5810 \pm 0{,}4263$	$1{,}4611 \pm 0{,}5188$	$1{,}1102 \pm 0{,}3631$

G.3. 3-D Motion and Behavior

As discussed in chapter F, based on the on-plane motion estimated from the tracking process, a full 3-D motion can be obtained for certain regions of the left ventricle. For the purposes of this thesis the left ventricle has been segmented on the SA images only. It is because there is a especial interest in the rotation and torsion by the cardiologists. Additionally, several clinical research studies have been developed under the parameters from the SA views[57, 38]. Thus, the interpolation scheme has been employed to complete the SA on-plane deformation.

The framework presented has been tested with a set of 12 patients. The imaging protocol consists of 6 parallel SA and 4 LA Tagged MR image views, and their corresponding CINE images. These have been aligned using the method presented in the chapter E. Then, the vectors aligned are transformed to the Tagged MR image planes such that these planes fit among them. It generates to a smoother and more accurate displacement maps.

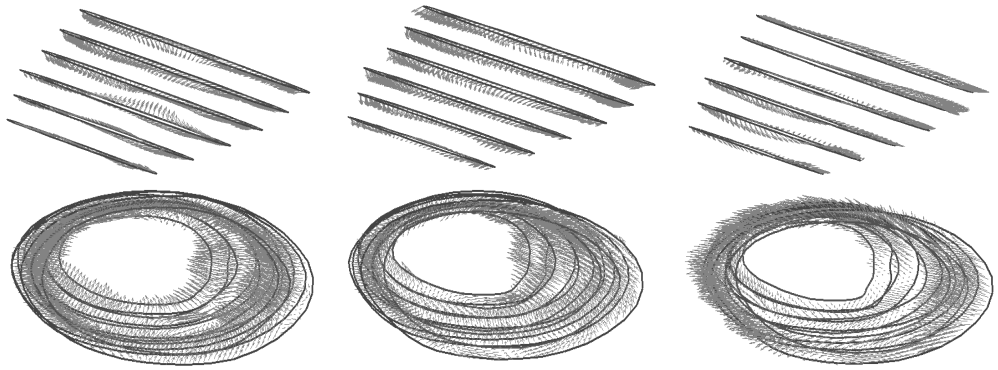

Figura G.7: 3-D Deformation fields calculated by the spread of the motion information from the intersection points. From left to right the systole time. On the top a long axis perspective is observed. On the bottom, the SA perspective is shown to illustrate the radial contraction and rotation.

Figures G.7 and G.8 show an example of the 3-D displacement information calculated for a healthy patient. It can be observed that during the beginning of the systole, the left ventricle starts to contract to its center of it and a rotation is presented. Another component along the long axis of the ventricle is appreciated from base to apex, and the nearer the apex the smaller it is. At first, this component is significant, but by reaching the end of the systole it becomes smaller as appreciated on the top of figure G.8. Here at the end of the systole, the ventricular motion is composed mainly of SA on-plane motion.

From the end-of-systole deformation maps, it can be appreciated a prominent motion component to one side. It represents the starting of the diastole where the ventricle returns to the least contraction stage. The side by which this process starts concords appropriately to the theory of Torrent-Guasp *et al.* where the heart releases its tension from the interventricular septum first [75, 76, 77, 78]. It correlates with the myocardial band theory which states that the heart is composed of a single band. Here, the ventricular cavities are defined by this band which describes two

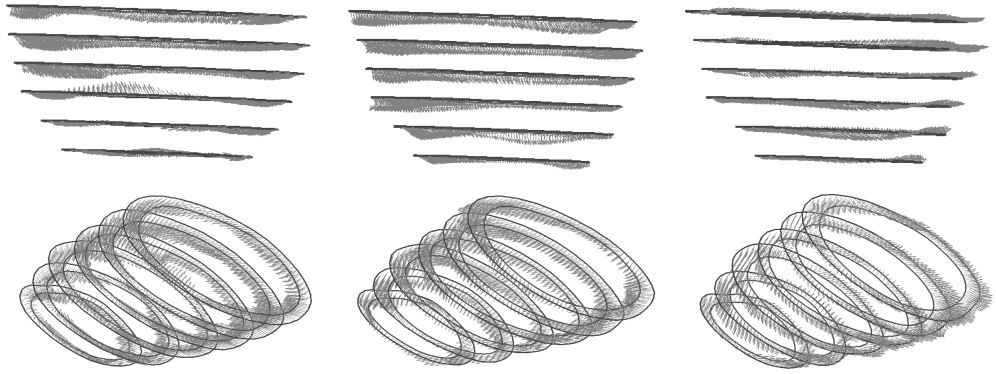

Figura G.8: Deformation field from two perspectives. From left to right the systole time. On the top a long axis perspective where the displacement information for 1 short axis component is observed. On the bottom a general view of the 3-D motion maps is depicted.

spiral loops from the root of the pulmonary artery to the aortic root. It is twisted clockwise in the base while counterclockwise in the apex during systole. When the diastole starts, the band releases its tension from backwards, and from the ascending segment of the apical loop.

This behavior has been observed with the rest of the healthy patients as a quality validation and the results are consistent. It should be noted that this 3-D motion reconstruction method accepts variations in the imaging protocol. It is because there are not assumptions above either the location or the number of the planes. Thus, it represent a flexible and scalable framework to the 3-D motion estimation.

G.4. Myocardial Rotation: a Clinical Measure

According to the myocardial band theory, the left ventricle twists counterclockwise in basal regions and clockwise in apical ones[76]. To support this theory, here the myocardial rotation has been measured. In addition, certain cardiac diseases are correlated with dysfunctions of the cardiac rotation and torsion such as coronary artery disease and ischemia[38]. However, there has not been developed a reliable baseline of healthy patients to discriminate pathologies. In this section, it is presented a statistical study of healthy people to propose a rotation and torsion pattern.

To estimate the rotation of the left ventricle in SA images, it has been used the method presented in [4]. Here, it has been treated as a simple circle to find the rotation axis. The myocardium has been segmented in 6 regions according to the *American Heart Association* (AHA)[5], and the movement has been represented in polar coordinates where the angle difference between consecutive frames is obtained as a rotation measure. It provides an index for each region which can be averaged with the rest to produce a single one by SA view. Thus, it can be compared the general index for each ventricular SA slice with the others on the long axis. In addition, the difference between basal and apical rotations has been used as torsion,

which has been correlated with certain heart dysfunctions[57].

Figure G.9 shows an example of the rotation behavior for a basal SA. The regions depicted correspond to the segmentation according to AHA. Here, it can observed how some regions (AL,IL,IN) present higher rotation levels. It suggest a rotation pattern where the interventricular septum rotates less freely than the opposite wall of the left ventricle. It supports the activation order implied by the myocardial band theory[76]. To obtain a single rotation pattern along the systole, the regions have been averaged.

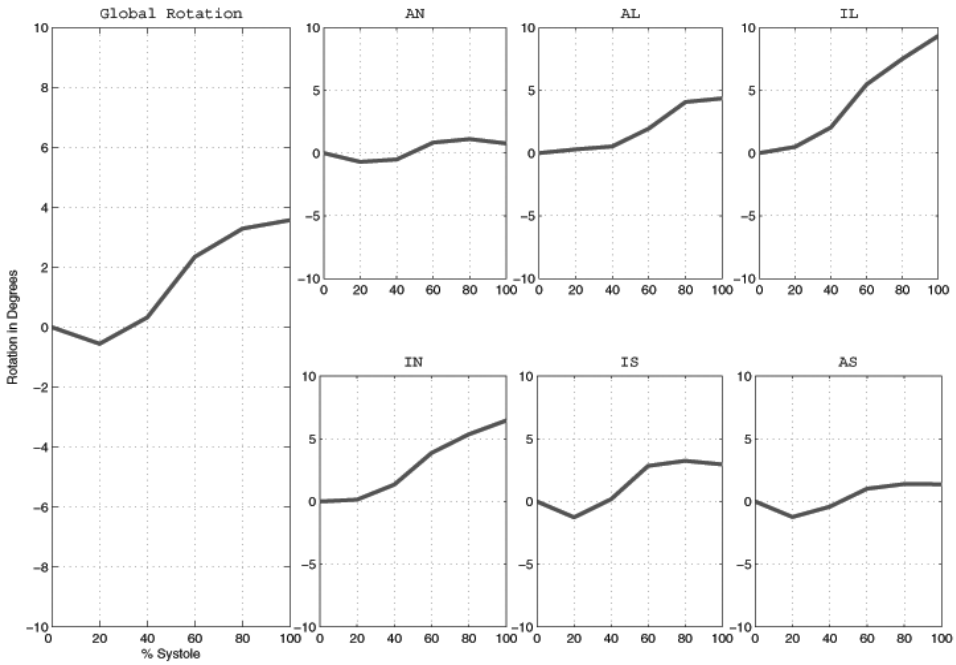

Figura G.9: Ventricular rotation of a basal SA plane for a healthy person described by regions. On the left the global pattern is depicted.

Once a general rotation behavior is calculated for each of the SA views, it can be compared these patterns from base to apex. As it is shown in figure G.10, at the base the myocardium rotates in counterclockwise orientation, while at the apex in clockwise direction. It correlates the myocardial band theory which states this orientation difference. It should be noted that these examples have been calculated for healthy patients. Here, the cardiac mechanic is expected to be normal. An analysis of several pathologies based on this measure is presented in [4, 57, 38].

In order to establish a reliable medical tool, the first step is to state a baseline for healthy people, where a certain pathology could be discriminated. In figure G.11 the rotation at the base and apex, and the torsion patterns are shown for a set of 12 healthy people. Here it can be observed how the basal rotation is meanly positive while the apical one is negative. Consequently, a positive torsion through the systole is generated even though at the beginning of systole the basal rotation is negative.

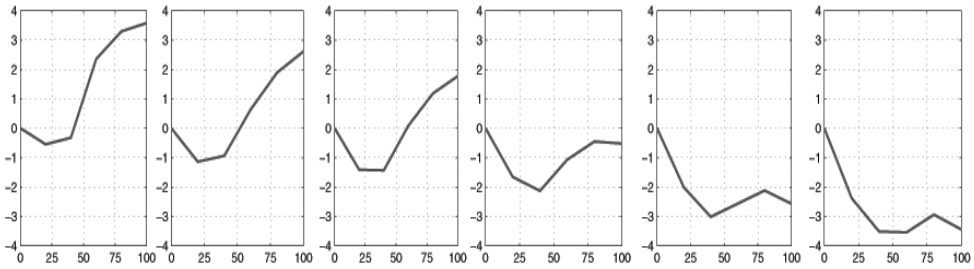

Figura G.10: Rotation behavior from base to apex for a healthy person in degrees during systole.

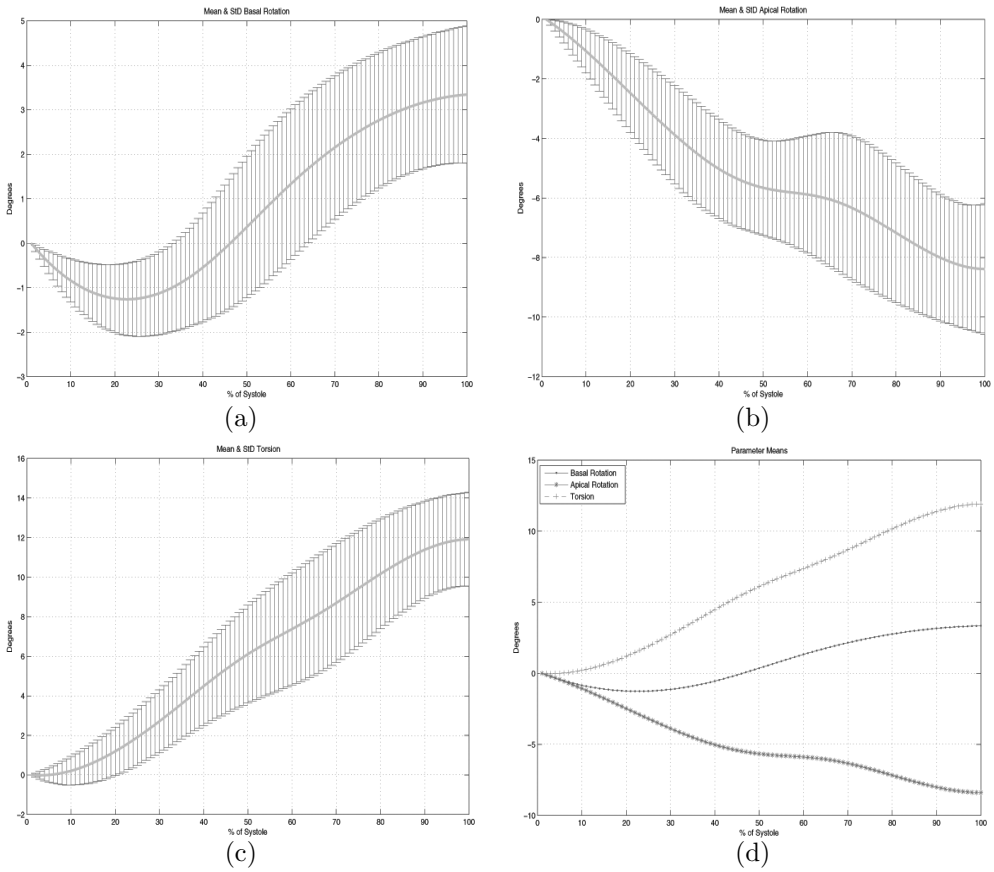

Figura G.11: Left ventricle patterns for a set of 12 healthy people during systole. (a) Basal rotation mean and its standard deviation. (b) Apical rotation mean and its standard deviation. (c) Torsion mean, i.e. basal and apical rotation difference, and its standard deviation. (d) General behavior of the three measures.

Apéndice H

Further Research

H.1. Conclusion and Discussion

A new approach to obtain the Angle Images from cardiac Tagged MR images has been described through the use of a Gabor filter bank. It has been presented an alternative method besides HARP and the proposed in [65], and demonstrated that it is more accurate than HARP and less expensive in computational cost than the proposed in [65]. Additionally, it has been applied a method able to obtain dense displacement maps for short axis MR images instead of recovering the tags only. Essentially, this method recovers the best of these techniques to generate a new approach in this issue.

The method presented is potentially an improved form to obtain more precise 3-D reconstruction and fully cardiac motion. It is due to the ability to recover more accurate Angle Images. Although the tracking process could be more controlled under a deformation model, the method has been left to converge freely assuming that for all points the displacement from frame to frame is less than a half of the tag period. Here, a postprocessing step could be added to smooth the deformation based on the neighborhood.

An accurate method to register LA and SA MR images by eliminating the misalignment artifact has been proposed. There has not been introduced any kind of bias in the movement behavior of the image slices, since these have been performed in the same global coordinate system instead of the left ventricle main axis. The image views have been treated as planes without thickness, which reduces the error of approximation that is significant for this case. It is because the myocardium could be represented by 4-6 pixels (7,9-11,9 mm) on the SA planes, while the slice thickness should not be less than 7 mm to achieve a good image equality. In addition, by treating the image data as voxels, some gaps between the SA planes are allowed, which introduce an error due to the interpolation between them, and hide part of the misalignment artifacts. Moreover, a minimum number of slice views are needed to register the image data using this idea which is not a requirement in our framework.

By inspecting the behavior of the alignment measure and the intersection vectors, it has been detected that there are more than one solution to the problem. It has been found good correspondences among the LA and SA slices at different locations, which suggests a number of displacement solutions. It is because, some

regions of the myocardium are uniform allowing a plane to move freely inside them. On the other hand, there are some regions near to the apex where an acceptable solution tends to be an exact displacement, particularly when the right ventricle is not appreciated.

Additionally, it has been observed that the misalignment artifact is an important issue in the 3-D volume reconstruction task of the left ventricle. A high percentage of patients, 75 %, has been identified with some level of movement. The inclusion of a rotation factor could help in the improvement of our registration method since the diaphragm provokes an orientation change in the image. However, this factor is not too significant when only the left ventricle is interested in as it is the case.

A non-biased method to recover the 3-D ventricular motion has been designed. It is based on the intersection points between a SA and a LA planes. A algorithm to combine the on-plane 2-D deformation vectors from each plane into 3-D displacement vectors has been performed. The spread of this motion information has been achieved to the missing dimension regardless of on-plane motion vectors calculated previously. This process has been computed a triangulation and interpolation steps. Here, the triangulation is used to obtain a more accurate solution since the available information is not equally distributed. Where the triangulation is not possible, the interpolation has been found from its nearest neighbor. It allows us to spread the motion information over the entire myocardium segmented in SA.

The 3-D reconstruction results have been correlated with the myocardial band theory. Here, the expected behavior has been achieved successfully. The method results have been observed to be stable and reproducible. In addition, the process is scalable and does not depend on either a model or a rigid imaging protocol. Here, the number of SA and LA frames can be variable and differently oriented among patients, and they can still be compared.

The myocardial rotation on SA views has been studied. A statistical analysis has been performed under a set of healthy people. This parameter has presented a characteristic pattern based on the segment analyzed. The basal rotation has depicted a counterclockwise orientation at the base, which has become to be opposite gradually as the the region analyzed reaches the apex. This behavior has yielded to a distinctive ventricular torsion pattern. In addition, it has been supported part of the myocardial band theory, which suggests the rotation difference between base and apex during systole.

A complete method to obtain the myocardial motion from Tagged MR images has been presented. From the characterization of the images to the estimation of 3-D displacements and a medical application have been depicted. The approach has been developed by stages which can be analyzed and enhanced independently. A medical measure has been studied although others parameters could be extracted and studied showing the impact of a solution to the problem.

H.2. Further Research

The method developed to improve the Angle Images has been used to provide a more reliable feature to track instead of the gray level. Here, this process has not been influenced by the neighborhood which could produce discontinuities especially near the boundaries. A postprocessing step can be suitable to improve the final

tracking. Based on the Gabor filter responses, it is possible to obtain a reliable level which can be used to smooth the output where this value is low.

The alignment method presented has been designed considering only a translation factor. However, it could be considered a rotation factor suggesting to find an axis. An analysis of how this factor impacts on the fitting could be an enhancement to the method. A process to combine the CINE MR images and the Tagged MR images would be able lead to a more efficient integration of both imaging techniques. Here, a more precise fitting could be obtained in the Tagged MR images, and an automatic method to segment and align the left ventricle could be developed.

To reconstruct the 3-D motion it has been used the intersection point vectors. The motion information have been spread through the SA to complete the on-plane displacements. A different interpolation method based on the polar coordinates could represent an improvement in the propagation. The 3-D motion information could be expanded to the gaps between SA planes where no motion information is available. Here, a more elaborate interpolation should be necessary. There might be isoparametric curves along the boundaries to achieve a reliable estimation.

To incorporate a new parameter in the clinical environment it is extremely important to test it with a huge number of healthy people, and create a baseline. Then, it can be compared statistically with several pathologies to determine its power. It is when a strong tool for diagnosis has been created. In the approach about rotation presented only a part of the first step of this process has been studied. The paucity of healthy patients in medical studious is a major issue which should be improved to continue the process.

Bibliografía

[1] World Health Organization. World Health Organization Statistics 2006. Available online at http://www.who.int/entity/healthinfo/statistics/.

[2] Geography National Institute of Statistics and Informatics. INEGI Digital Library . Available online at http://www.inegi.gob.mx/inegi/default.asp.

[3] Leon Axel, Albert Montillo, and Daniel Kim. Tagged Magnetic Resonance Imaging of the Heart: a survey. *Medical Image Analysis*, 9:376–393, 2005.

[4] J. Garcia Barnés, P. Radeva, and F. Carreras. Combining Spectral and Active Shape Methods to track Tagged MRI. In *Recent Advances in Artificial Intelligence Research and Development*, pages 37–44, 2004.

[5] Manuel D. Cerqueira, Neil J. Weissman, Vasken Dilsizian, Alice K. Jacobs, Sanjiv Kaul, Warren K. Laskey, Dudley J. Pennell, John A. Rumberger, Thomas Ryan, and Mario S. Verani. Standardized Myocardial Segmentation and Nomenclature for Tomographic Imaging of the Heart: A Statement for Healthcare Professionals From the Cardiac Imaging Committee of the Council on Clinical Cardiology of the American Heart Association. *Circulation*, 105:539–542, January 2002.

[6] J. Garcia Barnes and P. Radeva. Generalized Active Shape Models Applied to Cardiac Function Analysis. Technical Report 78, Computer Vision Center, July 2004.

[7] N. F. Osman, W. S. Kerwin, E. R. McVeigh, and J. L. Prince. Cardiac Motion Tracking Using CINE Harmonic Phase (HARP) Magnetic Resonance Imaging. *Mag. Res. Med.*, 42:1048–1060, 1999.

[8] K. McLeish, D. L. G. Hill, D. Atkinson, J. M. Blackall, and R. Razavi. A study of the motion and deformation of the heart due to respiration. *IEEE Trans. Med. Imaging*, 21(9):1142–1150, 2002.

[9] C. Studholme, D. L. G. Hill, and D. J. Hawkes. Automated three-dimensional registration of magnetic resonance and positron emission tomography brain images by multiresolution optimization of voxel similarity measures. *Medical Physics*, 24(1):25–35, Jan. 1997.

[10] J. Mathews. *Numerical Methods for Science and Engineering*. Prentice Hall, 1992.

[11] J. Garot, D. A. Bluemke, N. F. Osman, C. E. Rochitte, E. R. McVeigh, E. A. Zerhouni, J. L. Prince, and J. A. C. Lima. Fast Automated Assessment of Regional Left Ventricular Function from Tagged Cardiac Images by Harmonic Phase Magnetic Resonance Imaging,. *Journal of the American College of Cardiology*, 35(2):464, February 2000.

[12] Michael W. King. Muscle Action. Available online at http://web.indstate.edu/thcme/mwking/muscle.html.

[13] S. Girod and Anton Becker. Cardiac Muscle. Available online at http://en.wikipedia.org/wiki/Cardiac_muscle.

[14] Texas Heart Institute. Heart Information Center . Available online at http://texasheart.org/HIC/Anatomy/index.cfm.

[15] University of Kentucky Health Care. Basic Anatomy of the Heart. Available online at https://www.ukhealthcare.uky.edu.

[16] Zhi-Pei Liang and Paul C. Lauterbur. *Principles of Magnetic Resonance Imaging*, volume 1 of *Series In Biomedical Engineering*. IEEE Press, Reading, Massachusetts, 2000.

[17] Yale University School of Medicine. Atlas of Echocardiography . Available online at http://www.med.yale.edu/intmed/cardio/echo_atlas/contents/.

[18] L. Axel and L. Dougherty. Heart Wall Motion: Improved Method of Spatial Modulation of Magnetization for MR Imaging. *Radiology*, 172:349–350, 1989.

[19] Zerhouni E. A., Parish D. M., Rogers W. J., Yang A., and Shapiro E. P. Human Heart: Tagging With MR Imaging- a Method for Noninvasive assessment of Miocardial Motion. *Radiology*, 169:59–63, 1988.

[20] Dornier C., Ivancevic M., Lecoq G., Osman N., Foxall D., Righetti A., and Vallée J. Assessment of the left ventricle ejection fraction by MRI tagging: comparisons with cine MRI and ejection fraction by MRI tagging: comparisons with cine MRI and coronary angiography. In *ISMRM*, volume 10, page 1680, 2002.

[21] Daniel A. Moses and Leon Axel. Quantification of the Curvature and Shape of the Interventricular Septum. *Magnetic Resonance in Medicine*, 52:154–163, 2004.

[22] Kyoungju Park, DimitrisÑ. Metaxas, and Leon Axel. A Finite Element Model for Functional Analysis of 4D Cardiac-Tagged MR Images. In Ellis and Peters [79], pages 491–498.

[23] I. Haber, DimitrisÑ. Metaxas, and Leon Axel. Three-dimensional motion reconstruction and analysis of the right ventricle using tagged MRI. *Medical Image Analysis*, 4:335–355, 2000.

[24] Z. Qian, A. Montillo, D. Metaxas, and L. Axel. Segmenting Cardiac MRI Tagging Lines using Gabor Filter Banks. In *International Conference of Engineering in Medicine and Biology Society*, pages 630–633, 2003.

[25] Michael A. Guttman, Jerry L. Prince, and Elliot R. McVeigh. Tag and Contour Detection in Tagged MR Images of the Left Ventricle. *IEEE Trans. Med. Imaging*, 13(1):74–88, 1994.

[26] Amir A. Amini, Yasheng Chen, Rupert Curwen, Vaidy Mani, and Jean Sun. Coupled B-Snake Grids and Constrained Thin-Plate Splines for Analysis of 2D Tissue Deformations from Tagged MRI. *IEEE Transactions on Medical Imaging*, 17(3), 1998.

[27] Leon Axel, Ting Chen, and Tushar Manglik. Dense Myocardium Deformation Estimation for 2D Tagged MRI. In Frangi et al. [80], pages 446–456.

[28] Nael F. Osman and Jerry L. Prince. Angle Images for Measuring Heart Motion from Tagged MRI. In *ICIP (1)*, pages 704–708, 1998.

[29] Nael F. Osman and Jerry L. Prince. Visualizing myocardial function using HARP MRI. *Physics in Medicine and Biology*, 45:1665–1682, 2000.

[30] Nael F. Osman and Jerry L. Prince. On the Design of the Bandpass Filters in Harmonic Phase MRI. In *ICIP*, pages 625–628, 2000.

[31] Kyoungju Park, Albert Montillo, Dimitris Metaxas, and Leon Axel. Volumetric heart modeling and analysis. *Commun. ACM*, 48(2):43–48, 2005.

[32] Petia Radeva, Amir A. Amini, and Jiantao Huang. Deformable B-solids and implicit snakes for 3D localization and tracking of SPAMM MRI data. *Comput. Vis. Image Underst.*, 66(2):163–178, 1997.

[33] Li Pan, Jerry L. Prince, Joo A. C. Lima, and Nael F. Osman. Fast Tracking of Cardiac Motion Using 3D-HARP. *IEEE Transactions on Biomedical Eengineering*, 52(8):1425–1435, 2005.

[34] Raghavendra Chandrashekara, Raad Mohiaddin, and Daniel Rueckert. Analysis of 3-D myocardial motion in tagged MR images using nonrigid image registration. *IEEE Trans. Med. Imaging*, 23(10):1245–1250, 2004.

[35] Alistair A. Young. Model Tags: Direct 3D Tracking of Heart Wall Motion from Tagged Magnetic Resonance Images. In *MICCAI '98: Proceedings of the First International Conference on Medical Image Computing and Computer-Assisted Intervention*, pages 92–101, London, UK, 1998. Springer-Verlag.

[36] Xiang Deng and Thomas S. Denney Jr. Three-dimensional myocardial strain reconstruction from tagged MRI using a cylindrical B-spline model. *IEEE Trans. Med. Imaging*, 23(7):861–867, 2004.

[37] Yasheng Chen and Amir A. Amini. A MAP Framework for Tag Line Detection in SPAMM Data Using Markov Random Fields on the B-Spline Solid. *IEEE Trans. Med. Imaging*, 21(9):1110–1122, 2002.

[38] I. Paetsch, D. Foell, A. Kaluza, R. Luechinger, M. Stuber, A. Bornstedt, A. Wahl, E. Fleck, and E.Ñagel1. Magnetic Resonance Stress Tagging in Ischemic Heart Disease. *Am J Physiol Heart Circ Physiol*, 288:2708–2714, 2005.

[39] Albert Montillo, Leon Axel, and DimitrisÑ. Metaxas. Automated correction of background intensity variation and image scale standardization in 4D cardiac SPAMM-MRI. In *Proceedings of International Society for Magnetic Resonance in Medicine*, 2003.

[40] John G. Sled, Alex P. Zijdenbos, and Alan C. Evans. A Nonparametric Method for Automatic Correction of Intensity Nonuniformity in MRI Data. *IEEE Trans. Med. Imaging*, 17(1):87–97, 1998.

[41] Albert Montillo, Jayaram Udupa, Leon Axel, and Dimitris Metaxas. Interaction between noise suppression and inhomogeneity correction in MRI. In *SPIE: Medical Imaging Conference 2003*, pages 1025–1036, 2003.

[42] László G. Nyúl, Jayaram K. Udupa, and Xuan Zhang. New Variants of a Method of MRI Scale Standardization. *IEEE Trans. Med. Imaging*, 19(2):143–150, 2000.

[43] Dara L. Kraitchman, Alistair A. Young, Cheng-Ning Chan, and Leon Axel. Semi- Automatic Tracking of Myocardial Motion in MR Tagged Images. *IEEE Trans. Med. Imaging*, 14(3):422–433, 1995.

[44] Alistair A. Young, Dara L. Kraitchman, Lawrence Dougherty, and Leon Axel. Tracking and Finite Element Analysis of Stripe Deformation in Magnetic Resonance Tagging. *IEEE Trans. Med. Imaging*, 14(3):413–421, 1995.

[45] T. F. Cootes, C. J. Taylor, D. H. Cooper, and J. Graham. Active shape modelstheir training and application. *Comput. Vis. Image Underst.*, 61(1):38–59, 1995.

[46] Alejandro F. Frangi, Daniel Rueckert, Julia A. Schnabel, and Wiro J. Niessen. Automatic Construction of Multiple-object Three-dimensional Statistical Shape Models: Application to Cardiac Modelling. *IEEE Trans. Med. Imaging*, 21(9):1151–1166, 2002.

[47] Michael A. Guttman, Elias A. Zerhouni, and Elliot R. McVeigh. Analysis of Cardiac function from MR Images. *IEEE Computer Graphics and Applications*, 17(1):30–38, 1997.

[48] Albert Montillo, DimitrisÑ. Metaxas, and Leon Axel. Automated Segmentation of the Left and Right Ventricles in 4D Cardiac SPAMM Images. In *MICCAI '02: Proceedings of the 5th International Conference on Medical Image Computing and Computer-Assisted Intervention-Part I*, pages 620–633, London, UK, 2002. Springer-Verlag.

[49] Hans C. van Assen, Mikhail G. Danilouchkine, Alejandro F. Frangi, Sebastian Ordas, Jos J. Westenberg, Johan H. Reiber, and Boudewijn P. Lelieveldt. SPASM: A 3D-ASM for segmentation of sparse and arbitrarily oriented cardiac MRI data. *Medical Image Analysis*, 10(2):286–303, April 2006.

[50] M.R. Kaus, J. von Berg, J. Weese, W.J. Niessen, and V. Pekar. Automated segmentation of the left ventricle in cardiac MRI. *Medical Image Analysis*, 8(3):245–254, 2004.

[51] William E. Lorensen and Harvey E. Cline. Marching cubes: A high resolution 3D surface construction algorithm. In *SIGGRAPH '87: Proceedings of the 14th annual conference on Computer graphics and interactive techniques*, pages 163–169, New York, NY, USA, 1987. ACM Press.

[52] Joel Barajas, Jaume Garcia Barnés, Francesc Carreras, Sandra Pujadas, and Petia Radeva. Angle Images using Gabor Filters in Cardiac Tagged MRI. In Beatriz López, Joaquim Meléndez, Petia Radeva, and Jordi Vitriá, editors, *Artificial Intelligence Research and Development*, volume 131 of *Frontiers in Artificial Intelligence and Applications*, pages 107–114. IOS Press, 2005.

[53] Aymeric Histace, Christine Cavaro-Ménard, Vincent Courboulay, and Michel Ménard. Analysis of Tagged Cardiac MRI Sequences. In Frangi et al. [80], pages 404–413.

[54] Jerry L. Prince and Elliot R. McVeigh. Motion Estimation from Tagged MR Image Sequences. *IEEE Trans. Med. Imaging*, 11(2):238–249, 1992.

[55] T. S. Jr. Denney and J. L. Prince. Optimal brightness functions for optical flow estimation of deformable motion. *IEEE Transactions on Image Processing*, 3(2):178–191, 1994.

[56] Lawrence Dougherty, Jane C. Asmuth, Aaron S. Blom, Leon Axel, and Rakesh Kumar. Validation of an Optical Flow Method for Tag Displacement Estimation. *IEEE Trans. Med. Imaging*, 18(4):359–363, 1999.

[57] Yuichi Notomi, Randolph M. Setser, Takahiro Shiota, Maureen G. Martin-Miklovic, Joan A. Weaver, Zoran B. Popović, Hirotsugu Yamada, Neil L. Greenberg, Richard D. White, and James D. Thomas. Assessment of Left Ventricular Torsional Deformation by Doppler Tissue Imaging Validation Study With Tagged Magnetic Resonance Imaging. *Circulation*, 111:1141–1147, 2005.

[58] W.S. Kerwin, N.F. Osman, and J.L. Prince. Image Processing and Analysis in Tagged Cardiac MRI. Technical Report 99-04, JHU/ECE, April 1999.

[59] S.E. Fischer, G.C. McKinnon, M.B. Scheidegger, W. Prins, D. Meier, and P. Boesiger. True Myocardial Motion Tracking. *Magnetic Resonance in Medicine*, 31(4):410–413, 1994.

[60] Nael F. Osman, Smita Sampath, Ergin Atalar, and Jerry L. Prince. Imaging Longitudinal Cardiac Strain on Short-Axis Images Using Strain-Encoded MRI. *Magnectic Resonance in Medicine*, 46:324–334, 2001.

[61] Declerck J, J. Feldmar, and N. Ayache. Definition of a 4D continuous planispheric transformation for the tracking and the analysis of LV motion. *Medical Image Analysis*, 4(1):1–17, 1998.

[62] J. Huang, D. Abendschein, V. Davila-Roman, and A. Amini. Spatio-temporal tracking of myocardial deformations with a 4D B-spline model from tagged MRI. *IEEE Trans. Med. Imaging*, 18(10):957–972, 1999.

[63] Jyrki Lötjönen, Mika Pollari, Sari Kivistö, and Kirsi Lauerma. Correction of Movement Artifacts from 4-D Cardiac Short and Long-Axis MR Data. In Christian Barillot, David R. Haynor, and Pierre Hellier, editors, *MICCAI (2)*, volume 3217 of *Lecture Notes in Computer Science*, pages 405–412. Springer, 2004.

[64] L. Axel and L. Dougherty. MR Imaging of Motion with Spatial Modulation of Magnetization. *Radiology*, 171:841–845, 1989.

[65] Z. Qian, X. Huang, D. Metaxas, and L. Axel. Robust Segmentation of 4D Cardiac MRI-tagged Images via Spatio-temporal Propagation. In *SPIE, Medical Imaging*, 2005.

[66] J.G. Daugman. Uncertainty relation for resolution in space, spatial frequency, and orientation optimized by twodimensional visual cortical filters. *Journal of the Optical Society of America*, 2(A):1160–1169, 1985.

[67] Hans G. Feichtinger and Thomas Strohmer, editors. *Gabor Analysis and Algorithms: Theory and Applications*. Birkhäuser, 1998.

[68] Nael F. Osman and Jerry L. Prince. Regenerating MR Tagged Images Using Harmonic Phase (HARP) Methods. *IEEE Transactions on Biomedical Eengineering*, 51(8):1428–1433, 2004.

[69] A. C. Bovik, M. Clark, and W. S. Geisler. Multichannel Texture Analysis Using Localized Spatial Filters. *IEEE Trans. Pattern Anal. Mach. Intell.*, 12(1):55–73, 1990.

[70] Alejandro F. Frangi, Wiro J. Niessen, and Max A. Viergever. Three-dimensional modeling for functional analysis of cardiac images: A review. *IEEE Trans. Med. Imaging*, 20(1):2–5, 2001.

[71] John Moore, Maria Drangova, Marcin Wierzbicki, and Terry M. Peters. A high resolution dynamic heart model based on averaged mri data. In Ellis and Peters [79], pages 549–555.

[72] R. Gonzalez and R. Woods. *Image Processing*. Adison-Wesley, 1992.

[73] Carlo Tomasi. Mathematical Modeling of Continuous Systems. Lecture Notes, Duke University, September 2004. Available online at http://www.cs.duke.edu/education/courses/fall04/cps296.1/notes/book.pdf.

[74] D. T. Sandwell. Biharmonic Spline Interpolation of GEOS-3 and SEASAT Altimeter Data. *Geophysical Research Letters,*, 14:139–142, February 1987.

[75] Francesc Carreras, Manel Ballester, Sandra Pujadas, Ruben Leta, and Guillerm Pons Llado. Morphological and Functional Evidences of the Helical Heart from Non-Invasive Cardiac Imaging. *European Journal of Cardio-Thoracic Surgery*, 29:S50–S55, 2006.

[76] Francisco Torrent Guasp. La Mecánica Agonista-Antagonista de los Segmentos Descendente y Ascendente de la Banda Miocárdica Ventricular. *Revista Española de Cardiología*, 54:1091–1102, 2001.

[77] Francisco Torrent Guasp. Estructura y Función del Corazón. *Revista Española de Cardiología*, 51:91–102, 2006.

[78] Francisco Torrent Guasp, Mladen J. Kocica, Antonio F. Corno, Masashi Komeda, Francesc Carreras-Costa, Juan Cosin-Aguillar, and Han Wen. Towards New Understanding of the Heart Structure and Function. *European Journal of Cardiothoracic Surgery*, 27:191–201, 2005.

[79] Randy E. Ellis and Terry M. Peters, editors. *Medical Image Computing and Computer-Assisted Intervention - MICCAI 2003, 6th International Conference, Montréal, Canada, November 15-18, 2003, Proceedings, Part I*, volume 2878 of *Lecture Notes in Computer Science*. Springer, 2003.

[80] Alejandro F. Frangi, Petia Radeva, Andrés Santos, and Monica Hernandez, editors. *Functional Imaging and Modeling of the Heart, Third International Workshop, FIMH 2005, Barcelona, Spain, June 2-4, 2005, Proceedings*, volume 3504 of *Lecture Notes in Computer Science*. Springer, 2005.

Publicaciones Relacionadas

- J. Barajas, K. L. Caballero, J. García Barnés, F. Carreras, S. Pujadas, and P. Radeva. Correction of Misalignment Artifacts Among 2-D Cardiac MR Images in 3-D Space. In Proc. of *Computer Vision for Intravascular and Intracardiac Imaging Workshop from MICCAI 2006*, pages 114–121, 2006. Available online at http://www.scr.siemens.com/cvii/CVIIProceedings.pdf

- J. García Barnés, D. Gil, J. Barajas, F. Carreras, S. Pujadas, and P. Radeva, Characterization of Ventricular Torsion in Healthy Subjects Using Gabor Filters and a Variational Framework. In Proc. of *Computers in Cardiology 2006*, (in press)

- J. Barajas, K. L. Caballero, J. García Barnés, F. Carreras, S. Pujadas, and P. Radeva. Aligning 2-D Cardiac MR Images in 3-D Space using Normalized Mutual Information In Proc. of *Computer Vision: Progress of Research and Development. Proceedings of the 1st CVC Internal Workshop*, pages 1–6, Gráficas Rey. ISBN: 84-933652-8-9.

- J. Barajas, J. García Barnés, F. Carreras, S. Pujadas, and P. Radeva. Angle Images using Gabor Filters in Cardiac Tagged MRI. In Beatriz López, Joaquim Meléndez, Petia Radeva, and Jordi Vitriá, editors, *Artificial Intelligence Research and Development*, volume 131 of *Frontiers in Artificial Intelligence and Applications*, pages 107–114. IOS Press, 2005. ISBN: 1-58603-560-6.

- J. García Barnés, J. Barajas, F. Carreras, and P. Radeva. An Intuitive Validation Technique to Compare Local versus Global Tagged MRI Analysis. In Proc. of *Computers in Cardiology 2005*, pages 29–32, IEEE 2005. ISBN: 0-7803-9337-6.